INVERSE TECHNIQUES FOR THE ESTIMATION OF MULTIPLE PARAMETERS USING STEADY STATE HEAT TRANSFER EXPERIMENTS

Thesis

Submitted in partial fulfillment of the requirements for the Degree of

DOCTOR OF PHILOSOPHY

By

HARSHA KUMAR MK
(138030ME13F14)

DEPARTMENT OF MECHANICAL ENGINEERING
NATIONAL INSTITUTE OF TECHNOLOGY KARNATAKA
SURATHKAL, MANGALORE – 575025

July, 2018

DECLARATION

By the PhD research scholar

I hereby declare that the Research Thesis entitled **"INVERSE TECHNIQUES FOR THE ESTIMATION OF MULTIPLE PARAMETERS USING STEADY STATE HEAT TRANSFER EXPERIMENTS"** which is being submitted to the **National Institute of Technology Karnataka, Surathkal** in partial fulfilment of the requirements for the award of the Degree of **Doctor of Philosophy** in **Mechanical Engineering** is a *bonafide report of the research work carried out by me*. The material contained in this Research Thesis has not been submitted to any other Universities or Institutes for the award of any degree.

Register Number: **ME13F14**

Name of the Research Scholar: **HARSHA KUMAR MK**

Signature of the Research Scholar:

Department of Mechanical Engineering

Place: NITK-Surathkal

Date:

CERTIFICATE

This is to certify that the Research Thesis entitled **"INVERSE TECHNIQUES FOR THE ESTIMATION OF MULTIPLE PARAMETERS USING STEADY STATE HEAT TRANSFER EXPERIMENTS"** submitted by **Mr. HARSHA KUMAR MK (Register Number: 138030ME13F14)** as the record of the research work carried out by him, *is accepted as the Research Thesis submission* in partial fulfilment of the requirements for the award of the Degree of **Doctor of Philosophy.**

Dr. Gnanasekaran N
Research Guide
Date:

Dr. Narendranath S
Chairman-DRPC
Date:

ACKNOWLEDGEMENT

Words are not enough to express my gratitude and indebtedness to my guide **Dr. Gnanasekaran N**. who constantly guided and supported me throughout my research period. His words of experience helped me continue my research in worthwhile direction. He is indeed a source of inspiration for me. He always treated his students in a friendly way caring for their needs.

My deepest gratitude to **Prof. C. Balaji, IITM** for his valuable guidance and words of advice.

I am extremely grateful to HOD, **Dr. Narendranath S**. for making available all the facilities needed for the smooth progress of my research work. My special thanks to **Dr. Gangadharan K. V.** for providing DAQ facilities to conduct the experiments. I am also thankful to my RPAC committee members **Dr. Vadivuchezhian Kaliveeran** and **Dr. Ajay Kumar Yadav** for their guidance during my presentation. I would like to thank **Dr. Kumar G.N.** for his constant support and guidance during my research tenure. I would also like to thank secretary DRPC, **Dr. Ranjith M.** for being available whenever I approached him and making my presentations happen in a smooth way. I would also like to thank **Mr. Mahesh B.K.**, of CAD lab for helping me establish the experimental setup.

My heartfelt thanks to my friends **Vishweshwara, Narendran, Kotresh, Anil Kadam, Vignesh, Venkatesh, Suhas, Thippeswamy, Nuthan, Deepak, Bhaskar, Sharath, Sagar, Bala Ganesh, Balaji, Suyog, Pallav, SaiKrishna, Bhargav, Amey** and list seems to be endless. I am extremely thankful to the department of Mechanical Engineering, NITK, Faculty and non- teaching staff for providing all the facilities to carry out my research work.

Words cannot explain my gratitude to my mother **Smt. Umavathy** for supporting me and her blessings helped me in my research work. I would also like to thank my two elder sisters **Bharathi, Arathi** and brother-in-laws **Shreesha, Laxman** and kids **Thushar, Rajath, Lakshya** and **Shreeya** for supporting me in my work and making my research process a pleasant one. My special thanks to my wife **Supriya** who helped me in every step of my life, supported continuously during my research time and lots of love to my daughter **Prathyusha.**

I would like to thank all my relatives and friends who have who supported me in one way or the other and their best wishes were always there for me.

Finally I am greatly indebted to almighty for giving me this opportunity.

ABSTRACT

The aim of the present research work is to estimate the unknown parameters by using the information obtained from in-house steady state heat transfer experiments and to employ stochastic inverse techniques. With the advent of latest technologies in the field of advance computing, conjugate heat transfer problems that are highly complex can easily be solved to obtain temperature distributions.

In the present work, suitable mathematical models are proposed as forward models for a class of conjugate heat transfer problem. The first problem solved was a conjugate heat transfer from a mild steel fin. The numerical model is developed using ANSYS FLUENT with an extended model which facilitates natural convection heat transfer. Based on the experimental temperatures and with accompanying mathematical model, heat flux is estimated using Genetic Algorithm as inverse method. To accelerate the inverse estimation, Genetic algorithm is assisted with the Levenberg- Marquardt method for the estimation of the heat flux, thus making the whole process as hybrid estimation. In the second problem, 3-D conjugate fin model is proposed for the estimation of heat flux and heat transfer coefficient using Artificial Neural Network (ANN) method. The novelty of the work is to inject the experimental temperature methodologically in to the forward model which is trained by Neural network thereby the forward model is driven by experimental data and to accomplish the task of parameter estimation, ANN is used as inverse method that leads to a non-iterative solution.

The concept of a *priori* information is then introduced for the simultaneous estimation of heat flux and heat transfer coefficient using experimental data. This was accomplished using Bayesian framework along with Markov Chain Monte Carlo (MCMC) method to condition the posterior probability density function. A powerful Metropolis-Hastings algorithm is exploited in order to attain stable Markov chains during the process of inverse estimation. Finally, this was followed by estimation of heat generation and heat transfer coefficient from a Teflon cylinder within the Bayesian framework.

Keywords: inverse, conjugate, estimation, apriori, CFD, GA, ANN, Bayesian, MCMC, Metropolis-Hastings

TABLE OF CONTENTS

LIST OF FIGURES

LIST OF TABLES

NOMENCLATURE

A	heat transfer area of fin, m^2
ANN	artificial neural network
CFD	computational fluid dynamics
g	gravitational constant, 9.81m/s^2
h	heat transfer coefficient, W/m^2K
I	Current, A
J_{ij}	sensitivity coefficient
k	thermal conductivity of the fin material, W/m K
m	fin constant, $\sqrt{\frac{hP}{kA}}$, 1/m
LM	Levenberg- Marquardt
MCMC	Markov chain Monte Carlo
MH	Metropolis Hasting
N	number of testing data used in the network
p	perimeter of the fin, m
P_f	Likelihood function
P_{pr}	Prior density function
q	heat flux, W/m^2
q_v	volumetric heat generation, W/m^3

r	Cylindrical radial coordinate, m
T	temperature, K
T_∞	ambient temperature, K
T_{actual}	target data used in neural network, K
$T_{network}$	output from neural network, K
T_{sim}	simulated temperature, K
T_{meas}	measured temperature. K
T_{ANN}	temperature from neural network, K
T_{CFD}	temperature from simulation, K
T_{Exp}	experimental temperature, K
u	velocity in x direction, m/s
u_r	velocity in radial coordinate of the cylinder, m/s
u_θ	velocity in θ coordinate of the cylinder, m/s
u_z	velocity in z coordinate of the cylinder, m/s
v	velocity in y direction, m/s
V	Voltage, volts
w	velocity in z direction, m/s
Y_{meas}	measured temperature, K
Y_{sim}	simulated temperature, K

Greek symbols

ϑ	kinematic viscosity, m^2/s
β	Boussinesq approximation, 1/K

α	thermal diffusivity, m^2/s
σ	standard deviation
μ	mean
ϵ	error criteria

Subscripts

al	Aluminum
Exp	experimental
meas	measured
ms	Mild steel
p	parameter
pr	prior
sim	simulated

CHAPTER 1

INTRODUCTION

Of interest in heat transfer problem is the determination of the parameters involved in the mathematical formulation of the physical model. The focal point in any mode of heat transfer is the determination of temperature distribution along the region of interest for the applied boundary condition. Determination of temperature when the boundary conditions and other parameters are known will be a direct approach and such problems are called as *direct* problem. Direct problems are also referred as well-posed problems. But, when the information about any of the parameters is not known, the objective is then to estimate the unknown parameter with the knowledge of the temperature data. Such an approach is called *inverse* method which is often referred to as ill-posed problems. The parameters that can be estimated using inverse techniques include thermal conductivity, heat transfer coefficient, boundary heat flux, emissivity, thermal diffusivity, specific heat capacity.

Inverse parameter estimation problems form a class of estimation problems, where one is keen to determine the unknown 'quantity' from 'measurements', given the knowledge about the physical process. The concept of well-posed problem should satisfy the three conditions (Hadamard, 1923):

- Existence of the solution
- Uniqueness of the solution
- Stability of the output data for small changes in the input

(Beck et al. 1985) provides the importance and practical nature of the inverse heat conduction problems. Estimation of parameters is an important inverse problem in thermal sciences. Estimation techniques can broadly be classified as deterministic and stochastic methods. Deterministic methods are invariably calculus based, while stochastic methods by definition involve some probabilistic rules associated with the procedure. Generally, stochastic methods are better in terms of robustness in solving multi-parameter problems which are ill-posed and do not satisfy either one of the requirements of existence: uniqueness or stability (Mota et al. 2010).

Inverse problem is primarily focused on minimisation of the objective function,

$$F(x) = \sum_{i=1}^{N} [\boldsymbol{Y}_i - T_i(\boldsymbol{P})]^2 \quad (1.1)$$

where i is the number of measurements, ***Y*** is observation data, ***T(P)*** is the solution obtained from the forward or mathematical model for the assumed value of the parameter **P**. A general depiction of the estimation method is shown in Figure 1.1. In the Figure 1.1, T_{meas} represents experimental or simulated temperature and T_{sim} represents temperature data from forward model for the assumed input. R^2 is the error between the forward model temperature and experimental/simulated temperature and generally represented as L2 Norm. When the error is within the limit, the estimation process is terminated and the solution to the problem is the initial guess which was given as input to the forward model. In accordance to this, when the calculated error is not within the limit then a suitable inverse model is incorporated to generate a new sample and the process is continued until the objective function is minimized.

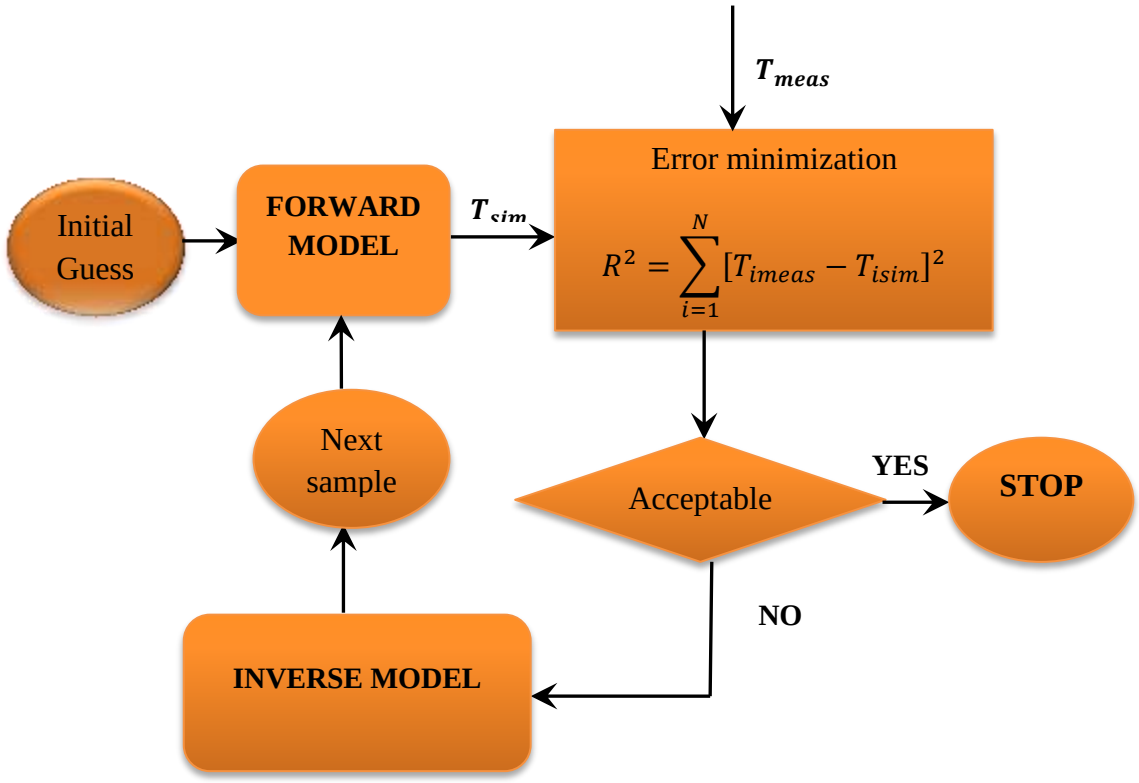

Figure 1.1 General representation of the Inverse problem

Stochastic methods provide reasonably accurate results even when the input data is noisy or corrupted due to measurement errors. Stochastic methods require generation of large amount of data for the forward calculations.

The widely used stochastic techniques include Genetic Algorithm (GA), Simulated Annealing (SA), Artificial Neural Network (ANN) and Bayesian inference etc. GA works on the basis of natural selection and mimic the process of biological evolution. Fitness function is treated as the objective function (Balaji and Thaseem 2009), wherein the objective is to minimize the fitness function or cost function. From the initial solution, the parents are selected to mate based on probabilistic rules to produce the offsprings. These offsprings form the new solution, and they once again repeat the process of mating to produce the new one until the fitness function is satisfied. Simulated annealing is a search technique where probabilistic rules are employed to decide whether a subsequent iterate is acceptable. This process is very much similar to the annealing process in metal treatment where the hot metal is cooled on a controlled manner so that desired material property can be obtained.

ANN method mimics the learning process of the human brain and progresses by training a large set of forward calculations in order to correlate the output against the input by using weights (Balaji and Thaseem 2009). It is a non-iterative technique in the inverse estimation.

Bayesian statistical framework includes probability distribution models constructed separately and explicitly for measurement and the unknown parameters (Mota et al. 2010). The *likelihood* function appearing in the Bayesian framework includes not only the information about the forward model and measurements but also takes in to account the uncertainty associated with the experiments. Any information regarding the unknown parameter can be incorporated in the *prior* model. In fact, this information is available before performing experiments. Finally the solution to the inverse problem is obtained in the form of posterior probability density function. Therefore, the Bayesian framework can be represented in terms of Posterior Probability Density Function which is proportional to Likelihood Density Function times Prior Density Function.

Some specific applications of the inverse problem include (Ozisik and Orlande 2000),

- Estimation of the boundary heat flux in natural convection and forced convection
- Estimation of thermophysical properties of the materials
- Estimation of inlet conditions and boundary heat flux in forced convection inside tubes
- Estimation of the interfacial heat transfer coefficient during the solidification process
- Estimation of the source strength
- Estimation of radiative heat transfer properties
- Estimation of interface conductance between periodically contacting surfaces.

1.1 FORWARD PROBLEM

Satisfactory results in parameter estimation by using inverse approach are possible when an appropriate forward model is used. In thermal sciences, the output from the forward model is usually temperature with the known boundary conditions/source term and material properties. The forward model or the mathematical model can be represented in terms of ordinary or partial differential equations which explains the complete physics of the problem domain along with boundary conditions and initial conditions. The forward problem forms an integral part of the inverse approach. When the computations of the forward model become complex due to time consuming CFD solutions or complex geometry, there is a need for *fast forward model*. Hence, in this thesis, artificial neural network (ANN) is used as the fast forward model which involves training a network between the known input and desired output.

1.2 INVERSE MODEL

The solution from the inverse model yields the retrieved parameter based on the error minimization criteria. The inverse model is classified into two main frameworks: deterministic and probabilistic methods. The use of deterministic methods is rendered passive because they have the tendency to get trapped in local minima and maxima (Gnanasekaran and Balaji 2011), requirement of

known constant standard deviation and prior information are not accepted. With the use of stochastic methods the problem of getting trapped in the local minima and maxima is avoided. Methods such as GA, PSO, SA etc are extensively used as optimization techniques in literature. In Bayesian Inference any prior information about the unknown parameter can be incorporated in the estimation process. In this work GA, ANN and Bayesian Inference is used as the inverse model for the estimation of single and multi-parameter.

1.2.1 Genetic Algorithm (GA)

Introduction (Sivanandam and Deepa 2008) of the evolutionary computation is based on Darwin's principle "Survival of the fittest". Genetic Algorithm is one such evolutionary computational technique which is based on the evolution of the biological species. It is a stochastic algorithm where randomness forms the essential role in the process of marching towards the solution. The biological species have solved the problem of chance, chaos, nonlinear interactivities and existence duration. In other words these problems can be related to the classic methods of optimization. Organisms which are most capable of using resources and sustain themselves are the ones which carry forward and undergo the function of evolution. These organisms are selected over the less capable organisms and are said to be fit. These evolutionary principles are embedded in Genetic Algorithm. The objective of the algorithm is to optimize the 'fitness function' either minimize or maximise based on the problem considered. The first work in the field of Genetic Algorithm was started in the year 1975 by Holland.

1.2.2 Artificial Neural Network (ANN)

ANN resembles the biological nervous system and creates a relationship between the input and the output variables. ANN can be used as forward model and inverse model. It is composed of nodes which act as the processing elements and the channels are called the connections. ANN has the self-learning ability through which the weights are adjusted based on the error between the target and the network output. Development (Yegnanarayana 2005) in the work of neural network started in the year 1943 by Warren McCulloch and Walter Pitts, but the drawback

of this model is that the weights are fixed hence it lagged the quality of self-learning. Later in the year 1949, Donald Hebb proposed a learning scheme for adjusting the connection weights. In 1954 a learning machine was developed by Marvin Minsky, in which the connection strengths could be adapted automatically. Finally in the year 1958, Rosenblatt proposed the perceptron model containing weights adjustable by the perceptron learning law.

1.2.3 Bayesian Inference

Bayesian inference is used as a frame work to minimize the objective function or to condition the probability density function. The inverse model is based on the Bayes' theorem to relate the experimental/simulated data Y and the parameter x is as follows, **(**Wang and Zabaras 2004)

$$P(x/Y) = \frac{P(Y/x)\ P(x)}{P(Y)} \qquad (1.2)$$

where, P(x/Y) – posterior probability density function (PPDF); P(Y/x) – likelihood function or the forward model; P(x) – prior density function; P(Y) – normalizing constant.

Markov chain Monte Carlo method along with Metropolis Hastings algorithm is used to compute samples from the posterior space. The most commonly used MCMC sampling algorithm is the Metropolis-Hastings algorithm, where a value is generated from an auxiliary distribution and accepted with the assigned probability.

At the closure of this chapter it is well understood that estimation of single and multi-parameter is achieved by using ANN as the forward model and in the inverse approach stochastic method such as Genetic Algorithm and Bayesian Inference is used. The robustness of these methodologies is tested with simulated measurements. After successful estimations, it is further progressed to the experimental observations and the results were found promising. With this broad idea Figure 1.1 can be further reduced which is shown in Figure 1.2.

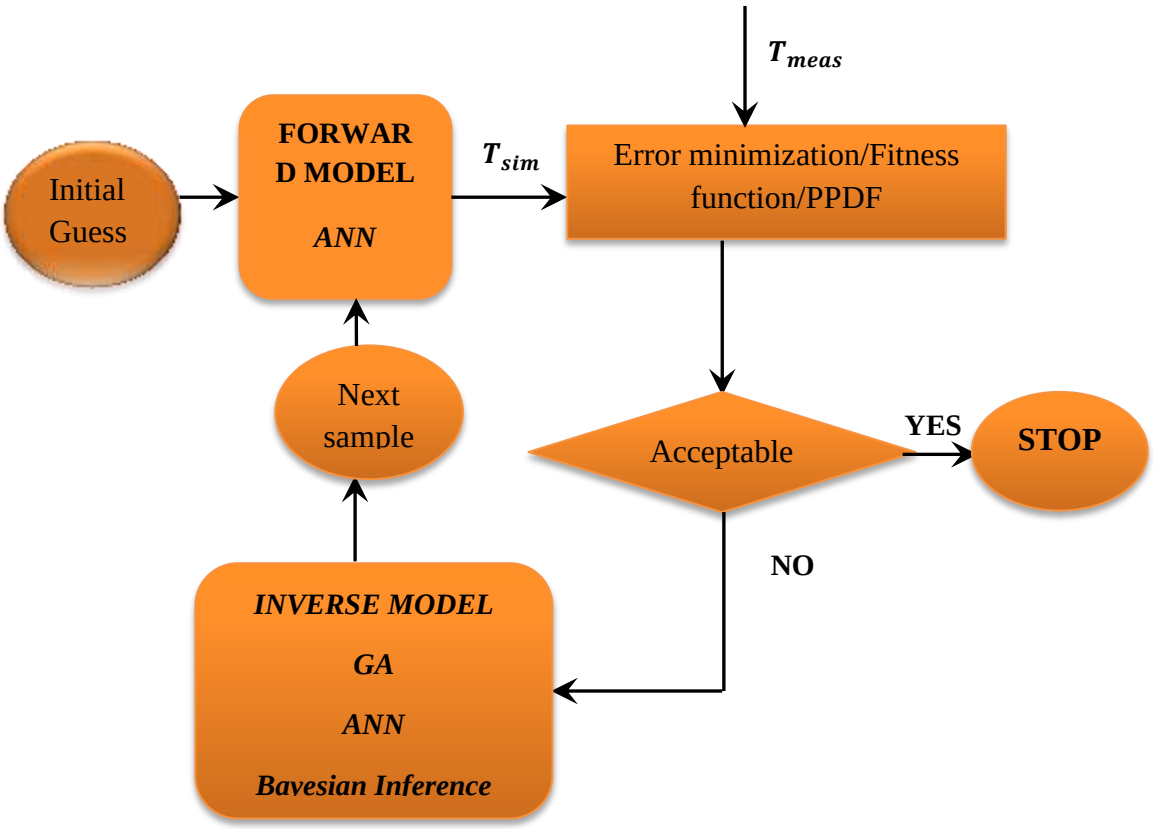

Figure 1.2 Inverse approach used in the present work

1.3 OVERVIEW OF THE WORK

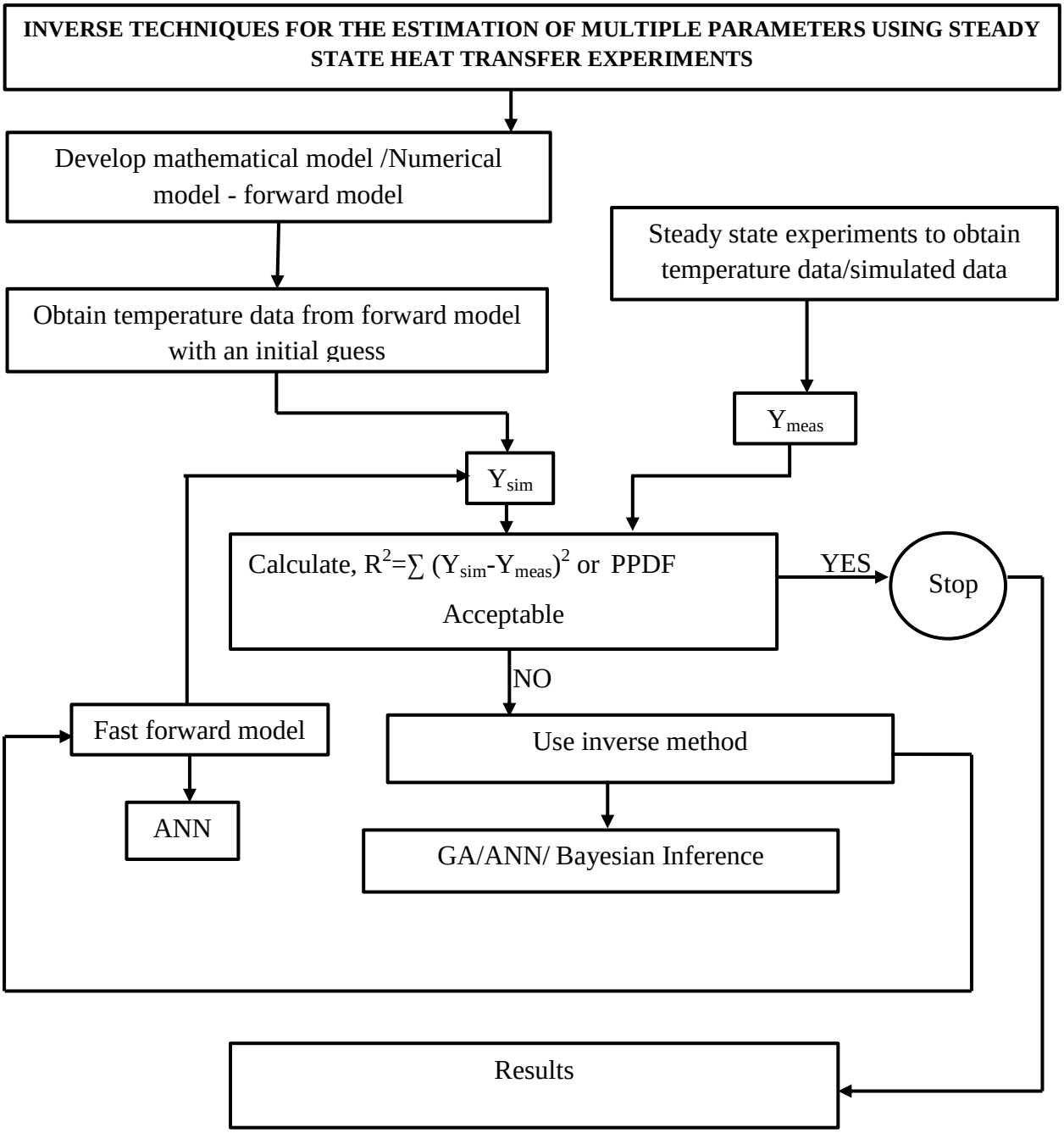

Figure 1.3 Overview of the work

1.4 ORGANIZATION OF THE THESIS

Chapter 1 provides a brief introduction about the estimation methodology for the solution of inverse heat transfer problems.

Chapter 2 highlights extensive literature review about the techniques used in the inverse estimation and its advantages. Weighted inputs were captured from the literature which helped in shaping the work in great deal.

Chapter 3 gives the constructional details of the experimental set up for each of the problems taken up for the investigation and various other instruments used in experimentation.

Chapter 4 explains the mathematical models of the forward problem. Methods such as Computational Fluid Dynamics (CFD) and Artificial Neural Network (ANN) are explained in detail.

Chapter 5 provides the details about the inverse methods used in the present work. Genetic Algorithm (GA) in conjunction with Levenberg Marquardt algorithm used for the estimation of the unknown parameters has been reported. ANN and Bayesian framework are also discussed in detail. Markov chain Monte Carlo along with Metropolis-Hastings algorithm for the sampling space within the Bayesian framework is extensively dealt with in this chapter.

In **Chapter 6** estimation of heat flux is accomplished for the two dimensional conjugate heat transfer from fin with horizontal base orientation using ANN as the forward model and evolutionary technique Genetic Algorithm as the inverse model. Hybrid technique is used by combining Levenberg Marquardt (LM) method with GA to obtain the solution. Information from steady state experiments is considered for the estimation.

In **Chapter 7,** the heat flux and the heat transfer coefficient is estimated for a 3D vertical orientation of the fin base setup. Steady state experiments are conducted on vertical orientation. ANN is used as both forward and inverse models. Experimental data is injected to the simulated data and training is accomplished. Using this trained data heat flux and heat transfer coefficient is estimated.

Chapter 8 deals with simultaneous estimation of heat flux and heat transfer coefficient for the horizontal base orientation of the fin setup using Bayesian Inference as an inverse approach. Estimation is also carried out for the measured

data. Initially 2D computational model is considered to obtain the simulated data in order to estimate heat flux as single parameter. This is used as the prior information for the simultaneous estimation. Later, 3D model is developed and simultaneous estimation of heat flux and heat transfer coefficient is accomplished. Sensitivity study has also been carried out.

In **Chapter 9** an application of the Bayesian frame work - Markov Chain Monte Carlo – Metropolis Hastings algorithm, for the simultaneous estimation of heat generation and heat transfer coefficient from Teflon cylinder which is a low thermal conducting material is attempted. ANN is used as the fast forward model. Sensitivity study is also carried out. This problem can be related to the estimation of the location and size of the tumour present in a human body.

The last chapter highlights the specific contribution made in the work along with the summary of the work. Also scope for future work is presented.

CHAPTER 2

LITERATURE REVIEW

Heat transfer phenomenon is found in all branches of science; hence the knowledge of temperature distribution and the cause for it is an interesting scenario. Direct problems, often referred to as forward approach, deal with the determination of temperature when the cause is known. But, when the cause is to be determined from the knowledge of its effect, say temperature, then such a challenging problem is termed as inverse problem in heat transfer. In recent years stimulating growth is observed in understanding the theory and application of Inverse Heat Transfer Problems (IHTP). Mechanical, chemical and nuclear engineers, aerospace, statistics, mathematics are the fields in which IHTP can be applied. The forward model is an integral part of the inverse approach. Optimizing the time taken by the forward model has created more interest among the investigators when the numerical model involves complex geometry and simultaneous partial differential equations to be solved. A common practice of an inverse problem is to develop systematic solutions to synergistically collaborate the simulation with experiments to obtain maximum information about the physical problem.

2.1 ESTIMATION OF MULTI-PARAMETERS USING EVOLUTIONARY ALGORITHM-GENETIC ALGORITHM (GA) AS INVERSE TECHNIQUE

Adili et al. (2010) applied Genetic Algorithm (GA) for the estimation of thermophysical properties of fouling deposited on internal surface of a heat exchanger tube caused due to the presence of inorganic salts. Estimation of thermophysical properties of the deposited fouling was important to improve the efficiency of the heat exchanger. Experimental temperature measurements are obtained from the copper tube that involves fouling. The simulated temperature were obtained by solving the one-dimensional linear inverse conduction problem, and by the use of the thermal quadrupoles formalism. Sensitivity study was carried out to determine the dependency of the parameters. The parameters like thermal diffusivity, thermal conductivity, volumetric heat capacity, heat transfer coefficients were estimated using GA.

Venugopal et al. (2009) used hybrid optimization technique to develop a Nusselt number correlation, in terms of relevant non-dimensional parameters, for turbulent forced convection flows in vertical channels for transient cooling experiments. The temperature-time curve obtained during the cooling of the hot plate is compared with temperature obtained numerically. As an inverse approach, GA along with Levenberg-Marquardt method constituting a hybrid approach is used to estimate the parameters by minimizing the fitness value. Another global optimization technique, Simulated Annealing (SA) was used for retrieving the parameters available in the correlation.

Miroslau et al. (1995) used GA to solve one-dimensional inverse heat conduction problem by using numerical data which is obtained from the solution of the direct problem. One dimensional transient heat conduction equation is considered as the direct problem. GA was used as inverse method for estimating the heat transfer by knowing the information about temperature. Noiseless and noise added data is considered. Regularization technique is used to improve the accuracy of the inverse method.

Hao and Xiang (2008) applied genetic algorithm (GA) combined with back propagation neural networks (BP) for the optimal design of plate-fin heat exchangers (PFHE). Two kinds of case study were considered wherein GA was used as an optimization tool to minimise the weight of heat exchanger and to minimise the total annual cost of PFHE. GA along with BP algorithm when used as an optimizing tool provided better efficiency than the traditional GA method.

Louis et al. (2009) presented a review paper on the utilization of GA in the field of heat transfer. They identified three main classes of problems for which GA could be used, (i) thermal systems design problems, (ii) inverse heat transfer problems, and (iii) development of heat transfer correlations. Problems including modeling, number of variables, and GA settings have also been presented in their work.

Imani et al. (2006) simultaneously estimated temperature dependent thermal conductivity and heat capacity using modified elitist genetic algorithm (MEGA). The forward model temperatures are obtained by solving one dimensional conductive

model using Finite Difference Method. They used hydridization technique by combining MEGA with Levenberg-Marquardt method to improve accuracy in the results. They considered measurements at single location for the estimation and also suggested that the estimates can be improved by increasing the number of sensors.

Sepehr and Hassan (2010) used GA for thermal modelling and optimal design of compact heat exchangers. Maximum effectiveness and minimum total annual cost were considered as two objective functions for which fin pitch, fin height, fin offset length, cold stream flow length, no-flow length and hot stream flow length were considered as parameters. Non-dominated sorting genetic-algorithm (NSGA-II) was used to satisfy the objective function. They proposed a correlation between the optimal values of two objective functions. Based on the estimation of energy saving of the equipment the pay back period was also calculated.

Reza et al. (2013) combined least squares and genetic algorithm for determining temperature in an inverse heat conduction problem. The results suggested that excellent estimation was obtained by the implementation of sequential genetic algorithm and parallel genetic algorithm for a computer with 2.7GHz speed and 16-core processor.

Fung-Bao (2008) estimated unknown heat source for an inverse heat conduction problem using modified genetic algorithm. An additional cost function was added to the real valued genetic algorithm to obtain the modified genetic algorithm in order to improve the computational efficiency. The results obtained from modified genetic algorithm were compared with real-valued genetic algorithm, and reduction in the computational time was observed. The results also revealed that the accuracy in the estimation is inversely proportion to the measurement errors.

Swati and Balaji (2007) estimated simultaneously conduction–radiation parameter, the optical thickness and the boundary emissivity from the information of the measured temperature profile of combined conduction and radiation in a plane parallel participating medium using Genetic Algorithm. The solution to the forward model is obtained from finite volume method. Effect of noise on estimated parameters was studied and it was observed that the error in estimation increased with noisy data.

Woodbury and Suprasanna (2006) conducted a comparison between binary coding and real number encoding for solving a one dimensional heat conduction equation with specified boundary conditions considering a test case. It was observed that when more number of parameters is to be estimated, the values retrieved by GA deviates from the observed value compared to the evolutionary algorithms.

Woodbury et al. (2004) developed and demonstrated a genetic algorithm based on a simple problem of determining the equation of a straight line. Later, GA was modified and implemented to estimate the temperature distribution in a gas based on the measured infrared transmissivity distribution. The prime objective of the inverse method was to determine the gas composition based on these transmissivity measurements.

Balázs and Gyula (2012) simultaneously estimated temperature dependent volumetric heat capacity and thermal conductivity of a solid material based on transient temperature data. Several data points were considered to obtain the temperature distribution. Temperature is recorded during the cooling process with the help of sensors. The inverse problem was solved by a real-valued genetic algorithm using simulated measurement results. New genetic operators (smooth initialization and smooth mutation) were developed and applied. The accuracy of the inverse solution was studied in two test cases including linear, square, and sinusoidal functions. They analyzed the effects of regularization and random noise in the temperature histories.

Damian (2008) applied GA to design inverse Stefan problem. They considered the problem of reconstructing the function describing the heat transfer coefficient. The solution to the Stefan problem involves finding the positions of the moving interfaces corresponding to the heat transfer. The objective of the work was to identify the heat transfer coefficient in the inverse three-phase Stefan problem. For numerical calculations genetic algorithm, Tikhonov regularization and generalized alternating phase truncation methods were used. They compared the results from the application of genetic algorithms with the results obtained from the Nelder–Mead method and found the results of GA to be superior.

Ling et al. (2004) proposed a new experimental procedure based on genetic algorithm for analyzing exterior wall surface heat transfer process and determine exterior wall surface heat transfer coefficient subject to actual conditions. They conducted tests for wide range of conditions and obtained value for heat transfer coefficient varying from 14.315 to 24.412 W/m^2 K for wind speed ranging from 1.04 to 7.36 m/s and developed a correlation based on wind speed. The use of GA suggested improving the experimental condition, by adopting flux meter for the estimation of heat transfer coefficient accurately.

Arash et al. (2014) proposed a combined cycle based on the Brayton power cycle and the ejector expansion refrigeration cycle that can provide heating, cooling and power simultaneously. The working fluid used was CO_2. The effects of the thermodynamic parameters on the system performance and the exergy destruction rate in the components were examined by carrying out parametric study and exergy analysis. They observed that the combined cycle saved around 46% of energy compared with other system producing the same output. The objective of the evolutionary based genetic algorithm was to minimize the heat exchanger size and maximize exergy efficiency. They also proposed a correlation between the exergy efficiency and total heat exchanger length. Based on the results, the combined cycle was recommended for buildings and outside regions.

Morales et al. (2015) used ANN to predict the coefficient of performance (COP) of an absorption heat transformer with a new physical design consisting of compact components, and its inverse (ANNi) was used to optimize the performance of the system, coupled for the water purification. The temperature (T), concentration of the solution (X), pressure (P) and mass flow ($\dot{m}$) are considered as input to the neural network. Using the inverse ANN model they developed a strategy for optimization of a generator and an evaporator input temperatures and the solution was obtained using the method of genetic algorithms (GAs).

Chyi-Tsong and Hung-I (2013) achieved multi-objective optimization design of plate-fin heat sinks equipped with flow-through and impingement-flow air cooling systems. Simultaneous minimization of the entropy generation rate and the material cost of the

heat sinks were attained with the help of Genetic algorithm with direction-based crossover operator. Simulation results showed that the plate-fin heat sink with flow-through air cooling system, having larger size, is better than that with impingement-flow one in heat dissipation.

Hotta et al. (2015) used an optimization strategy by combining ANN and GA for configuring five heat rectangular heat sources placed on the substrate board at the test section of the low speed horizontal wind turbine. Volume of the five heat sources, power input and their centroid distance from x and y axis is considered as input to the neural network and maximum temperature from the five heat sources is considered as output. The objective of GA was to estimate the heat source location that reduced the maximum temperature excess considering all possible configurations. The data to GA was provided from ANN and experimental data is used as input to ANN. From the results they concluded that the combined ANN–GA technique was more accurate compared to the λ-based heuristic optimization method.

Ponnada et al. (2016) estimated the dimensions of the heat sink cavity for obtaining the maximum melt time and maximum thermal performance of the heat sink by the use of ANN based GA. Using the commercially available FLUENT software transient three-dimensional simulations were done for a phase-change material (PCM)-based heat sink subjected to constant heat flux of 1.59 kW/m^2. The numerically obtained temperature data was validated with the experimental data. Simulations were carried out with 30 different geometric configurations to determine the time required for complete melting. With the estimated optimal configuration numerical calculations were done and the resulting melting time showed a good match with ANN-GA predicted values.

2.2 ANN AS FORWARD AND INVERSE MODEL

Balaji and Padhi (2010) used ANN in conjunction with Markov Chain Monte Carlo method to solve an inverse heat conduction problem. The paper reports a steady state two dimensional heat conduction from a square slab with uniform volumetric internal heat generation. Heat transfer coefficient, heat generation and thermal conductivity are estimated for the simulated data with noise and without noise. They replaced the

forward model (conduction equation) with the neural network. Noise was added to the data in order to validate the capability of the hybrid technique. Estimation was carried out by considering various prior values. The retrieved values obtained using hybrid technique is compared with ANN retrieved values and it was observed that the results from hybrid technique are superior to the results obtained using ANN as inverse technique. This hybrid technique resulted in reduced computational cost and time.

Guanghui et al. (2003) presented a review paper on the prediction of critical heat flux for natural or forced convection under low pressure and oscillation conditions by using ANN. They considered six input parameters into the network pressure, mean mass flow rate, relative amplitude, period, inlet subcooling and heated length to diameter of tube ratio and one output parameter F (nondimensionalized factor of CHF). The effect of all these input parameter on F under working conditions is also studied. They proposed that the number of neurons in the hidden layer is the product of the number of neurons in the input and output layer.

Najafi and Woodbury (2014) used ANN as an digital filter for online estimation of heat flux from temperatures measured within the domain. The performance of ANN was compared with digital filter coefficient. Triangular non-dimensional heat flux is used as input in the neural network. They used 38 sets of data with 70% for training, 15% for testing and 15% for validation. The RMS value of 0.0702 was found between the exact solution results and ANN predicted values. They concluded that for the geometry and boundary condition the number of future and past time steps required to predict the heat flux at the current time step can be minimized.

Deng and Hwang (2006) used ANN as both forward and inverse models for estimating unknown boundary condition. In the forward model continuous-time analogue Hopfield neural network is used to obtain temperature distribution for an heat conduction problem. The inverse problem uses the back propagation network (BPN) for estimating the unknown boundary condition. The numerical results of one dimensional cartesian coordinate, one dimensional cylindrical coordinate and two dimensional cartesian coordinates under transient conditions are considered. A clear layout of Hopfield network and BPN are provided in their work. They concluded that the proposed technique estimates the parameter with acceptable error.

Juan (2011) estimated auto-ignition temperature (AIT) of organic compounds using ANN. He used the combination of group contribution method (GCM) with ANN and replacing the traditional back propagation algorithm with particle swarm optimization (PSO). AIT of 93 organic compounds was estimated using the combination GCM, ANN and PSO and then compared with the values reported in literature. It has been observed that the values obtained by using this combination were better in comparison to others. He also concluded that the large differences between the structure, physical and chemical properties created difficulties in estimation and these problems were taken care by ANN and PSO. The results were compared with the experimentally measured value of auto ignition temperature and found to be very efficient.

Kumar et al. (2016) estimated the volumetric heat generation of a Teflon cylinder with aluminium heater as the heat source. Simulation of three dimensional conjugate heat transfer problem is carried out to obtain temperature distribution over the Teflon cylinder and heater temperature. Simulation data is used for training ANN. When ANN is used as forward model heat capacity is used as input and temperature as output, and while using ANN as inverse method, temperature is considered as input and heat capacity as output. Estimation of heat generation was also done for noise added data. A maximum error of 7% is observed in the estimation for noise added data.

Balázs et al. (2013) used ANN as the inverse technique for the identification of the temperature dependent volumetric heat capacity of a solid body. The network input was represented in 2 types of relations one with the classical temperature versus time representation and the novel time versus temperature representation. They observed that the time versus temperature representation contained more information than the classical one. The forward problem includes the solution of the direct heat conduction problem with noise and without noise. The inverse method uses the back propagation (BP) and radial basis function (RBF) for the estimation volumetric heat capacity from transient data. The time versus temperature representation significantly outperformed the temperature versus time representation resulting in better accuracy in the case of both noiseless and noisy inputs. The best accuracy was provided by the RBF network with time versus temperature representation. They also concluded that the RBF

provided better accuracy than the BP algorithm, but when limited data sets are available, BP algorithm would serve better with little loss in accuracy.

Jambunathan et al. (1996) estimated convective heat transfer coefficients from experimental observations using neural networks. Back propagation algorithm was selected and numerous network combinations were considered and they selected 3-6-3-1 (network structure) arrangement which resulted in minimum error. The experimental temperature information was obtained using liquid crystal thermography. The neural network consists of 3 inputs θ, thermal diffusivity α, time t and the output is heat transfer coefficient h. The error obtained from the network arrangement of 3-6-3-1 when compared with the actual value of h was found to be 2.7%.

Jose et al. (2011) predicted heat capacity of the ionic liquid at constant pressure using ANN and mass connectivity index concept. The data required for training the network was obtained from the literature and different types of multi-layered feed forward model back propagation algorithm were studied. They considered 31 ionic liquids and 477 data points as input for the neural network. They used one hidden layer in their training architecture and Matlab codes were used for training and testing. Based on the deviation between the predicted heat capacity and the values available from the literature they concluded that the network with 5, 10, 1 neurons in the input, hidden and output layer respectively was selected. The absolute deviation between the correlated heat capacity and the literature values was less than 1.2%.

Ghadimi et al. (2014) estimated the heat flux generated by the locomotive brake disc by using artificial neural network and sequential function method as the inverse approach. A three dimensional turbulent, unsteady and conjugate heat transfer problem was considered. The governing equations subject to boundary conditions is solved numerically for 47 different heat flux values. Temperature information at 18 different locations inside the brake disc is obtained. The effect of varying the number and location of the sensors on the estimation was also studied. Effect of noise on the estimated result has also been dealt with. Back propagation algorithm was used for training. Their study concluded that the sensor location must be close to the heat source for increasing the accuracy of the estimation. With more input data, the

stability of the estimate can be improved and the mean square error of the flux estimation is a linear function of the standard deviation of temperature when noise is added.

Sablani et al. (2005) solved the inverse heat conduction problem by estimating heat transfer coefficient for a solid/fluid assembly from the temperature information available within the domain. They considered two examples, linear and nonlinear problems. The first case included a cube with constant thermophysical properties and second one with semi-infinite plate with temperature dependent thermal conductivity. Neural network was obtained between the dimensionless temperature and the dimensionless heat transfer coefficient. Two models were used for estimating the heat transfer coefficient at the surface of the cube and semi-infinite plate, in the first model the ANN was trained to predict Biot number considering the slope of the dimensionless temperature ratio versus Fourier number as input to the network. In the second model an ANN model was used to predict the dimensionless heat transfer coefficient using non-dimensional temperature as input to the network. The maximum estimation error was found to be 2.5%.

Mitra and Balaji (2010) estimated the size and position of a spherical tumour in a human breast using artificial neural networks. The temperatures measured on the surface of the breast through a breast thermogram were used as the input to the network. They employed the Pennes bio-heat transfer equation for solving heat conduction equation in a cancerous breast using a finite element based commercial solver COMSOL. The solution was provided considering two types of heat sources inside the tumour, with constant heat generation and variable heat generation. When no noise was considered the accuracy in estimation of position and size of the tumour for constant heat generation was found to be 90% and 95% respectively and similarly for varying heat generation the accuracy observed was 88% and 98% respectively. The effect of size of the data on the estimated parameters is studied through sensitivity coefficient. A maximum of 22% error in position and 10% error in radius of the tumour is recorded when noise is increased from 0.1K to 0.5K.

Yasar (2003) predicted the heat transfer rate of the wire-on-tube type heat exchanger by applying artificial neural network. Back propagation algorithm is used as the

learning algorithm. C++ program was used to solve the algorithm. The mean absolute error between the experimental value and the ANN predicted value was below 3%.

Sablani (2001) carried out a non-iterative procedure using an artificial neural network (ANN) for calculating the fluid to particle heat transfer coefficient, h_{fp}, in fluid particle systems. The importance of this problem is found in agitation processing of cans containing liquid/particle mixtures where the fluid temperature varying with time. He considered two configurations of input and output parameters for the neural network. In the first one, the fluid and particle temperature which is the input parameter and Biot number the output parameter were considered on a linear scale and in the second case, the input and output parameters were converted using logarithmic and arctangent scales. The network was constructed using 3 hidden layers and the Biot number estimated was in the range of 0.1 to 10 with less than 2% error.

Elham et al. (2016) predicted relative viscosity of nanofluid in broad ranges of operating parameters. A feed-forward back-propagation multilayer perceptron artificial neural network was developed along with Levenberg–Marquardt training algorithm. They considered 1490 experimental data points on relative viscosity of different nanofluids. Temperature, nanoparticle size, density, volume fraction, and base fluid viscosity are considered as input to the network. Two hidden layers were considered in the network structure. The average absolute relative deviation (AARD) is 0.41%, and maximum average relative deviation (ARD) is 6.44 % which was observed between the ANN predicted values and the experimental data.

Mohsen et al. (2017) used artificial neural network to evaluate the effects of energy utilization, energy efficiency and utilization ratio, exergy loss and efficiency on the drying process. Two layered feed forward network was constructed considering inlet temperature, velocity and depth of bed of the dryer. The results revealed that energy utilization, efficiency and utilization ratio increased by increasing the air velocity and depth of the bed. They also observed that by increasing the inlet temperature, velocity and depth of the bed the exergy loss and the efficiency could be improved.

Tan et al. (2009) used artificial neural network models to simulate the thermal performance of a compact, fin-tube heat exchanger with air and water/ethylene glycol anti-freeze mixtures as the working fluids. The objective of the ANN was to predict

the overall heat transfer rate between the liquid and air is a heat exchanger and to prove its superiority over the non-linear regression models in dealing with the non-linear problem. The results obtained were in close agreement with the experimental data. The results obtained were potent enough for monitoring the conditions of the heat exchangers.

Soteris and Milorad (2000) used ANN for the prediction of the energy consumption of a passive solar building consisting of one room and an inclined room. They considered two cases for the analysis, a fully insulated building and a building with one wall made of masonry and the other walls with combination of masonry and thermal insulation for two different seasons winter and summer. Multi-layered neural network with back propagation was used to model the thermal behaviour of the building by creating a simulation programme for the prediction of the energy consumption. The results from this model were compared with the dynamic thermal building model that was constructed on the basis of finite volumes and time marching. The performance of ANN was found to be much faster than the dynamic model.

Mohammad (2017) used ANN for processing the experimental data on the flow and heat transfer in a nanofluid-based double tube heat exchanger. Nanofluid concentration and Reynolds number were the network inputs. The working fluid used was Ag/water. Radial basis function (RBF) algorithm was used to predict pressure drop and Nusselt number. The results proved that despite the presence of noise in the data the RBF algorithm was capabale enough to predict the results with desirable accuracy. The results also concluded that the pressure drop and Nusselt number are dependent on the nanoparticle volume fraction.

Hamzaoui et al. (2015) optimized the useful life (UL) of the failure assessment in blades of steam turbines using artificial intelligence. The artificial neural network inverse (ANNi) integrated with Nelder Mead optimization method was used to estimate resonance stress when the UL of the blades is required. When ANN was used as forward model, UL was considered as the output. And using ANNi the unknown parameter resonance stress is estimated.

Mohammad et al. (2015) predicted thermal conductivity and dynamic viscosity of ferromagnetic nanofluids using ANN. Experimental data in terms of temperature,

diameter of particles and solid volume fraction is considered as input to the neural network. The maximum error observed in the prediction of thermal conductivity and dynamic viscosity was 2% and 2.5% respectively. Based on the ANN outputs, they developed two correlations for determining thermal conductivity and dynamic viscosity and the results showed that the correlations were in good agreement with the experimental data.

Unal et al. (2009) conducted experiments for analysing heat transfer in oscillating flow. Nusselt number is calculated based on experimental results. Neural network is trained considering kinetic Reynolds number, dimensionless amplitude, filling heights and heat flux as input and Nusselt number as output. Sigmoid function was considered as the activation function. 45 sets of experimental data were considered for the training of the neural network. A maximum error of 4.47% was found between the experimental values and the ANN predicted values.

Kemal et al. (2007) proposed feed-forward back-propagation artificial neural network (ANN) algorithm for heat transfer analysis of phase change process in a finned-tube, latent heat thermal energy storage system. Initially the investigation of effect of fin and flow parameter on heat transfer is carried out numerically by solving the governing equations heat transfer fluid, pipe wall and phase change material. Heat transfer area, Reynolds number, inlet temperature, time are considered as inlet to the network and energy stored was considered as output from the network. The absolute mean relative error of 5.58% was observed which confirmed that ANN can be used for thermal analysis of latent and sensible energy storage systems.

Elham et al. (2016) estimated the depth, size, and metabolic heat generation rate of a tumour using dynamic neural network. The forward model included the finite element model. The Pennes bio-heat equation was solved to obtain surface and depth temperature distributions which can be used as the input to the neural network. Neural network trained for FEM breast model is tested for the thermal breast image. Trained neural network is used as inverse method.

Masoud et al. (2016) proposed a correlation to predict relative viscosity of MWCNTs-SiO2/AE40 nano-lubricant using experimental data. Optimal artificial neural network was designed using minimum prediction error. Experimental data was considered as

input to the neural network. The results confirmed that the output from ANN is better than the empirical relation and a deviation of 1.5% was observed from the output of optimal neural network.

Reza and Masoud (2012) developed neural network to estimate heat transfer and friction factor in helically coiled tubes. Two separate ANN models were constructed for estimating the Nusselt number and the friction factor. Reynolds number, Prandtl number, curvature ratio and coil pitch were used as input to the network and Nusselt number is considered as output. For friction factor as the output, Reynolds number, curvature ratio and coil pitch were used as input to the network. Results showed very good agreement with experiments.

Unal et al. (2016) considered a flat plate having constant heat flux subjected to a transversely pulsating jet and estimated heat transfer rate by using ANN. The experimental setup includes the flat copper plate heater located in a wind tunnel. Dimensionless parameters of Reynolds number (Re), blowing ratio (M), dimensionless amplitude (Ao) and Womersley number (Wo) were used as input to the neural network. Back propagation algorithm was used for training and the error obtained was less than 1%.

Zeke et al. (2006) proposed ANN-based forecasters to match with the additional non-linearities in the load pattern for US utility arising due to the competitive electricity market environment. The problem of over-fitting caused due to the lack of data is overcome by using some common generalization methods such as Early-Stopping, Bayesian Regularization, Adaptive-Regularization and Genetic Algorithm-based regularization GARNET. Results showed that forecasters trained by using the generalization learning techniques produced lower prediction error compared to standard error minimization method.

Jesus et al. (2014) applied Artificial Neural Networks (ANNs) for the prediction of thermodynamic properties of refrigerants in vapour - liquid equilibrium. To ensure simple design and safe working of the equipment determination of the refrigerant properties plays a vital role, that has been predicted using ANN. The use of ANN eliminated the necessity of equation of states for determining the thermodynamic properties of the refrigerants. With temperature as input to the network, pressure,

density of liquid, specific volume of vapour, enthalpy of liquid, enthalpy of vapour, entropy of liquid and entropy of vapour were the output from the network. They used Monte Carlo cross validation and Wilcoxon signed-rank test for selection of the proper ANN model.

2.3 ESTIMATION OF MULTI-PARAMETERS USING BAYESIAN INFERENCE AS INVERSE TECHNIQUE AND STUDY ON SENSITIVITY ANALYSIS.

Kaipio and Somersalo (2004) in their book developed statistical approach as a solution to inverse problem which considered numerical modelling. Construction of the prior models, modelling of the noise involved in measurements and Bayesian estimation has been discussed in detail. The use of the technique for the real world application is also cited in their work.

Mota et al. (2010) considered one dimensional nonlinear heat conduction equation and simultaneously estimated volumetric heat capacity, thermal conductivity and boundary heat flux using the Bayesian approach. Markov chain Monte Carlo approach along with Metropolis Hastings algorithm was employed for the estimation process.

Wang and Zabaras (2004) used Bayesian inference for the solution of inverse heat conduction problem. The posterior probability density function is obtained for the unknown heat flux using MCMC sampling algorithm.

Giralomi M. (2008) proved that the Bayesian influential framework provides consistent approach in the estimation of unknown parameters and also provided an introduction to Bayesian methodology as applied to system models represented as differential equations. .

Liang et al. (2009) considered one dimensional transient heat conduction problem and estimated the Robin coefficient using Bayesian inference. MCMC algorithm was used to sample the unknown parameters and proved that Bayesian inference method can provide accurate estimates as well as uncertainty for the problem considered.

Parthasarathy and Balaji (2008) applied Bayesian inference to estimate multiple parameters in a two-dimensional conduction problem with convection boundary condition and convection-radiation boundary condition. The focus of the work was to

determine the effect of noise and prior information on the retrieval results. Different a-priori models were used for single and multiple parameter estimations.

Zabaras (1988) analysed the usefulness of stochastic methods for solving inverse heat conduction problems especially in the context of estimation of boundary heat flux where in temperature is known.

Gnanasekaran and Balaji (2011) used the Bayesian approach to estimate average heat transfer coefficient ‘h’ and thermal conductivity ‘k’ from fin heat transfer. Steady state, simple experiments were conducted on mild steel fin where the heat transfer from fin to surrounding is by natural convection. Markov Chain Monte Carlo method was used as inverse method to estimate unknown average heat transfer coefficient and thermal conductivity with and without subjective priors. Since heat transfer coefficient and thermal conductivity are correlated, an informative and subjective prior information about one of the parameter was used for the successful estimation of ‘k’ and ‘h’.

Konda et al. (2012) carried out transient experiments on rectangular fin and obtained temperature data using the transient Liquid Crystal Thermography (LCT) technique, treating the inverse problem as an estimation problem, the difference between the measured temperature from LCT and simulated temperatures were minimized with the Bayesian methodology in the inverse model to determine the point estimates.

Cheung and Beck (2009) investigated Hybrid Monte Carlo method to show that it can be used to solve higher dimensional Bayesian model updating problems. New formulae for Markov chain convergence assessment were derived. Practical issues for the feasibility of the Hybrid Monte Carlo method to such problems were addressed, and improvements were proposed to make it more effective and efficient for solving such model updating problems. The effectiveness of the proposed approach were illustrated with a simulated data example.

Gnanasekaran and Balaji (2013) conducted in-house simple and inexpensive transient experiments under natural convection with mild steel fin subjected to constant heat flux at the base. MCMC sampling algorithm was used to estimate fin parameter ‘m’ and thermal diffusivity ‘α’ for the measured values. Initially single parameter estimation was carried out and continued with simultaneous estimation of both fin

parameter and thermal diffusivity. Results obtained by using Bayesian technique without MCMC and with MCMC are compared. The usefulness of priors was also investigated.

Somasundharam and Reddy (2016) used MH-MCMC sampling algorithm in Bayesian Inverse frame work and estimated thermal conductivity, heat transfer coefficient and emissivity. The paper reported the use of Parallel Tempering (PT) and Evolutionary Monte-Carlo (EMC) along with MH-MCMC to sample through correlated PPDF to retrieve the above three thermal properties. It has been concluded that at high noise levels Parallel Tempering (PT) and Evolutionary Monte-Carlo (EMC) performs equally and estimates the parameter with the maximum deviation of 9%.

Renjith et al. (2015) used Bayesian Inference for single parameter estimation, specific heat and multi-parameter estimation which included specific heat and emissivity by combining with MCMC based sampling models. The results were reported in terms of MAP, mean and SD. They used Range-Kutta method of the order four as the forward model to obtain time dependent temperature for the assumed values of heat capacity and emissivity.

Hamilton et al. (2012) used pressure measurements taken inside the combustion chamber of a spark ignition engine to estimate overall time-dependent heat transfer coefficient within the Bayesian framework. Transient zero-dimensional process based on the First Law of Thermodynamics for a perfect gas was used to model the combustion process, and the fuel burned fraction was modelled through a Wiebe's function model.

Orlande et al. (2014) improved the accuracy of the inverse problem by using two models namely the Delayed Acceptance Metropolis-Hastings (DAMH) Algorithm and the Enhanced Approximation Error Model (AEM). Spatially varying heat flux generated using laser source is estimated using MCMC with the help of these two prior models.

Naveira-Cotta et al. (2010) used combined approach of integral transform method and the generalised integral transform technique (GITT) for solving two dimensional

steady state convection problem and used MCMC and MH sampling algorithm as an inverse approach for the simultaneous estimation of the momentum and thermal accommodation coefficients related to gas flow and heat transfer for laminar forced convection within micro-channels, later Biot number was also estimated. The direct problem included the combination of numerical and analytical solution, hence termed hybrid. The prior information regarding the parameters was used in the form of Gaussian distributions.

Orlande et al. (2008) used radial basis functions for the interpolation of the likelihood function for estimation of parameters. They used Bayesian Inference as an estimation approach for two different cases, in the first case Bayesian technique was used to estimate soil properties such as dispersion of tracers in soil columns and in the second case estimation of thermal conductivity in an orthotropic medium considering transient case. The incorporation of the interpolation of the likelihood function reduced the cost of computation and the estimated values were found to be close to the actual value.

Naveira-Cotta et al. (2011) estimated spatially varying thermal conductivity and thermal diffusivity in 1D heat conduction in heterogeneous media. The information of temperature is obtained using infrared thermography. The experimental measurements obtained from the spatial domain are compressed by using integral transformation of the temperature at each measured time. The transformed temperature was then considered as the forward model. This transformation was attained by using Generalised Integral Transform Technique (GITT). The application of the Bayesian inference using MCMC method was to estimate thermophysical properties in heterogeneous media. Gaussian prior and uniform prior were used as priors in the process of estimation. With the use of data reduction model the time consumed in the estimation process was reduced.

Patrick et al. (2007) used MCMC sampling algorithm to estimate the gas plume content from hyper-spectral thermal image data. Bayesian inference was used as inverse technique based on the quality that it will automatically take care of the uncertainties associated with the estimation. They used nonlinear Bayesian regression

algorithm to produce better estimate from hyper-spectral data. They showed that the regression models are dependent on the prior information.

Phippe et al. (2006) conducted two parameter estimation for a roof mounted radiant barrier system (RBS). Sensitivity analysis was carried out to know the most influential parameter in order to design and improve the thermal model. Based on this study two heat transfer coefficients, upper convective coefficient of the ceiling and lower convective coefficient of the RBS were found to be the parameters with high sensitivity coefficients. Bayesian Inference was used as the inverse method in the estimation process. Effect of different priors in the estimation process was also examined. It was observed that by using Bayesian technique even with the far-away prior there was improvement in the characteristics of the PPDF.

Fudym (2008) considered one-dimensional heat conduction problem for comparing least-squares, maximum a posteriori and Markov Chain Monte Carlo methods in the estimation of spatially-dependent thermophysical properties like thermal diffusivity. Finite volume method was used to solve the direct problem considering simulation temperature, with noise added. They found that only MCMC method was able to estimate the spatially varying thermal diffusivity accurately.

Gnanasekaran and Balaji (2011) conducted transient experiments for turbulent mixed convection by sandwiching heater between two aluminium plates, placed in middle of two walls. A correlation for Nusselt number was obtained in terms of Richardson number. The Bayesian inference is used as the inverse approach to estimate the constants proposed in the correlation. These values were compared with the experimentally determined values. They also suggested that by running limited steady state experiments different prior information can be obtained which can improve Nusselt number correlation and reduce standard deviation.

Shubhankar and Prasanta (2015) used MCMC algorithm along with MH sampling for the reconstruction of the internal hot spot in a 2D conductive domain by determining its size, location and boundary temperature. Synthetic data was used initially for the determination process which was continued with experimental data. Boundary collocation method was used as the forward model for obtaining the temperature at

discrete points in the domain. PPDF plot with uncertainty and without uncertainty is plotted. They observed that the error involved in the estimation of eccentricity was more compared to radius and the boundary temperature. From linearity analysis they observed that sensitivity coefficients of source eccentricity, radius and temperature are not linearly independent. Hence prediction of these parameters simultaneously was not possible which basically acts as an obstruction for the reconstruction of the hot spot while considering synthetic and experimental data.

Julien et al. (2016) explored the use of Bayesian Inference for estimating both the thermal conductivity and the internal convective heat transfer coefficient of an old historic building wall. One year data of the room air temperature, surface wall temperature and temperature within the wall has been considered as the data for the estimation problem. Approximation error model has been used to compensate the error involved in the mathematical model. The building wall is composed of 3 layers lime coat, rubble stone and dressed stone. The results obtained from inverse estimation is compared with the standard values, thermal conductivity of rubble stone and dressed stone was found to be 8% higher and the internal heat transfer estimation was considered to be satisfactory. With the estimated parameters heat flux was determined; the difference between estimated heat flux and the standard value is 5.89kWh/m^2.

Xu and Tomasz (2017) used Bayesian framework for uncertainty quantification of nuclear reactor simulations using simulated data. They used direct numerical simulation and polynomial chaos expansion (PCE) as forward model. They observed that polynomial chaos expansion performed better in terms of efficiency and accuracy. When PCE was used as simulated model the simulation time was reduced by 2-3 orders of magnitude when compared with the direct simulation model. Performing inverse uncertainty quantification by using Bayesian analysis the calibration of the random input parameters was possible so that the simulation results are in better agreement with the experimental data. The parameters estimated are external reactivity insertion, Doppler reactivity coefficient and coolant temperature coefficient.

Dong et al. (2017) investigated statistical methodology in order to obtain the probability density function for the model parameters of RELAP5 code related to reflood phenomena obtained from flooding experiments with blocked arrays (FEBA) experimental data. The complex forward calculations were replaced by Radial basis function which was used as the direct problem. The objective of the work is to quantify the uncertainties associated with the Best Estimate (BE) models with the use of MCMC as the inverse method and the results are expressed in terms of mean and standard deviation. The efficiency of the simulated model was improved by an adaptive approach based on cross-entropy minimization to increase the density of the training samples at space of posterior probability density function.

Youssef and Dongbin (2009) used Stochastic collocation methods, which is based on generalized polynomial chaos (gPC), and used to construct a polynomial approximation of the forward solution with the help of the prior distribution. They carried out error analysis of the algorithm and established convergence of the retrieved posterior towards the exact posterior, also convergence rate was estimated. They showed that the convergence rate of the posterior density is same as the L2 convergence rate of the gPC expansion used for the forward solution, and hence clarified that if the gPC representation of the forward solution converges exponentially fast then even the posterior density will converge at the same rate. Demonstration of the convergence properties of the algorithm was carried out numerically by considering two examples: first on an infinitely smooth problem involving parameter estimation in the viscous Burgers' equation, and second with a forward model exhibiting discontinuous dependence on its input.

Zixi et al. (2017) in their work expressed that Bayesian Inference when used to estimate the unknowns of infinite dimensions performed at a slow rate since it is depending on dimensions. To overcome this they introduced new MCMC algorithm which is dimension independent and named it as preconditioned Crank-Nicolson (pCN) methods. By incorporating this method the sampling of infinite dimensional parameter was possible. They considered two examples; in the first one they considered simple inverse problem with forward model as the ordinary differential equation and in the second problem they estimated Robin coefficient for the one

dimensional heat conduction equation. They also highlighted the limitation of the model, since it determined the effective subspace from the prior distributions.

Xiang and Zabaras (2009) converted the deterministic forward model into a stochastic model by introducing the concept of stochastic prior state space in to the Bayesian formulation. The adaptive hierarchical sparse grid collocation (ASGC) method was used as the solution of the forward model. They used Hierarchical Bayesian formulation to derive the posterior probability density function (PPDF). Markov Chain Monte Carlo algorithm is used to explore the state space variables. They considered two numeric examples and confirmed that ASGC is much faster than FEM computation. The accuracy of the results was more dependent on the noise rather than the threshold value.

Charles et al. (2004) considered three dimensional climate model which included three parameters namely obliquity (Earth's tilt), longitude of the perihelion (celestial longitude at which Earth is at its closest approach to the sun), and eccentricity (degree of orbit circularity). The simulation results based on the simulated climate model is the variation of the surface temperature caused by arbitrary changes in these three parameters. Bayesian stochastic inversion along with very fast simulated annealing (VFSA) is used as the inverse approach. They observed that multiple VFSA is one to two orders of magnitude more efficient than the Metropolis/Gibbs sampler in estimation of the parameter uncertainties, when more importance is given to dimensionality of the parameter space analysis.

Kaipio and Colin (2011) presented a review paper on the view of helping researchers working in the area of inverse heat transfer. The paper provides the idea as to how modelling of uncertainties can be done which arise from real physical phenomena. Inverse problems in heat conduction, heat convection and heat radiation have been dealt. Prior modelling, noise and likelihood modelling also has been discussed in their work by considering examples.

Wang and Zabaras (2005) addressed uncertainties in the measured temperature data, temperature sensor locations and thermophysical properties using Bayesian statistical inference with hierarchical Bayesian formulations method for a heat conduction

problem. Numerical examples were conducted in which the thermal conductivity and the boundary heat flux are estimated. Effect of sensor location on the solution of inverse problem was also been dealt.

Naoya et al. (2016) used Bayesian Inference to estimate the maximum depth of corrosion in an oil storage tank. They proposed a new method combining extreme value analysis with Bayesian Inference using experimental data. Backside corrosion of oil storage was a major problem and the traditional way of measuring the thickness is by using discrete ultrasonic thickness measurements. They utilized the detected maximum depth of corrosion of discrete thickness measurements from the Japanese Fire Service Act (JFSA) guidelines for the year 2006 and 2011 which is considered as the measured value. The pulse reflection method was used to measure the thickness of the bottom floors of the tank with 12 sensors used to measure the thickness. The combined method of extreme value analysis and Bayesian inference provided effective results in terms of estimation the maximum depth of corrosion.

Pereyra et al. (2014) applied sensitivity analysis and parameter estimation to test heat transfer and material flow models. A forward-difference approximation was used to compute the sensitivity of the solution with respect to the unknown model parameters. The Levenberg-Marquardt (LM) method was applied to solve the nonlinear parameter estimation problem. The numerical models were developed by the finite element method (FEM).

Ewa et al. (2013) analysed the thin metal film subjected to the ultrashort laser pulse. The heat conduction in the domain considered has been described by two-temperature model consisting of the system of two coupled parabolic equations determining the electron and lattice temperatures. The sensitivity analysis of electron and lattice temperatures with respect to the parameters appearing in mathematical description has been discussed. The changes of temperatures due to the changes of coupling factor G and the film thickness L was estimated.

Cole et al. (2009) provided exact solutions for the transient temperature in flux-base fins with the method of Green’s functions (GF) in the form of infinite series for three

different tip conditions. The temperature was expressed as the function of parameters to be estimated, which help carry out sensitivity study.

2.4 MOTIVE AND SCOPE FOR THE PRESENT WORK

Based on the understanding from the review of literature, inverse heat transfer can be viewed as an independent area of research in the field of heat transfer and unrestrained work is being carried out in the past few decades. Few principal reasons behind this development are,

1. Availability of high precision measurement techniques

2. Rapid steps in the mathematical formulation of optimization problems

3. Availability of sophisticated computational resources to handle complex inverse problems that invariably involve repeated solutions to the forward model.

4. Among the new generation techniques to solve inverse heat transfer problems, GA yields results with few iterations, hence proving its robustness. A non-iterative technique ANN has also been used as inverse technique. As already stated the Bayesian framework gives scope to accommodate prior information and can eminently handle noisy measurement data.

In harmony with this, the primary focus of this thesis is the pursuit of the stochastic methods such as Genetic Algorithm, artificial neural network and Bayesian framework to solve inverse heat transfer problems. In consideration of this, the scope and objectives of the present study are,

2.5 OBJECTIVES OF THE PRESENT WORK

1. To develop an inexpensive heat transfer experimental setup in order to perform steady state experiments.
2. Estimation of boundary heat flux using ANN as the fast forward model and Genetic Algorithm as the Inverse model for the measured data from conjugate fin heat transfer.

3. Estimation of boundary heat flux and heat transfer coefficient using ANN as both fast forward model and Inverse model based on steady state fin heat transfer experiments.
4. Simultaneous estimation of boundary heat flux and heat transfer coefficient for the fin using ANN as the forward model and Bayesian Inference as the Inverse model for the measured data.
5. Simultaneous estimation of heat generation and heat transfer coefficient for Teflon cylinder using ANN as the forward model and Bayesian Inference as the Inverse model for the measured data.

2.6 Closure

A detailed discussion on the literature review apropos to the problems considered in this study was presented in this chapter. The objectives of the present work listed. In the next chapter, the experimental set up and the instruments used for experimentation is elucidated.

CHAPTER 3

EXPERIMENTAL SETUP

3.1 INTRODUCTION

This chapter explains the details of the experimental setup and the instruments used to perform steady state experiments. The experimental setup is designed such that the effect of surroundings is minimised to enable natural convection to take place. Steady state experiments are conducted for different power levels.

3.2 EXPERIMENTAL SETUP

In-house experimental setup has been developed to facilitate the natural convection heat transfer from fin. The layout of the experimental setup is shown in Figure 3.1. The mild steel fin with dimensions 150x250x6mm^3 is placed centrally on to the aluminium base of dimension 150x250x8mm^3. A nichrome wire wound over a mica

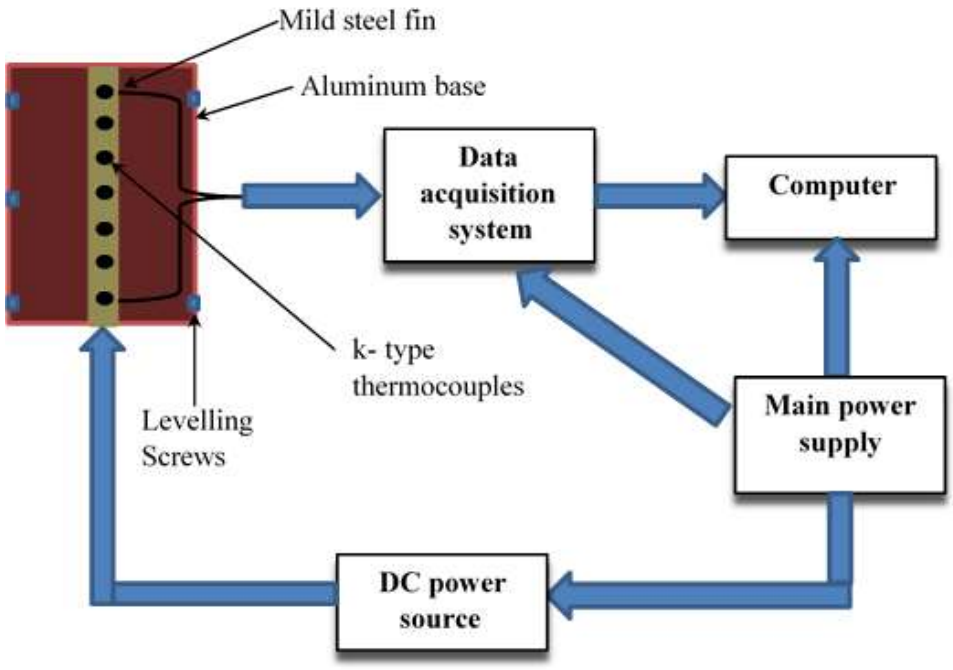

Figure 3.1 Layout of the experimental setup.

sheet is used as a heater, having the dimensions of the aluminium plate with thickness 1.4mm, shown in Figure 3.2. The sides of the aluminium base plate and bottom of the heater are insulated with glass wool to prevent heat loss. The fin setup is placed in an enclosed chamber of dimensions 975x995x930mm^3, so as to avoid disturbances from the surroundings. Holes of 3mm diameter are drilled for a depth of 20mm along the measuring length of the fin and also in the base plate. Calibrated K-type sheathed thermocouples are used to measure the temperature of the fin and the base plate. A heater, provided below the base plate, is powered by a DC power source that can supply constant power to the setup. The temperature recorded by the thermocouples is stored with the help of data acquisition system equipped with Labview software

Figure 3.2 Nichrome heater plate

supplied by the National Instruments. Figure 3.3 shows the experimental setup used in the present work. The temperature data is recorded for every 10s during the course of the experiment however, only steady state measurements are taken into account for the purpose of estimation. A typical natural convection fin experiment require 6-7 hours to reach steady state. The steady state is confirmed when the change in temperature is less than 0.2°C for the time duration of 10min. Experiments are conducted for different heat input values and corresponding steady state temperatures are stored. Two attachments are used so that estimation can be carried out for different orientation of base i.e vertical and horizontal. Figure 3.4 (a) and (b) shows the horizontal and the vertical attachment respectively.

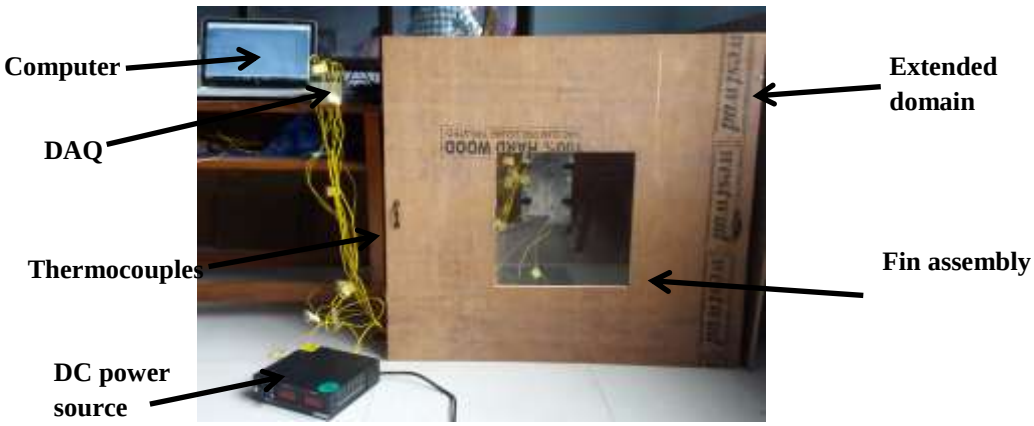

Figure 3.3 Photographic representation of the experimental setup.

(a) (b)

Figure 3.4 (a) Horizontal base **(b)** Vertical base

In addition to the fin setup the estimation of the parameter using inverse method is also extended to volumetric heat generation, to accommodate this, an experimental setup is developed using Teflon cylinder which is having low thermal conductivity. A Teflon cylinder of radius 50 mm and height 100 mm is considered consisting of the cylindrical heater placed at the centre. Figure 3.6 shows the dimensions of the Teflon cylinder along with the aluminium cylindrical heater. Same DC power source is used to supply power to the cylindrical heater placed in the Teflon cylinder. The power supply can deliver a range of power required for the experiments (voltage: 0-60V, current: 0-5A). K-type thermocouples are used to measure the temperature data at

several locations of the Teflon cylinder at various depths and also the temperature of the heater is measured. Steady state experiments are conducted for different values of heat generation and the temperature is recorded. A photographic view of experimental setup is shown in Figure 3.5. The thermocouples are fixed by drilling holes in the Teflon cylinder and then bonded using epoxy adhesive. The other end of the thermocouples is connected to a data logger to collect the data and using Lab view software the data is stored in the computer for every 5mins. The duration for single experiment starting from heating, continued as steady state and followed by cooling consumes 7 hours. In order to avoid the resistance created by the air inside the hole-gap, epoxy adhesive has been applied. Steady state experiments are carried out for different power levels and temperature is recorded. Steady state is said to have been reached when the temperature difference does not vary by more than 0.1°C within 10 minutes.

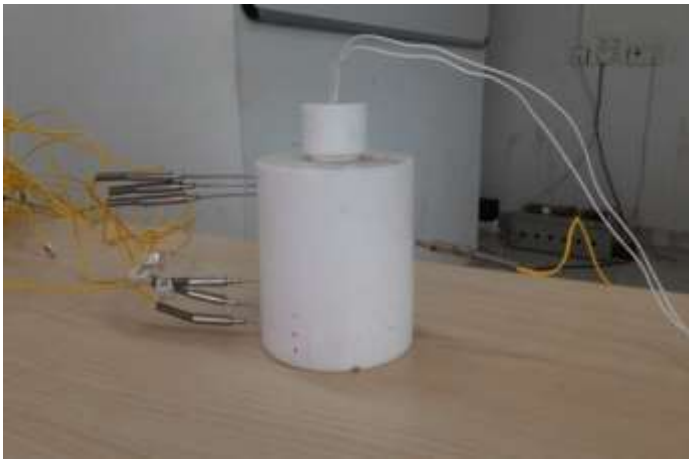

Figure 3.5 Teflon cylinder with thermocouples

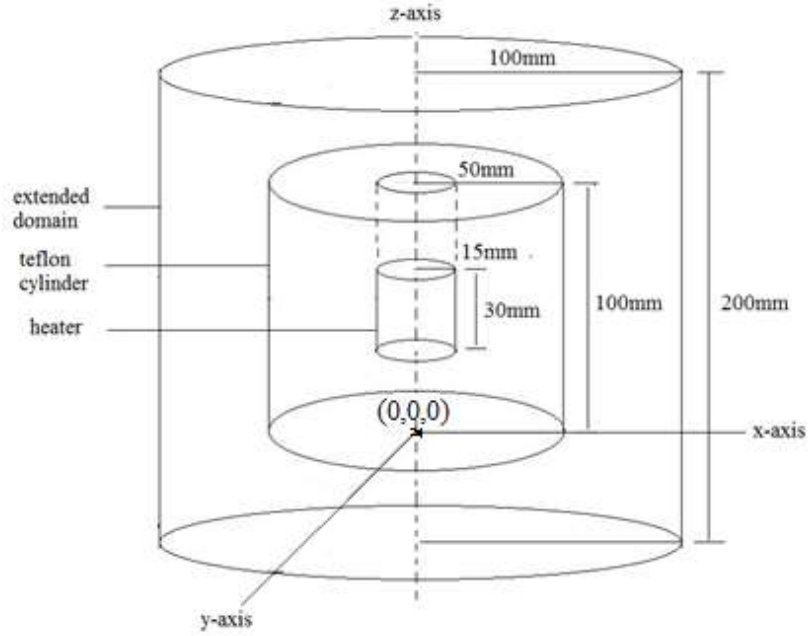

Figure 3.6 Schematic representation of the Teflon cylinder along with aluminum heater

3.3 INSTRUMENTATION

3.3.1 DC power source

DC power source is used to supply power to the heater. Different trials of experiments can be conducted by varying the range of power input to the heater. The specifications of the DC power source are shown in Table 3.1.

Table 3.1 Specifications of DC power source

Features	**Specifications**
Output Voltage	0-150V
Output Current	0-2A
AC input	1phase AC220V ±15%, 50/60Hz
Source voltage regulation	Constant voltage ≤0.2%
Load regulation	Constant voltage≤1%, constant current≤2%
Make	Proxim Asia Inc.

3.3.2 Data Acquisition system (DAQ)

The data acquisition system is supplied by the National Instruments. The DAQ used in the present work consists of 16 channels with the model no: NI 9213. Figure 3.7

shows the pictorial view of DAQ used in the present work. Using the labview software the measured temperature is stored. A simple network diagram is created using labview such that the temperature is stored for every 10 seconds. The temperature reading from beginning of the experiment till the end is stored in the system with the help of DAQ.

Figure 3.7 Data acquisition system

3.3.3 Digital Multimeter

Digital multimeter is used to measure the current flowing across the terminal of the DC power source into the heater. Voltage across the output terminal of the DC power source is also measured with the help of Digital multimeter. For the input voltage of 40V the voltage measured using multimeter is 39.7V. The photographic view of Digital multimeter is shown in Figure 3.8.

Figure 3.8 Digital Multimeter

3.3.4 Thermocouple

Temperature along the height of fin and the base is measured using thermocouples. Sixteen K-type sheathed thermocouples are used for measurement. Thermocouple with 3mm diameter is inserted into the holes created on the measuring side of the fin and base. The other end of the thermocouple is connected to the data acquisition system for recording the data. Before using the thermocouple for measurement it is calibrated with the standard thermostatic bath supplied by Thermo Scientific, with the range of -60°C to 200°C and with accuracy of 0.01°C. Table 3.2 shows the details of calibration.

Table 3.2 Calibration chart

Number of thermocouples	**Thermostatic bath temperature, °C**		
	50.5	**60.05**	**70.06**
	Thermocouple reading, °C		
1	50.02	59.48	69.31
2	50.04	59.45	69.41
3	50.1	59.49	69.4
4	50.16	59.51	69.44
5	50.2	59.56	69.45
6	50.19	59.57	69.45
7	50.12	59.51	69.48
8	50.24	59.55	69.35
9	50.08	59.57	69.48
10	50.32	59.63	69.54
11	50.22	59.54	69.51
12	50.12	59.5	69.57
13	50.08	59.6	69.47
14	50.24	59.57	69.41
15	50.14	59.61	69.45
16	50.2	59.46	69.61
Average percentage error	0.684	0.856	0.859

3.4 Closure

This chapter provided the details about the experimental setup and the equipments and attachments required for the smooth conduction of the experiment along with its specifications. The next chapter explains about the forward model used in the present work.

CHAPTER 4

FORWARD MODEL

4.1 INTRODUCTION

This chapter deals with the techniques which have been used as forward model in the present work. The forward model in this context refers to obtaining temperature as the output when heat flux or any other boundary condition is given as input. In any inverse estimation problem, the forward model becomes the integral part of it. Numerical simulation and ANN is used as the forward model. ANN replaces the conventional numerical simulation by optimizing the computational time without compromising much in accuracy and hence called as *Fast Forward Model*.

4.2 NUMERICAL SIMULATIONS

ANSYS fluent is used as the computational tool. 2D and 3D models representing the horizontal and vertical attachments of the fin setup are developed. Grid independence test is carried out to fix the number of grids for the numerical model that can be used for further study. Heat flux is given as the input for the numerical model and temperature is obtained as the output. Temperature distribution, velocity contour and information about heat transfer coefficient are obtained as output from the numerical simulations. Based on the residual value, the convergence criteria for continuity equation is specified as 10^{-4} and for momentum, energy equations it is specified as 10^{-6}. The governing equations are solved by using ANSYS fluent solver which employs finite volume method as its solution strategy. The velocities and the pressure are calculated using the semi implicit pressure linked equation solver (SIMPLE) algorithm. Second order upwind scheme is used to discretize the convective terms.

4.3 ARTIFICIAL NEURAL NETWORK (ANN)

ANN is a numerical tool which is used to correlate the inputs and outputs of a certain experiment. The name of this technique is inspired from the biological nervous system which acts according to the input stimulus, processes the information in the neurons taking into account the previous experiences and gives out the reactions as required. The artificial neural network simulates such a process. But still the

biological neural network is superior to even the most sophisticated artificial network in terms of robustness, flexibility, ability to deal with different data situations and collective computation. The main advantage of using ANN is that it can model nonlinear relationships between the inputs and outputs very well. The architecture of the artificial neural network consists of an input layer, variable quantity of hidden layers and an output layer. Figure 4.1 shows the layout of ANN. To train the network, the inputs and their corresponding outputs are filled in the input and output layers. The input and output data is obtained from CFD simulations or any other forward model. A perceptron in an ANN is the analogous element to the neuron in the biological nervous system. Each input and output is individually represented by a perceptron (neuron). The perceptron is a processing node which processes data and sends it to the next layer in the network. The number of hidden layers and the number of perceptron in the hidden layers can highly affect the accuracy of each architecture. Hence, there arises the task of fixing the number of neurons before using the network for obtaining the desired output. Each perceptron in the network has a weight associated with it to determine the importance of that particular information stored in that node. In the first iteration of the training, based upon the inputs and default weights, the network finds an output and compares this with the actual output. Based upon the error observed, the weights are modified in each successive iteration until the error becomes zero. The training is done using the back propagation algorithm.

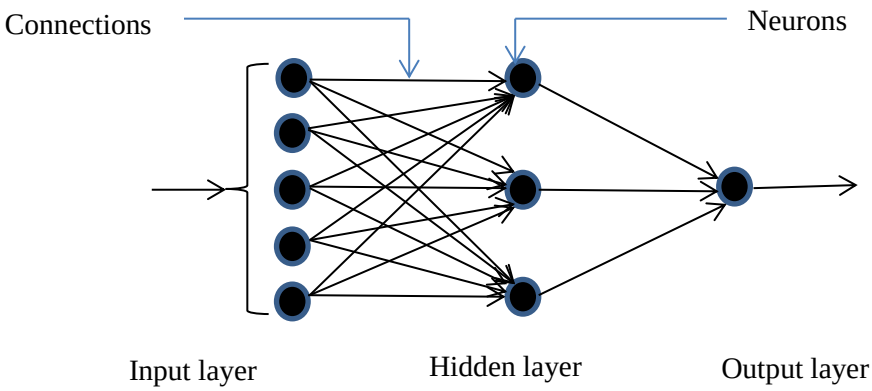

Figure 4.1 Basic layout of ANN

The process can be explained using an example, let the following be the mathematical model for the forward model network-

The matrix W is the matrix of all weights. The matrix F is the input matrix i.e the matrix of the flux data. Matrix B is the bias matrix which provides the required bias to get the desired output. The Matrix O signifies the output matrix which contains the temperature data.

$$\begin{bmatrix} w1 & w2 & w3 \\ w4 & w5 & w6 \\ w7 & w8 & w9 \end{bmatrix} \times \begin{bmatrix} f1 \\ f2 \\ f3 \end{bmatrix} \pm \begin{bmatrix} b1 \\ b2 \\ b3 \end{bmatrix} = \begin{bmatrix} t1 \\ t2 \\ t3 \end{bmatrix}$$

[W] [F] [B] [O]

f1, f2,and f3 are the fluxes as inputs and w1,w4 and w7 are the weights associated with the flux f1, w2, w5 and w8 with f2 and w3, w6 and w9 with flux f3. These weights are modified in each iteration so that the above LHS produces the desired RHS.

4.3.1 Backpropogation using Levenberg-Marquardt method

Training of artificial neural network is a process where the error between the actual outputs and desired outputs is computed and the weight matrix is modified such that in the next iteration, the disparity is reduced. This is done until the error vanishes or reduces below a threshold value. The backward propagation mainly works in two steps- first, the calculations are done in the forward direction, the outputs and derivatives are calculated. Second, the network is run backward and the pre-calculated derivatives are used to modify the weight matrix. We use a Levenberg-Marquardt method which is based on least square error curve fitting. This method is a combination of the gradient descent and Gauss-Newton algorithm and delivers the advantages of both. The error or activation function should be continuous and differentiable multiple times. The error square is defined as-

$$E = 0.5 \sum_{L=1}^{L} \sum_{O=1}^{O} e_{L,O}{}^{2} \tag{4.1}$$

L – index of patterns

O – index of outputs

e – error at each output using different patterns

The constant 0.5 will disappear when E is once differentiated. This small arrangement makes the function E easy to use.

The error gradient G is –

$$G = \left[\frac{\partial E}{\partial w_1}, \frac{\partial E}{\partial w_2}, ... \frac{\partial E}{\partial w_n} \right] \tag{4.2}$$

The Newton's method takes into account the descent of the error gradient i.e

$$\frac{\partial G}{\partial w_j} = \left[\frac{\partial^2 E}{\partial w_i \partial w_j} \right] \tag{4.3}$$

And in the process defines a Hessian matrix H where

$$h_{i,j} = \frac{\partial^2 E}{\partial w_i \partial w_j} \tag{4.4}$$

From these equations, the modifications to be made in weights can be found to be $\Delta w = -H^{-1}G$ i.e

$$w_{m+1} = w_m - (H^{-1})_m G_m \tag{4.5}$$

m - count of the iteration.

But the Hessian matrix involves calculating double differentials which to calculate each time is computationally expensive. Hence the Gauss-Newton method defines a jacobian matrix J

$$J_{i,j} = \frac{\partial e_{L,O}}{\partial w_n} \tag{4.6}$$

Such that

$$G = Je$$

$$H = J^T J \tag{4.7}$$

Substituting (4.7) in (4.5)

$$w_{m+1} = w_m - (J^T J)^{-1}{}_m (Je)_m \tag{4.8}$$

The Hessian matrix sometimes may not be invertible and will create problems during calculations. The trick to evade this problem is to try to make all the diagonal elements of H larger than zero. Hence, the Levenberg-Marquardt method states an approximation that

$$H = J^T J + \lambda I \tag{4.9}$$

λ is always positive and is called combination coefficient

I is the identity matrix

This approximation changes (4.8) as follows

$$w_{m+1} = w_m - (J^T J + \lambda I)^{-1}{}_m (Je)_m \tag{4.10}$$

This equation can be efficiently used to modify weights in each iteration and stop the process when the error gradient reaches its minimum. One disadvantage of the backward propagation algorithm is that it might stop at the local gradient minima and would not wait for the global minima to be achieved which will affect the accuracy of the output drastically. Hence this algorithm can be used appropriately in small or moderately hard problems where the error functions are not changing extremely.

Neuron independence is carried out to fix the number of neurons while training the network for the forward model. Number of neurons in the hidden layer is fixed based on the performance of certain characteristics given below (Balaji and Padhi 2010).

Mean Relative Error:

$$MRE = \frac{1}{N}\sum_{i=1}^{N} \frac{|T_{actual,i} - T_{network,i}|}{T_{actual,i}} \tag{4.11}$$

Correlation Coefficient:

$$R^2 = 1 - \frac{\sum_{i=1}^{N}(T_{actual,i} - T_{network,i})^2}{\sum_{i=1}^{N}(T_{actual,i})^2} \tag{4.12}$$

4.4 Closure

This chapter provided the details of the forward model used in the present work. The parameters used in CFD simulation and the algorithm used in training the artificial neural network were discussed. The next chapter provides an insight to the inverse model used.

CHAPTER 5

INVERSE MODEL

5.1 INTRODUCTION

This chapter provides an insight to the inverse model used in the present work. The word inverse highlights the fact of estimating the cause for the observed effect. The observed effect is the measured temperature. The objective of any inverse method is to minimise the error between measured and simulated temperatures. Genetic Algorithm (GA), Artificial Neural Network (ANN) and Bayesian Inference are used as inverse methods.

5.2 GENETIC ALGORITHM (GA)

Genetic Algorithm (GA) is a search method which is basically devised to model adaptation process and is based on natural selection. The basic principles of GA was first introduced by Holland in the year 1960, which is well explained in nature, individuals in a population compete with each other for resources such as food, water and shelter. It was later developed by Goldberg in 1989 (Goldberg 2006). It works on the principle of evolution of species where in the best individual in the species survives and will be predominant, hence becoming a successor in continuing its generation. GA is a kind of evolutionary algorithm, a search technique which models the natural selection and survival of the fittest in the biological world. These algorithms are search techniques which search from a 'population' of solutions. Every individual in the population represents a potential solution to the problem and is implemented as a data structure. Each solution is evaluated to give some measure of fitness. Then the individuals with more fit values are selected to form a new population. New solutions are formed from the population by undergoing some transformations. The transformation in the population is carried out by genetic operators. Creating a new offspring by making a small change in a single individual is termed as unary transformation. When changes are made in more than one individual higher order transformation is accomplished creating new individual. After some number of generations the algorithm converges and it is expected that the best individual represents a near optimum solution.

The concept of survival of fittest can effectively be used in solving various engineering problems. To solve such problems, defining an objective function as shown in Equation (5.1) is very much necessary, which can be either maximizing or minimizing.

$$S(P) = \sum_{m=1}^{M} \sum_{n=1}^{N} [\boldsymbol{Y}_{im} - \boldsymbol{T}_{im}(\boldsymbol{P})]^2 \quad (5.1)$$

where $\boldsymbol{P}$ is the estimated parameter in vector form. $\boldsymbol{Y_{im}}$ is the i^{th} observation from the m^{th} measurement; M and N are the number of measurements and observations, respectively. $\boldsymbol{T_{im}(P)}$ is the simulated temperature obtained from the forward model of the problem considered. Based on Equation (5.1) the unknown parameter is estimated by minimizing the sum of the squared difference between the simulated and the measured temperatures.

The basic steps of GA are population initialization, evaluation of the fitness function, selection, crossover, mutation and generation of off springs. Population initialization is the creation of set of individuals which are called chromosomes. Each chromosome is made of genes. The fitness function values are evaluated for each chromosome and the ranking of the chromosomes is carried out based on the fitness values. The chromosome with the best fitness value will be retained for the next generations and worst chromosome is rejected. The selected set of chromosomes will be allowed to produce a new offsprings by the process called crossover where the chromosomes are randomly swapped at random cross over sites to generate new offsprings. Even two point or multipoint crossover can be used. This new set of chromosomes has a great tendency to produce good performance in retrieving the solution. Mutation process is the modification in the genes, where few genes of particular chromosome which has a capability to enhance the liability to vary the population. Figure 5.1 shows the crossover site and mutation. From the new population, every location of bit in the chromosome will go through random change in with identical probability. Thus the new born population is used to find the fitness function and the process is continued until the stopping criterion is reached. Figure 5.2 shows the flowchart for the execution of genetic algorithm.

Steps used in Genetic Algorithm

Every genetic algorithm incorporates the following basic steps:

i. A population of possible solutions is initialized randomly.
ii. The fitness of each solution is determined according to an appropriate fitness function.
iii. Pairs of the population are selected to be parents of the new generation. This selection of parents is based on the most-fit members of the current population.
iv. The selected parent pairs combine to form children, which constitute the new population.
v. Variation is introduced into the new population through mutation, crossover, and creep.
vi. Steps (ii)-(v) are repeated until the program ends according to user-specified criterion.

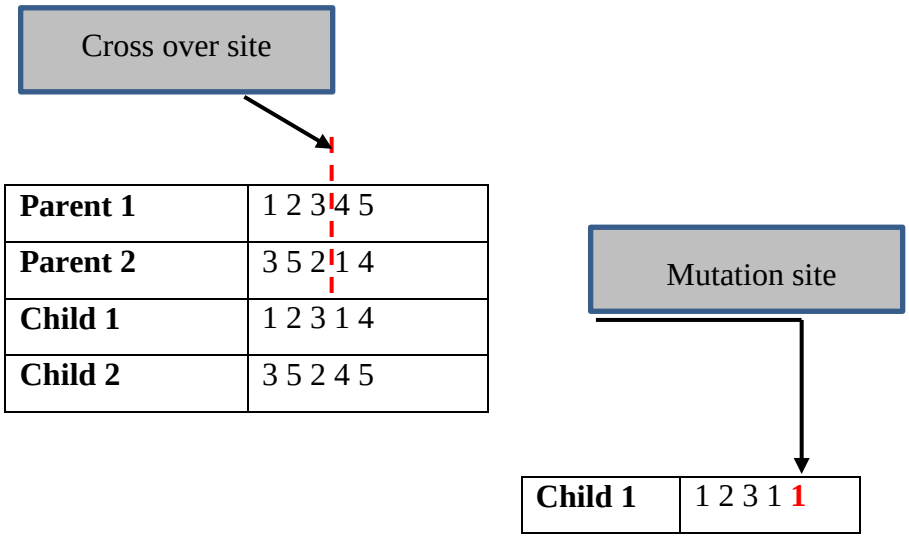

Figure 5.1 Crossover and Mutation

5.2.1 Levenberg Marquardt Method (LM- method)

Levenberg Marquardt method is an iterative method used for solving nonlinear least square problem of parameter estimation. It was first derived by Levenberg in the year 1944 and later modified by Marquardt in 1963. Estimation of the parameter using LM

method requires proper selection of the initial guess. With poor selection of the initial guess the chances of getting trapped in the local minima is more likely to occur. In this work the output from the GA is provided as the initial guess to LM algorithm.

The LM algorithm is as follows. It is based on minimization of the ordinary least squares norm which is given as:

$$S(P) = \sum_{i=1}^{I}[Y_i - T_i(P)]^2 \tag{5.2}$$

Where, S = sum of squares error or objective function

P^T = $[P_1, P_2, \ldots P_N]$, vector of unknown parameters

$T_i(P) =$ estimated temperature,

Y_i = measured temperature,

N = number of unknown parameters

I = number of measurements, where $I \geq N$

Step 1: The forward problem is solved using P^k as the initial guess to obtain temperature vector. (set k=0 for initial guess and μ^0=0.001)

Step 2: Compute $S(P^k)$ from Equation (6.20)

Step 3: Compute the sensitivity matrix J^k and Ω^k using the current value of P^k, where J^k is given as $J(P) = \left[\frac{\partial T^T(P)}{\partial P}\right]^T$ and $\Omega^k = diag[(J^k)^T J^k]$

Step 4: Calculate the new set of estimate P^{k+1},

$$P^{k+1}=P^k+[(J^k)^T J^k + J^k\Omega^k]^{-1}\,(J^k)^T\,[Y - T(P^k)] \tag{5.3}$$

Step 5: Solve the direct problem for the new estimate P^{k+1} to obtain $T(P^{k+1})$.

Step 6: Compute $S(P^{k+1})$

Step 7: If $S(P^{k+1}) \geq S(P^k)$, replace μ^k by $10\mu^k$ and return to step 4.

Step 8: If $S(P^{k+1}) < S(P^k)$, accept the new estimate P^{k+1} and replace μ^k by $0.1\mu^k$

Step 9: Check the stopping criteria. If the criteria is satisfied, then stop the iterative procedure otherwise replace *k* by *k+1* and move to step 3. The stopping criteria is given as $S(P^{k+1}) < \epsilon_1$.

5.3 ARTIFICIAL NEURAL NETWORK (ANN)

The ability of ANN to learn from examples, manage large number of variables and respond to changes in the information makes it a versatile technique. A non-iterative technique like ANN with this potential quality is also used as Inverse technique in

estimation process. In the preceding chapter ANN as forward model has already been explained. The structure of the neural network remains the same when used for inverse process. While using ANN as the inverse model the input considered is the temperature and the output will be heat flux or any other parameter of interest.

.

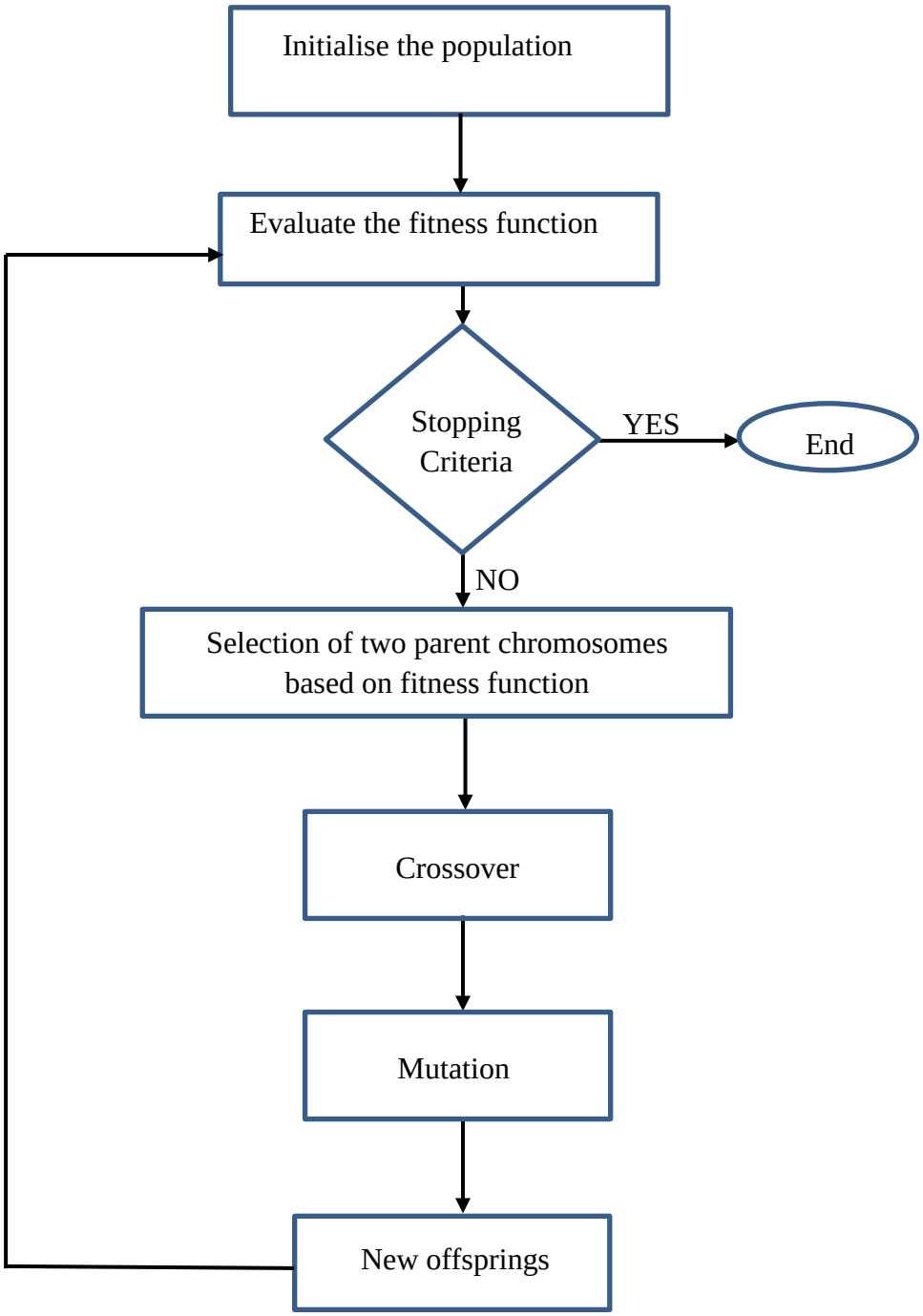

Figure 5.2 Flowchart for Genetic Algorithm

5.4 BAYESIAN INFERENCE

Gaining statistical knowledge about the unknown variables when the model and the measured data are available require certain attractive techniques such as the Bayesian Inference. The name Bayesian inference comes from the frequent use of Baye's theorem in the inference process. The primary objective of the Bayesian estimation is to deduce the probability distribution of the unknown parameters based on the available data. It is used to relate the experimental measurement $\boldsymbol{Y}$ and the unknown parameter $\boldsymbol{P}$ for the continuous random variables and is given as follows:

$$\pi(\boldsymbol{P}/\boldsymbol{Y}) = \frac{\pi(\boldsymbol{Y}/\boldsymbol{P}) \times \pi(\boldsymbol{P})}{\pi(\boldsymbol{Y})} \tag{5.4}$$

Where $\pi(\boldsymbol{P}/\boldsymbol{Y})$ is the posterior probability density function (PPDF) that the variable $\boldsymbol{P}$ caused the measurement $\boldsymbol{Y}$, $\pi(\boldsymbol{Y}/\boldsymbol{P})$ is the likelihood function, $\pi(\boldsymbol{P})$ is the prior knowledge about the parameter $\boldsymbol{P}$ and can be incorporated in the analysis in the form of a distribution within the Bayesian framework, $\pi(\boldsymbol{Y})$ is the normalizing constant.

The likelihood function is arrived at by computing the temperature for the assumed values of the parameter $\boldsymbol{P}$ based on the forward/mathematical model and then calculating the probability based on the simulated and experimental temperatures. This is then represented as likelihood probability density function. Assuming the temperature data to be additive, uncorrelated, Gaussian, with zero mean and constant standard deviation, the likelihood can be written as (Orlande et al. 2008),

$$\pi(\boldsymbol{Y}/\boldsymbol{P}) = \frac{1}{(2\pi\sigma^2)^{\frac{n}{2}}} exp\left[-\frac{(\boldsymbol{Y}-\boldsymbol{T}(\boldsymbol{P}))^T\,(\boldsymbol{Y}-\boldsymbol{T}(\boldsymbol{P}))}{2\sigma^2}\right] \tag{5.5}$$

Where $T(\boldsymbol{P})$ is the calculated temperature for the given value of parameter **P**, $n = N \times M$ is the total number of temperature measurements, σ is the standard deviation.

The prior $\pi(\boldsymbol{P})$ is assumed to be normal distribution with mean μ_P and standard deviation σ_p, and is expressed as :

$$\pi(\boldsymbol{P}) = \frac{1}{\left(2\pi\sigma_p^2\right)^{0.5}} exp\left[-\frac{\left(\boldsymbol{P}-\mu_p\right)^2}{2\sigma_p^2}\right] \tag{5.6}$$

The prior density function $\pi(\boldsymbol{P})$ typically follows a uniform or normal distribution. In case of a uniform prior, $\pi(\boldsymbol{P})$ is same for all values of $\boldsymbol{P}$**.** Equation (5.6) is used when normal prior is incorporated. Use of normal prior would result in sharper PPDF and also low values of standard deviation. PPDF as shown in Equation (5.4) is the product of likelihood function and the prior function and is given as:

$$\pi(\boldsymbol{P}/\boldsymbol{Y}) = \frac{1}{(2\pi\sigma^2)^{\frac{n}{2}}} exp\left[-\frac{(\boldsymbol{Y}-\boldsymbol{T}(\boldsymbol{P}))^T(\boldsymbol{Y}-T(\boldsymbol{P}))}{2\sigma^2}\right] \times \frac{1}{\left(2\pi\sigma_p^2\right)^{0.5}} exp\left[-\frac{\left(\boldsymbol{P}-\mu_p\right)^2}{2\sigma_p^2}\right] \quad (5.7)$$

When uniform prior is used in the estimation, then PPDF will be decided by the likelihood function alone and is given by:

$$\pi(\boldsymbol{P}/\boldsymbol{Y}) \propto \frac{1}{(2\pi\sigma^2)^{\frac{n}{2}}} exp\left[-\frac{(\boldsymbol{Y}-\boldsymbol{T}(\boldsymbol{P}))^T(\boldsymbol{Y}-T(\boldsymbol{P}))}{2\sigma^2}\right] \quad (5.8)$$

In order to calculate the unknown estimates based on Equation (5.4), numerical integration must be performed. If analytical treatment of the posterior probability function is not possible, one can use Markov chain Monte Carlo methods to draw samples from a distribution.

MCMC is the most widely adopted numerical method used for exploring the posterior state space. Samples are to be generated and an efficient sampling algorithm is required for the successful implementation of the Bayesian method. Solution procedure of the Bayesian framework can be split up into three steps (Diego et al. 2012). In the first step prior probability density function can be evaluated with the available information about the parameter $\boldsymbol{P}$. In the second step the forward model or the likelihood function $\pi(\boldsymbol{Y}/\boldsymbol{P})$ can be calculated for the given value of $\boldsymbol{P}$. And the third step includes developing models to explore the posterior probability density $\pi(\boldsymbol{P}/\boldsymbol{Y})$. Hence numerical techniques like MCMC are used to perform the third step. MCMC is used to obtain samples that accurately represent the posterior probability density. Metropolis-Hastings algorithm is the most commonly used MCMC sampling

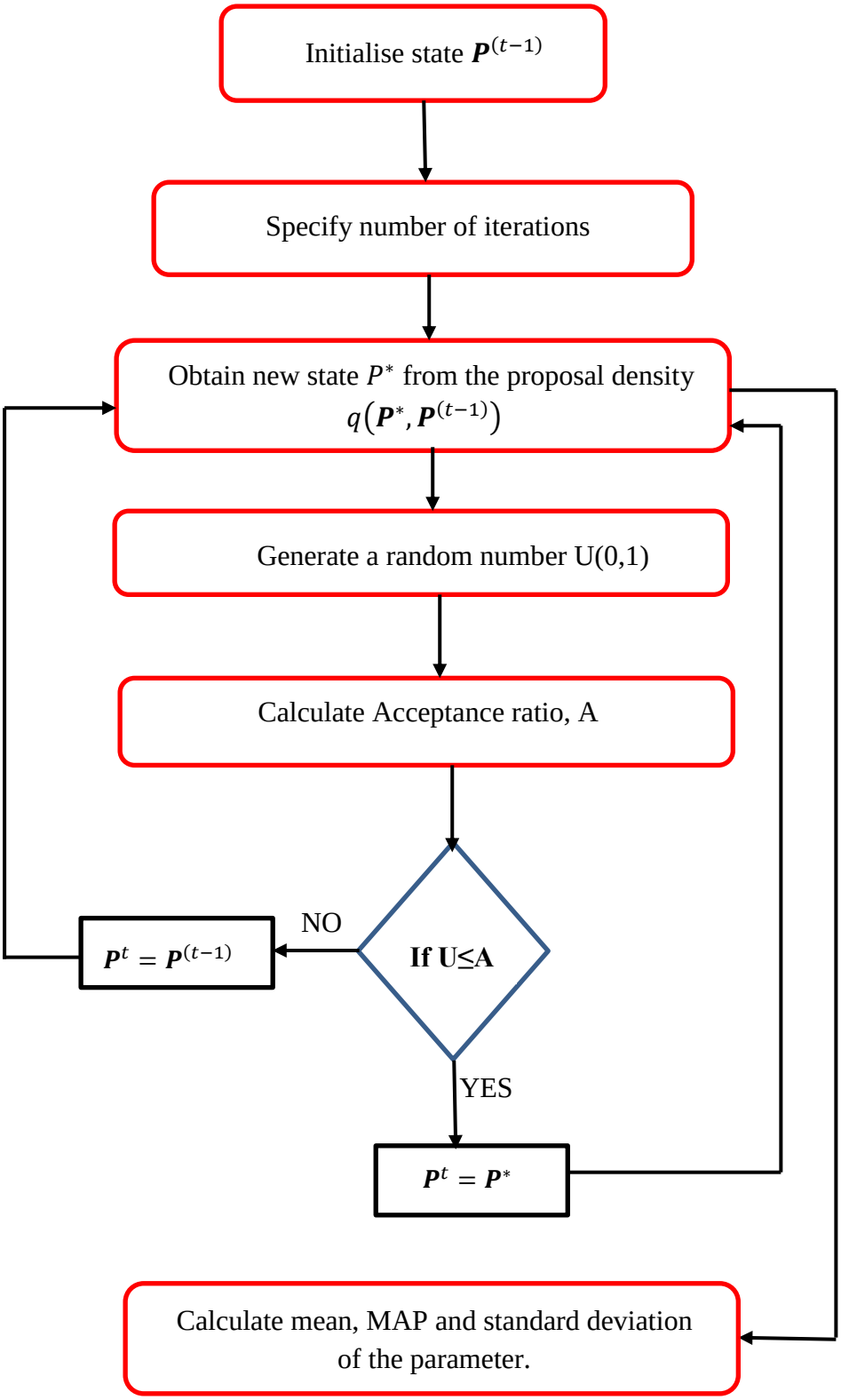

Figure 5.3 Flow chart for MH algorithm

algorithm. Since the posterior state space has high dimension and it is required to obtain the marginal distributions of individual parameters. MCMC is one such

algorithm used to accomplish this task. A class of algorithms used generally for computational inference is called Markov Chain Monte Carlo methods. The process followed in MH algorithm is showed in the form of flow chart in Figure 5.3.

The steps involved in MCMC-MH algorithm for single parameter estimation can be summarised as (Orlande et al. 2008),

i. Sample a candidate P^* from the distribution $q\left(\boldsymbol{P}^*, \boldsymbol{P}^{(t-1)}\right)$.

ii. Generate a random number U uniformly distributed on (0,1).

iii. Calculate the acceptance ratio, $A\left(\boldsymbol{P}^*, \boldsymbol{P}^{(t-1)}\right) = min\left[1, \frac{\pi(\boldsymbol{P}^*/\boldsymbol{Y})q\left(\boldsymbol{P}^{(t-1)}, \boldsymbol{P}^*\right)}{\pi\left(\boldsymbol{P}^{(t-1)}/\boldsymbol{Y}\right)q\left(\boldsymbol{P}^*, \boldsymbol{P}^{(t-1)}\right)}\right]$

iv. If U$\leq$ A, then $\boldsymbol{P}^t = \boldsymbol{P}^*$; otherwise $\boldsymbol{P}^t = \boldsymbol{P}^{(t-1)}$.

v. Return to step 1 so that the sequence $\{\boldsymbol{P}^1, \boldsymbol{P}^2, \ldots\ldots \boldsymbol{P}^n\}$ can be generated.

Hence stochastic iterative techniques like GA, non-iterative technique ANN and Bayesian Inference are successfully used as inverse techniques in the estimation process.

5.5 Closure

This chapter discussed about the methods used as inverse approach in the present work. The methods are explained with the help of flow chart. Further chapter deals with the application of these inverse techniques for the estimation purpose.

CHAPTER 6

ESTIMATION OF HEAT FLUX USING COMBINED ANN-GA AND EXPERIMENTAL BASED TECHNIQUE FOR A CONJUGATE HEAT TRANSFER PROBLEM

6.1 INTRODUCTION

This chapter deals with the estimation of heat flux at the boundary for the vertical fin on a horizontal base. A two dimensional numerical fin model is created for the analysis of temperature distribution for the known heat flux at the base. Navier Stokes equation is solved by incorporating Boussinesq approximation. Using the 2D simulation data, a neural network is developed as the forward model. The conjugate heat transfer NN model is now coupled with Genetic algorithm (GA) for the solution of the inverse problem. Initially, GA is applied to the pure simulated data, the results are then used as input to the Levenberg-Marquardt (LM) method and such hybridization is proven to result in accurate estimation of the unknown heat flux. The hybrid method is then applied for the experimental temperature to estimate the unknown heat flux.

6.2 FORWARD MODEL

The forward problem proposed is a 2D conjugate heat transfer from fin. The numerical model consists of a mild steel fin of dimension 250x150x6mm^3, which is placed vertically on an aluminum base of dimension 250x150x8mm^3. A known heat flux is specified at the base beneath the aluminum plate. The computational domain is simplified to a two dimensional model because of its symmetry. An extended domain is created for the air to flow on to the fin during natural convection. The flow is assumed as incompressible and laminar with constant fluid properties. But the density change with temperature in the buoyancy term is taken into account for the analysis. Simulation is carried out for different values of heat flux as input and the temperature data is recorded. Figure 6.1 shows the computational model used for the present study.

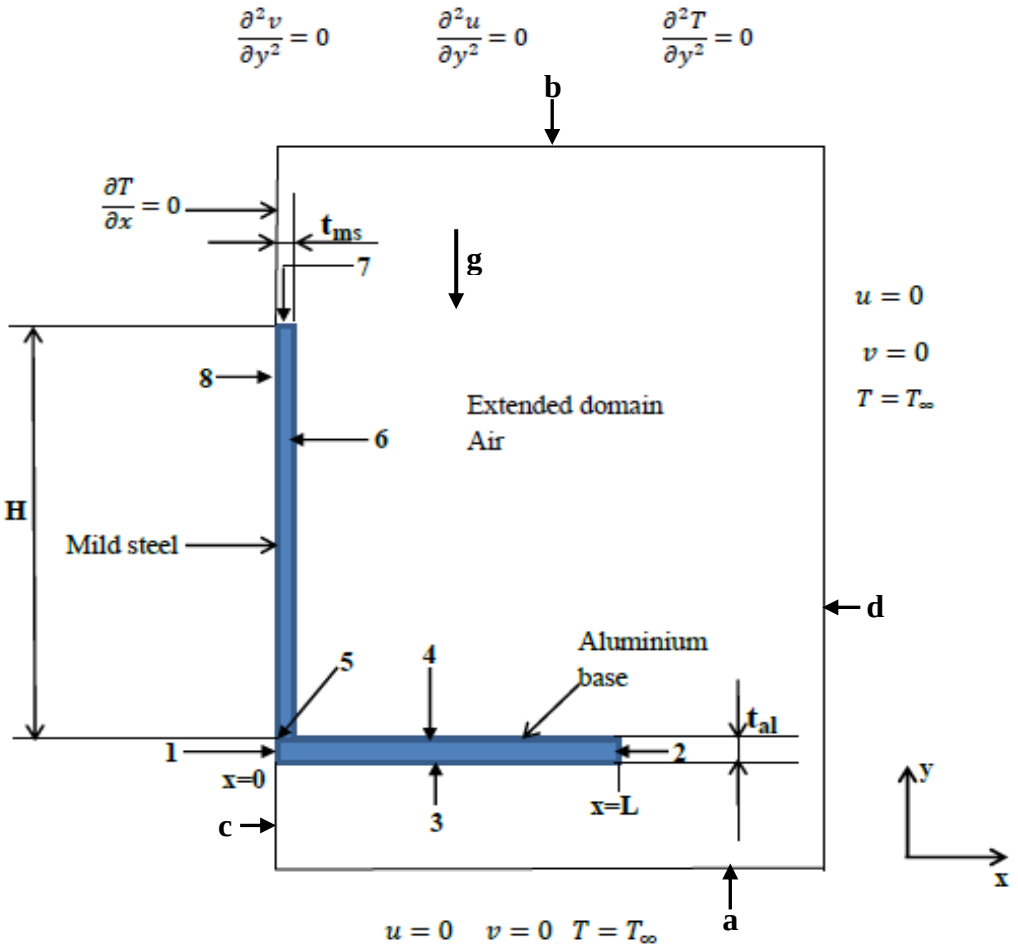

Figure 6.1 2D computational domain

The steady state two-dimensional equation of continuity, momentum and energy is:

Continuity:

$$\frac{\partial u}{\partial x} + \frac{\partial v}{\partial y} = 0 \tag{6.1}$$

X-momentum equation:

$$\rho\left(u\frac{\partial u}{\partial x} + v\frac{\partial u}{\partial y}\right) = -\frac{\partial p}{\partial x} + \mu\left(\frac{\partial^2 u}{\partial x^2} + \frac{\partial^2 u}{\partial y^2}\right) \tag{6.2}$$

Y-momentum equation:

$$\rho\left(u\frac{\partial v}{\partial x}+v\frac{\partial v}{\partial y}\right)=-\frac{\partial p}{\partial y}+\mu\left(\frac{\partial^2 v}{\partial x^2}+\frac{\partial^2 v}{\partial y^2}\right)+\rho g\beta(T-T_\infty) \quad (6.3)$$

Energy equation for fluid:

$$\rho c_p\left(u\frac{\partial T}{\partial x}+v\frac{\partial T}{\partial y}\right)=k_f\left(\frac{\partial^2 T}{\partial x^2}+\frac{\partial^2 T}{\partial y^2}\right) \quad (6.4)$$

where ρ is the density (kg/m^3), k_f is thermal conductivity of fluid (W/mK), c_p is the specific heat (J/kgK), g is the gravity constant (m/s^2), $\beta=\frac{1}{T}$ (K^{-1}), μ is dynamic viscosity (Ns/m^2).

Along the solid walls no slip condition is applied and the flow velocities on these walls are set to zero. The base of the aluminium plate is subjected to constant heat flux thermal boundary condition. The sides of the base are subjected to adiabatic conditions. Details of these conditions are given below after presenting the governing equation for the aluminium base and the mild steel fin. The inlet and outlet boundary conditions, also other applied boundary conditions are as follows.

Velocity and temperature at the inlet at 'a',

$$u=0\ ,\ v=0,\ T=T_\infty \quad (6.5)$$

Outlet boundary conditions at 'b',

$$\frac{\partial^2 v}{\partial y^2}=0,\ \frac{\partial^2 u}{\partial y^2}=0,\ \frac{\partial^2 T}{\partial y^2}=0 \quad (6.6)$$

The left side of the computational extended domain i.e 'c' exhibits symmetry boundary condition and is represented as,

$$\frac{\partial T}{\partial x}=0 \quad (6.7)$$

The right side of the computational extended domain i.e 'd' exhibits the following boundary conditions,

$$\frac{\partial u}{\partial x}=0,\ \frac{\partial T}{\partial x}=0,\ u=0 \quad (6.8)$$

Aluminum base:

$$k_{al}\left(\frac{\partial^2 T}{\partial x^2}+\frac{\partial^2 T}{\partial y^2}\right)=0 \quad (6.9)$$

At regions 1 and 2, i.e. x =0 and x=L

$$\frac{\partial T}{\partial x} = 0 \tag{6.10}$$

At region 3, i.e. at y=0

$$-k_{al}\frac{\partial T}{\partial y} = q_0 \tag{6.11}$$

where q_0 is the heat flux (W/m^2), k_{al} is the thermal conductivity of the aluminium base plate (W/mK).

At region 4, i.e. at y =t_{al} and $t_{ms} \leq x \leq L\text{-}t_{ms}$

$$k_{al}\frac{\partial T}{\partial n} = k_f\frac{\partial T}{\partial n} \qquad \text{and} \qquad T_{aluminum} = T_{fluid} \tag{6.12}$$

where k_f is thermal conductivity of fluid (W/mK) and t_{al} is thickness of the aluminium base plate, t_{ms} is thickness of mild steel fin.

Mild steel fin:

$$k_{ms}\left(\frac{\partial^2 T}{\partial x^2} + \frac{\partial^2 T}{\partial y^2}\right) = 0 \tag{6.13}$$

At region 8 i.e x=0

$$\frac{\partial T}{\partial x} = 0 \tag{6.14}$$

At region 6 i.e. x=t_{ms} and $t_{al} \leq y \leq H$

$$k_{ms}\frac{\partial T}{\partial n} = k_f\frac{\partial T}{\partial n} \qquad \text{and} \quad T_{mildsteel} = T_{fluid} \tag{6.15}$$

where k_{ms} is the thermal conductivity of the mild steel fin (W/mK)

Region 5 which is at y = t_{al} and $0 \leq x \leq t_{ms}$. It is the intersection between aluminum base and mild steel fin,

$$q_{cond,aluminum} = q_{cond,mild\ steel\ fin} \tag{6.16}$$

$$k_{al}\frac{\partial T}{\partial n} = k_{ms}\frac{\partial T}{\partial n} \quad \text{and} \quad T_{aluminum} = T_{mildsteel} \tag{6.17}$$

At region 7 i.e. y=H and $0 \leq x \leq t_{ms}$

$$k_{ms}\frac{\partial T}{\partial n} = k_f\frac{\partial T}{\partial n} \quad \text{and} \quad T_{mildsteel} = T_{fluid} \tag{6.18}$$

6.3 EXPERIMENTAL SETUP

The experimental setup was elaborately discussed in Chapter 3. Experiments are performed in a careful and closed environment in order to prevent the effect of external disturbances. The fin is heated from the ambient temperature to the steady state temperature for a time duration of 4 to 5 hours and the steady state temperature is confirmed when the temperature difference is found to be ±0.1°C for a time interval of 10 mins. Upon reaching the steady state temperature, the power supply is turned off and the fin is allowed to cool. The temperature distribution thus obtained contains the information about heating, steady state and cooling zones. The total duration of the experiment will be approximately 6 hours. Figure 6.2 shows the temperature recorded by a thermocouple located along the height of the fin. Three zones namely heating, steady and cooling can be seen in the plot obtained during experimentation. The estimation methodology of the present work is shown in terms of flow chart in Figure 6.3.

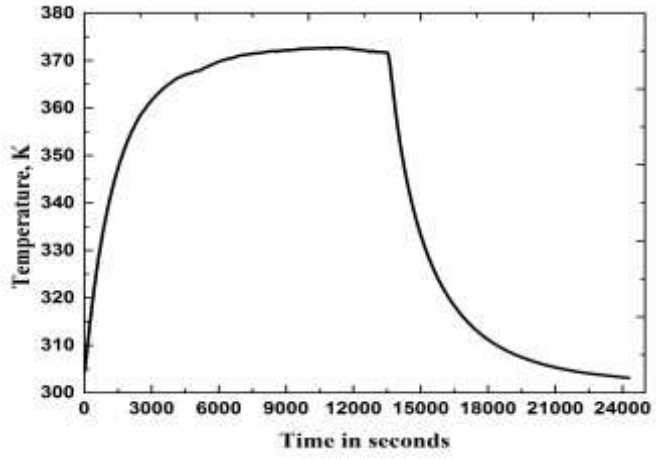

Figure 6.2 Typical experimental plot for heat input of 2133W/m^2

6.3.1 Uncertainty Analysis

The uncertainties involved in the measurements of various quantities for the DC power supply is shown in Table 6.1.

Table 6.1 Uncertainty involved in the devices used in the present study

Instrument	**Uncertainity**
DC power source	±0.2%
Digital multimeter	±1.6%

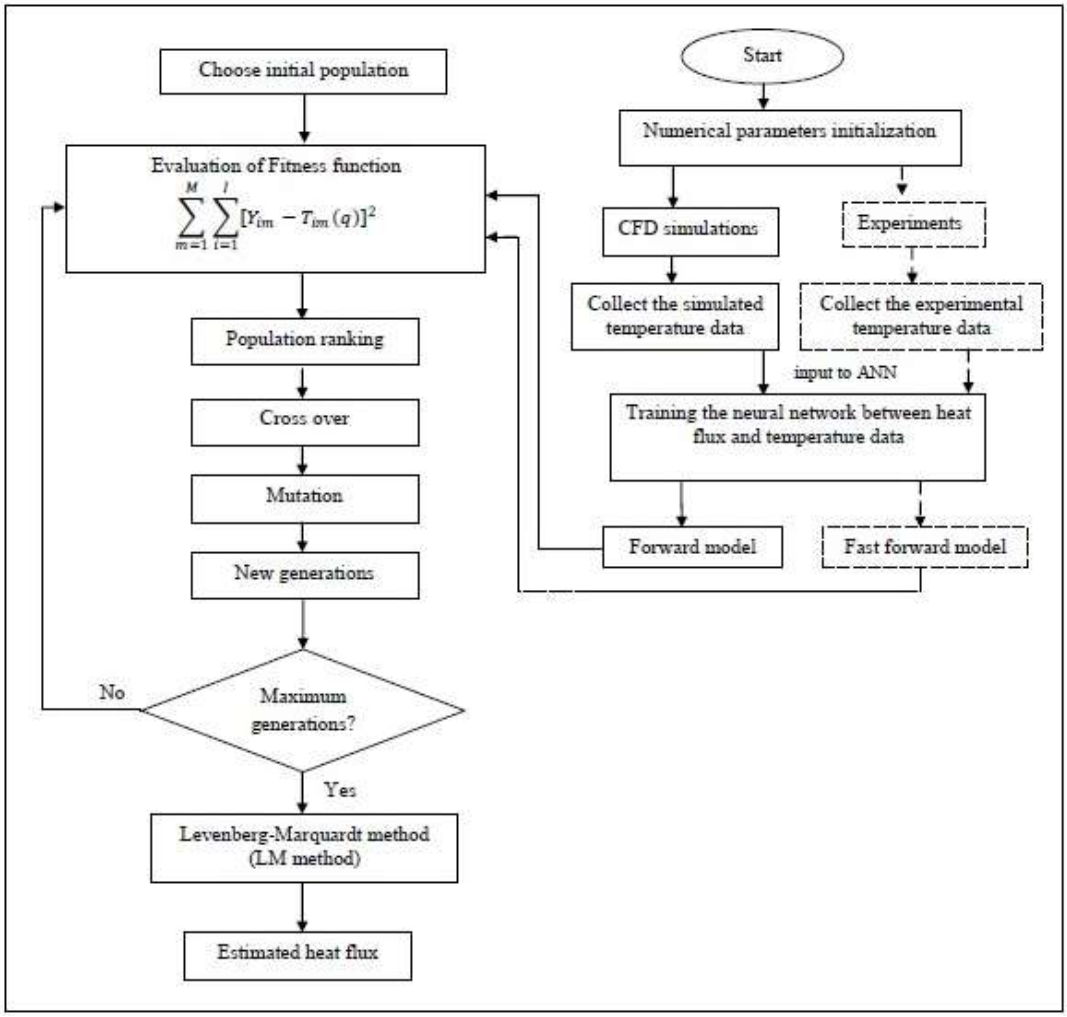

Figure 6.3 Flowchart of the estimation methodology

P = VxI, W

$$\pm\sqrt{\left(\frac{\partial P}{\partial V}\sigma_V\right)^2 + \left(\frac{\partial P}{\partial I}\sigma_I\right)^2} \tag{6.19}$$

$$\pm\sqrt{((0.91)(0.002))^2 + ((60)(0.016))^2}$$

± 0.921W or 1.6%

6.4 ANN AS FORWARD MODEL

In solving the inverse conjugate natural convection heat transfer problem, the estimation of unknown heat flux can be accomplished with the help of known temperature distribution from the fin. The use of ANN as forward model reduces the

complexity of the computational process. The following steps are considered to develop a relation between the heat flux and temperature distribution.

1. Training the network: The training sets include heat flux and temperature vectors by solving the forward model. While training the network, the range of heat flux is important in order to match the target temperature.
2. Network building: The proper selection of network depends on the size of the input and output vectors. There are number of algorithms to develop a proper training process and the number of hidden neurons used is also a function of the algorithm selected.
3. Network training: During training, the network tries to understand the facts between input and output. Training can be accomplished with the help of learning algorithms and training the network is continued till the error is reasonably small.
4. Network testing: With the trained network, the input which is not contained during the training process is chosen to test the neural network. If the error is more, the training process is again executed till the testing part is satisfied.

The above procedure is used to construct network between heat flux and simulated temperatures. A neuron independence study is carried out and is shown in Table 6.2. A comparison between the simulation temperature and the temperature obtained from the network is shown in Table 6.3 and Table 6.4 shows the comparison between experimental temperature and the neural network output. The deviation between the temperatures obtained from simulation and ANN also between experimental temperature and ANN is shown in Figure 6.4 and Figure 6.5 respectively

Table 6.2 Neuron Independence study

Sl.no	Neurons	MRE	R^2
1	6	0.006107889	0.999998511
2	**8**	**0.003859184**	**0.999999476**
3	10	0.003875978	0.99999797

Table 6.3 Comparison between simulated and ANN temperature.

Position of thermocouple from base,m	1800W/m^2		2300W/m^2		2700W/m^2	
	T_{sim}, K	T_{ANN}, K	T_{sim}, K	T_{ANN}, K	$T_{sim,}$ K	T_{ANN}, K
0.006	445.12	444.61	472.30	472.67	497.38	497.93
0.045	428.60	427.86	451.70	450.45	473.21	472.50
0.084	414.62	413.04	435.01	432.11	453.28	451.52
0.110	408.41	406.66	427.42	424.53	444.66	442.82
0.148	403.86	402.08	421.88	419.31	438.39	436.60

Table 6.4 Comparison between experimental and ANN temperature.

Position of thermocouple from base,m	533W/m^2		1200W/m^2		1624W/m^2	
	T_{Exp}, K	T_{ANN}, K	T_{Exp}, K	T_{ANN}, K	$T_{Exp,}$ K	T_{ANN}, K
0.006	323.86	324.07	344.68	345.02	355.37	357.78
0.045	320.36	320.43	337.45	338.50	344.42	346.03
0.084	318.20	318.27	333.04	333.21	338.33	339.40
0.110	317.34	317.42	331.21	331.76	335.59	334.58
0.148	316.89	316.99	330.20	330.40	334.18	332.55

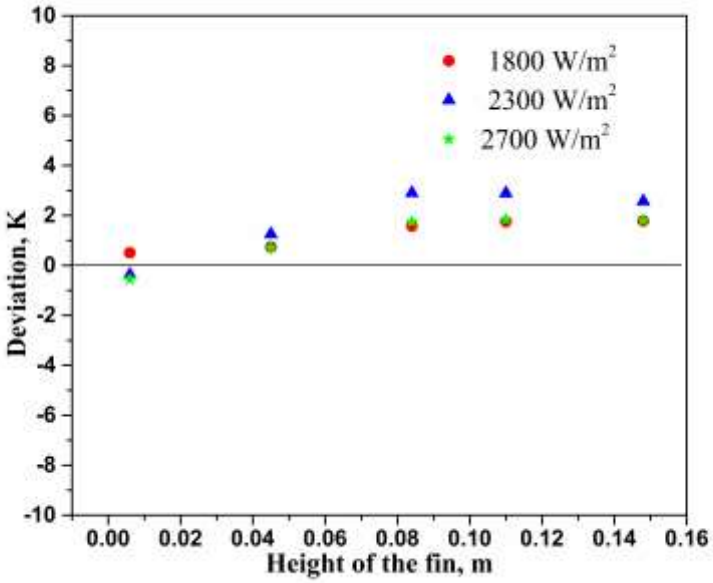

Figure 6.4 Error plot for the simulation temperature and ANN temperature

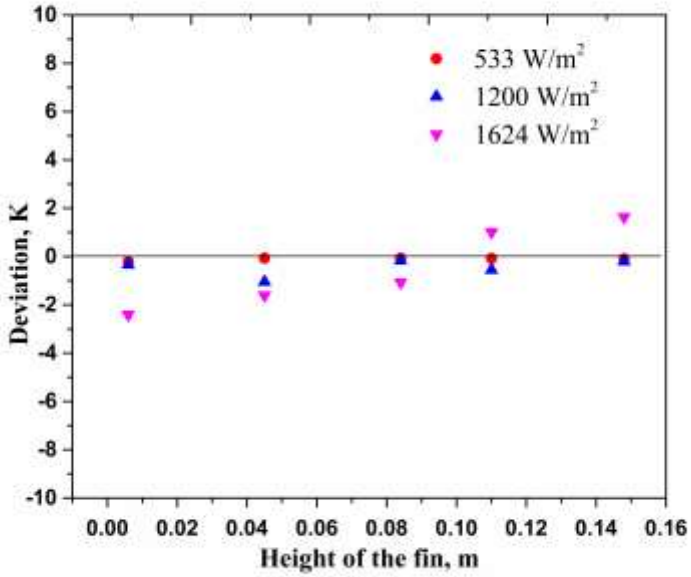

Figure 6.5 Error plot for the measured temperature and ANN temperature

6.5 GA AS INVERSE METHOD

The detailed discussion on GA has been provided in Chapter 5. The objective of GA is given in Equation (5.8). Simulated temperatures are obtained by executing the ANN model for an assumed or known heat flux input. Now in GA, the desired accuracy level and the range of the unknown parameter must be selected to represent them in the form of binary string. For the present case, the lower range and upper range of heat flux is 266 and 3700 W/m^2, respectively. The whole process in GA is represented in binary form so the maximum number of binary required is chosen as 3700 W/m^2, which is the upper range of the unknown heat flux. The binary for the upper and lower cases is specified in Table 6.5.

Table 6.5 Binary representation of string

Heat flux, W/m^2	Binary representation
266	000100001010
3700	111001110100

In the process of GA, the cost function is evaluated for all populations and corresponding decimal is obtained. Then, the cost function is calculated for the decimals obtained and sorting of those values is done according to the objective function, minimum or maximum. If the problem under consideration is minimization, the value corresponding to the minimum cost function is rated top because this is the best individual or fitness among the population. It is pertinent to mention here that the simulated temperatures in the objective function are obtained from ANN, which is considered to be the forward model of the problem. Once the cost function is evaluated for the population and sorted according to the requirement, the next phase is to choose parents among the population for the process of crossover. The best individual has the privilege to produce children by the process of crossover among the population i.e., the operation involves exchanging the substrings of the chromosomes in the population. Most of the time, the chromosomes, which is rated least will be discarded as it is of no use for the fitness function or objective function. Moreover, the selection of population can be random and it is not necessary to retain entire population for crossover process. As mentioned earlier, one can vary the number of population and the effect on the objective function can also be studied. The concept of mutation is applied in this work. Such operation takes each chromosome from the mating pool and changes the chromosomes randomly i.e., the bit is replaced from 0 to 1, or vice versa. Generally, the mutation rate varies from 0.01 to 0.2 and it plays only a minor role in the whole process. Subsequently, the problem of trapping in local minima can be avoided and the procedure takes care of attaining global minima. The concept of elitism plays important role in the convergence process. Elitism is the process of retaining the best individual from the initial iteration to the end for faster convergence. For the subsequent iterations, the average fitness function or the average objective function reduces which is the sign of attaining global minima.

6.6 RESULTS AND DISCUSSION

6.6.1 Estimation of heat flux from simulated data

The numerical model is subjected to the boundary condition and on solving Equation (6.1) – (6.18) temperature distribution is obtained as the output for different values of heat flux as input. The temperature data is now given as input to the inverse approach.

As explained in earlier section 6.5, the number of chromosomes and genes are fixed as 8 and in-house GA code has been developed with commercial software. Figure 6.5 shows the mean, maximum and minimum fitness functions for a heat flux of 1800 W/m^2.It is clearly seen in Figure 6.6 that the best chromosome is stable compared to

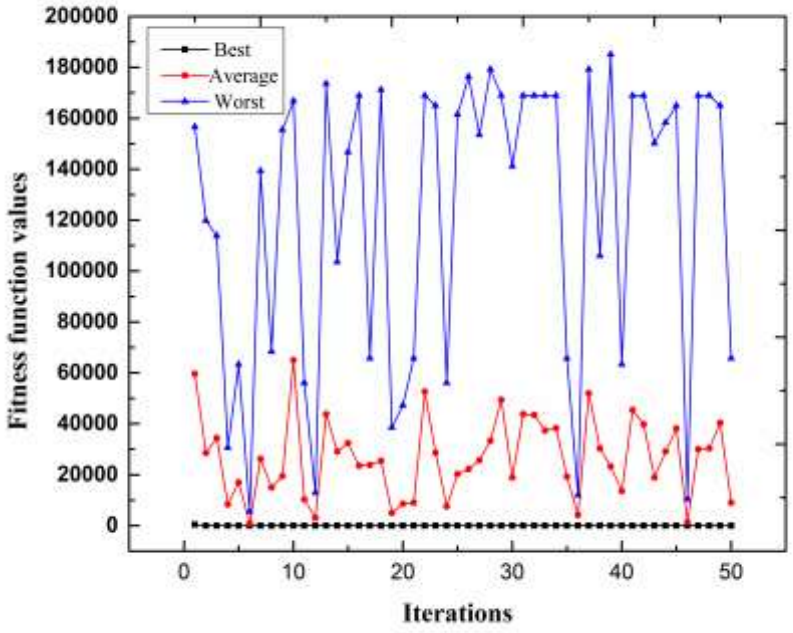

Figure 6.6 Best, average and worst fitness function values in the population for each iteration for heat flux of 1800W/m^2 with chromosomes=8 and genes=8

worst and average chromosomes. The best and worst refers to the minimum and maximum of the fitness function respectively. The number of iteration was limited to 50. The convergence based on the best chromosome for a heat flux of 1800 W/m^2 is plotted in Figure 6.7. Even though the generations specified as 50, the convergence of the heat flux takes place within 15 iterations. Similarly, the search procedure is extended to two more initial guesses for the same heat flux and the convergence study is shown in Figure 6.8 as run 1, 2 and 3. Hence, different runs generate different initial guess solution. Eventually, the trend of the fitness functions seems to converge in a similar fashion thereby providing highly independent initial guess solutions. One of the advantages of using Genetic Algorithm to solve the inverse problems is that the initial guesses of the unknown quantities can be chosen arbitrarily. The estimated heat

flux is further examined with the actual value and results are reported in Table 6.6. Even though the estimated heat flux is very close to the actual heat flux, an attempt is made to obtain the accurate estimate thereby resulting in hybrid search approach. The hybrid search approach is a combination of Genetic Algorithm and Levenberg-Marquardt algorithm.

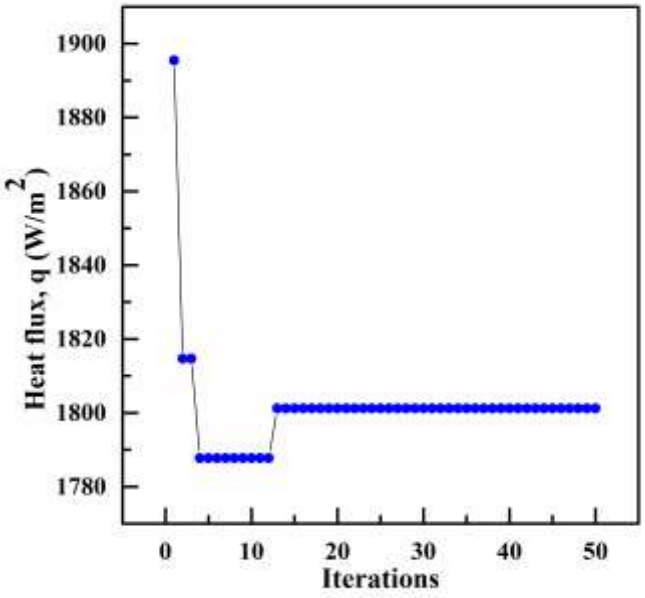

Figure 6.7 Convergence study of fitness function for heat flux of 1800W/m^2, genes=8, chromosomes=8

After selecting the number of population, the estimate is obtained by executing the GA code. The result is now given as input to the LM algorithm and finally the unknown parameter is estimated with less uncertainty. It is pertinent to mention that the number of iterations/generations can be changed to study the effect on the performance of the algorithm, but such a study does not help achieve significant

Table 6.6 Estimation of heat flux using GA and LM for the heat flux 1800 W/m^2

Sl no	Number of chromosomes	GA, heat flux(W/m^2)	Time(s)	LM_heat flux(W/m^2)
1	6	1801.2	9.43	1800
2	8	1801.2	9.63	1800
3	12	1801.2	14.12	1800

contribution to the solution because of the fact that the simulated data used contain no noise. Thus the hybrid search (Venugopal et al. 2009) provides the actual value of heat flux for different chromosomes. In addition to the estimates, Table 6.6 also provides information about the computation time involved in solving the inverse algorithm using GA. The computation time increases as the number of chromosome increases.

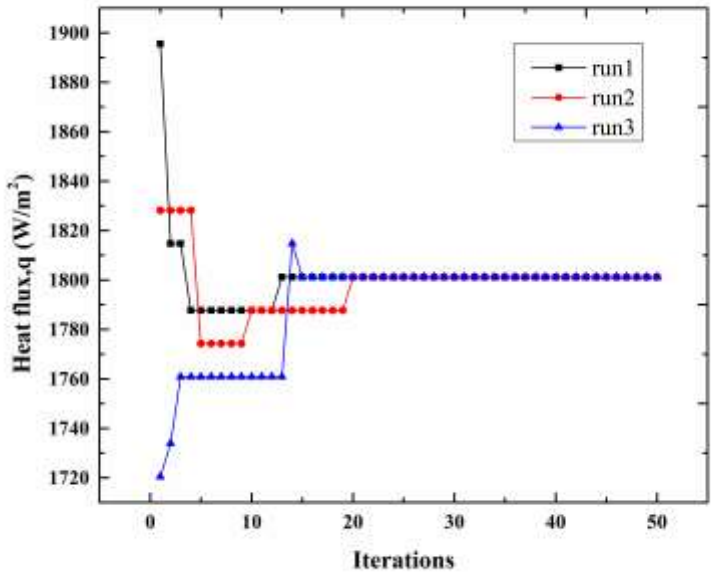

Figure 6.8 Convergence studies of fitness function for the heat flux of 1800 W/m^2, genes=8, chromosomes=8

Even though there is increase in computational time with respect to chromosomes, the estimates are consistent thereby proving the robustness of the inverse methodology. All the numerical simulations are performed on a computer system with intel core i5, 1.70 GHz, 12GB. Similarly, a study based on change of mutation rate and genes is

Table 6.7 Estimation of heat flux using GA and LM for the heat flux 1800 W/m^2 for different mutation rate

Sl no	**Mutation rate**	**GA heat flux(W/m^2)**	**Time(s)**	**LM heat flux(W/m^2)**
1	0.05	1801.2	10.33	1800
2	0.1	1801.2	9.555	1800
3	0.15	1801.2	9.51	1800

Table 6.8 Estimation of heat flux using GA and LM for the heat flux 1800 W/m^2 for different genes

Sl no	Number of genes	GA_heat flux(W/m^2)	Time(s)	LM heat flux(W/m^2)
1	8	1801.2	9.63	1800
2	12	1799.7	9.8	1800

presented in Table 6.7 and 6.8. The mutation rate is varied from 0.05 to 0.15 and the estimation is carried out for fixed gene and chromosome. The results show that the mutation rate sometimes increases the computational time because the chances of retaining the best solution in every iteration is less. The temperature residual is calculated in order to assess the model used in the inverse analysis. To achieve this parity plot is drawn between the temperature values obtained from the forward model heat flux and temperature values obtained from the estimated heat flux. Figure 6.9 shows such an exercise in which the forward model heat flux is 1800W/m^2 and the estimated value of the heat flux is obtained from Table 6.7 with GA as the inverse method. The inverse method is further tested for a heat flux of 2250 W/m^2 and such a test case is shown in Figure 6.10. Therefore, first level of inverse estimation using GA is well established for the conjugate natural convection problem and the next discussion is about the estimation of heat flux for actual temperature measurements.

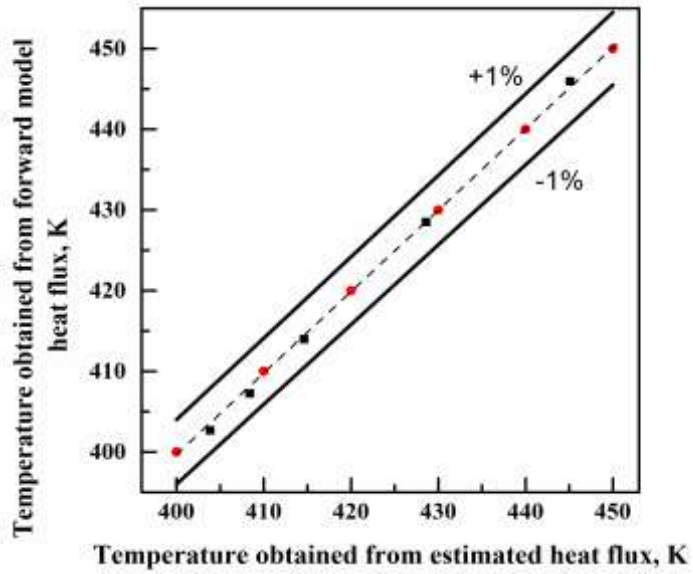

Figure 6.9 Parity plot for the temperature obtained from the forward model heat flux and the estimated heat flux

6.6.2 Estimation of heat flux from measured data

Having proved the robustness of the retrieval methodology in the previous section, the approach for the estimation of unknown heat flux is the same as the previous section but the simulated temperature is now replaced with the actual measurement temperature. However, the observed temperature data may contain measurement errors therefore a neural network is trained for the measurement data thereby eliminating the complexity in matching the temperature between the neural network trained using CFD simulations and experiments. This in turn reduces the complexity associated in modelling and simulating the numerical model.

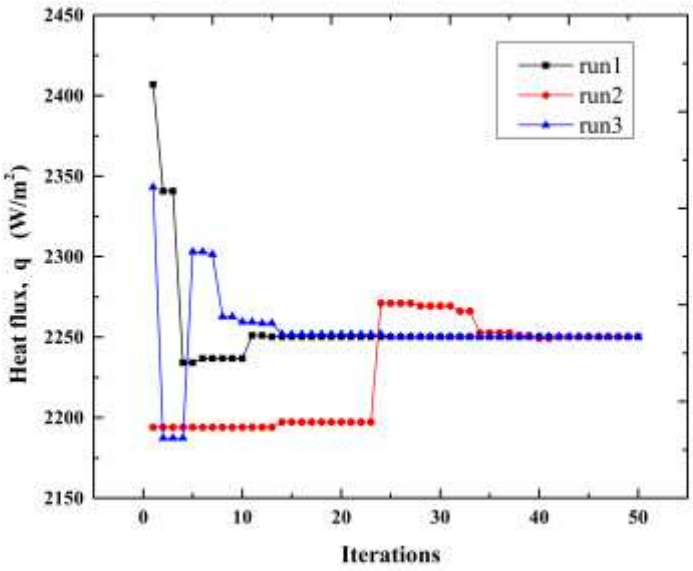

Figure 6.10 Convergence study for the heat flux of 2250 W/m^2, genes=8, chromosomes=8

The neuron independence study for the experimental neural network has been carried out and selected neurons is found to be 10. The trained neural network temperature is compared with the experimental temperature and already shown in Table 6.4. The deviation between the experimental and NN temperatures is clearly given in Figure 6.4 and the variation is less than 2.5K.

To ascertain the estimated heat flux, several trail run has been conducted and fitness function in terms of best, average and worst for the experimental heat flux of 826.66W/m^2 is shown in Figure 6.11 which proves that GA is able to estimate the

unknown heat flux even for the measured temperatures. Figure 6.12 shows the convergence study for the heat flux of 826.66 W/m^2 for different runs. The percentage

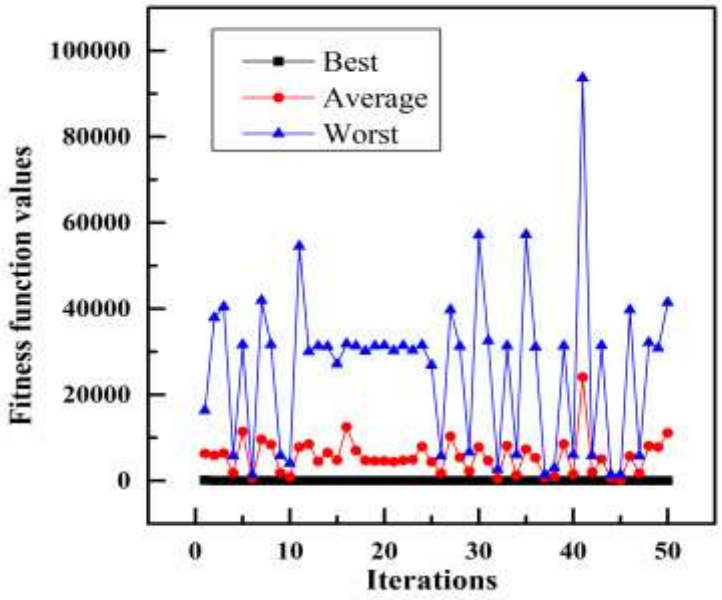

Figure 6.11 Fitness function for the heat flux of 826.66 W/m^2, genes=8, chromosomes=8

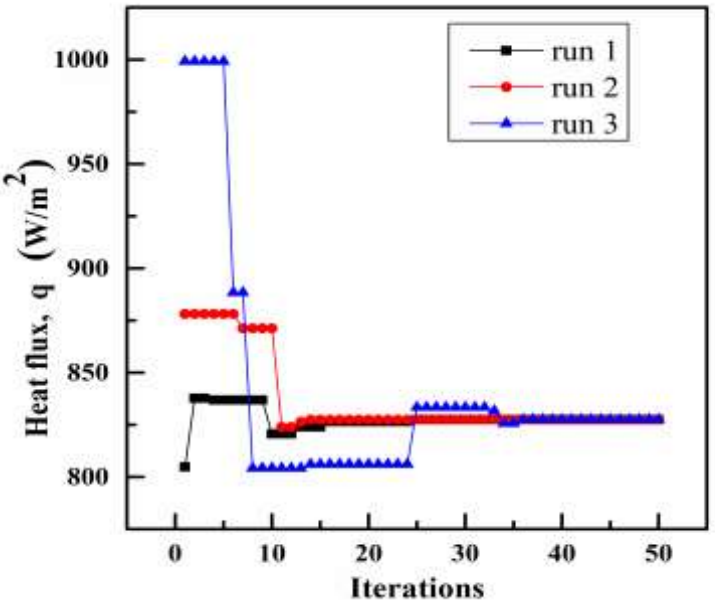

Figure 6.12 Convergence study for the heat flux of 826.66 W/m^2, genes=8, chromosomes=8.

Table 6.9 Estimation of heat flux using GA and LM for the heat flux 826.66 W/m^2 for the measured temperature

Sl. no	Number of chromosomes	Heat flux (W/m^2)	Time, s	LM GA heat flux (W/m^2)	% error
1	6	827.42	6.24	826.53	0.107
2	8	827.42	8.4	826.53	0.107
3	12	827.42	12.77	826.53	0.107

error reported in Table 6.9 for the heat flux of 826.66 W/m2 is very less which further corroborates that reliable solution can be obtained even for the measured data. It can also be seen from Table 6.9 that the estimates using hybrid GA improves only to a small extent and thereby suggesting that the plain GA itself is a robust and powerful inverse methodology for the estimation of the heat flux.

6.7 CONCLUSION

An inverse approach has been demonstrated to estimate the unknown heat flux for a conjugate heat transfer problem. Fluid flow and heat transfer from two dimensional fin with base being heated by uniform heat flux was first solved by ANSYS to determine the velocity and temperatures in the domain of interest. These calculations are validated with limited in-house experiments. Following this a back propagation Neural Network was developed that returns the temperatures of the fin for a given heat flux. This was then used to drive a Genetic Algorithm engine to estimate the un-known heat flux with known measurement. Finally, the output of the Genetic Algorithm was given to Levenberg Marquardt Algorithm to improve the accuracy of the estimate. The important conclusions of the present study are:

- ANN-GA is robust and efficient method to estimate problems of this class.
- ANN can be efficiently used to replace the time consuming CFD model.
- There is little to choose between a plain GA and hybrid GA method.

6.8 Closure

This chapter dealt with the estimation of heat flux using simulated data and experimental data using ANN as the forward model and GA as inverse method considering 2D geometry. A hybrid inverse approach was incorporated by combining deterministic method, Levenberg Marquardt algorithm with stochastic method,

Genetic Algorithm. Next chapter explains the use of ANN as both forward and inverse problem.

CHAPTER 7

ESTIMATION OF HEAT FLUX AND HEAT TRANSFER COEFFICIENT USING ANN AS FORWARD AND INVERSE METHODS

7.1 INTRODUCTION

This chapter reports the usefulness of incorporating back propagation neural (BPN) network as forward and inverse models in the estimation of unknown heat flux and heat transfer coefficient for the vertical base fin setup. The main aim of this work is to reduce the computational cost of the inverse estimation. Furthermore, the effect of addition of experimental temperature in to the forward model is also studied in order to improve the solution of the inverse estimation. The solution procedure begins with the simulated data and limited number of experiments is injected in to the simulated data for the estimation of heat flux and heat transfer coefficient. The novelty of the work is to perform very few numerical simulations and experiments and finally combining these two to provide a quick solution to the experimental data driven forward model.

7.2 FORWARD MODEL

In this work, the numerical model consisting of the fin and base assembly is modelled as a three dimensional conjugate heat transfer problem, which is shown in Figure 7.1 with related boundary conditions. The base plate of the fin is placed vertically to ground, the extended domain is modelled to study the effects of convection and also to obtain velocity information. The medium considered in the extended domain is air which is considered to be of constant thermo-physical properties except for the density so as to model natural convection. Boussinesq approximation is incorporated to treat density as a constant with the momentum and the continuity equations but vary with temperature in the energy equation.

w

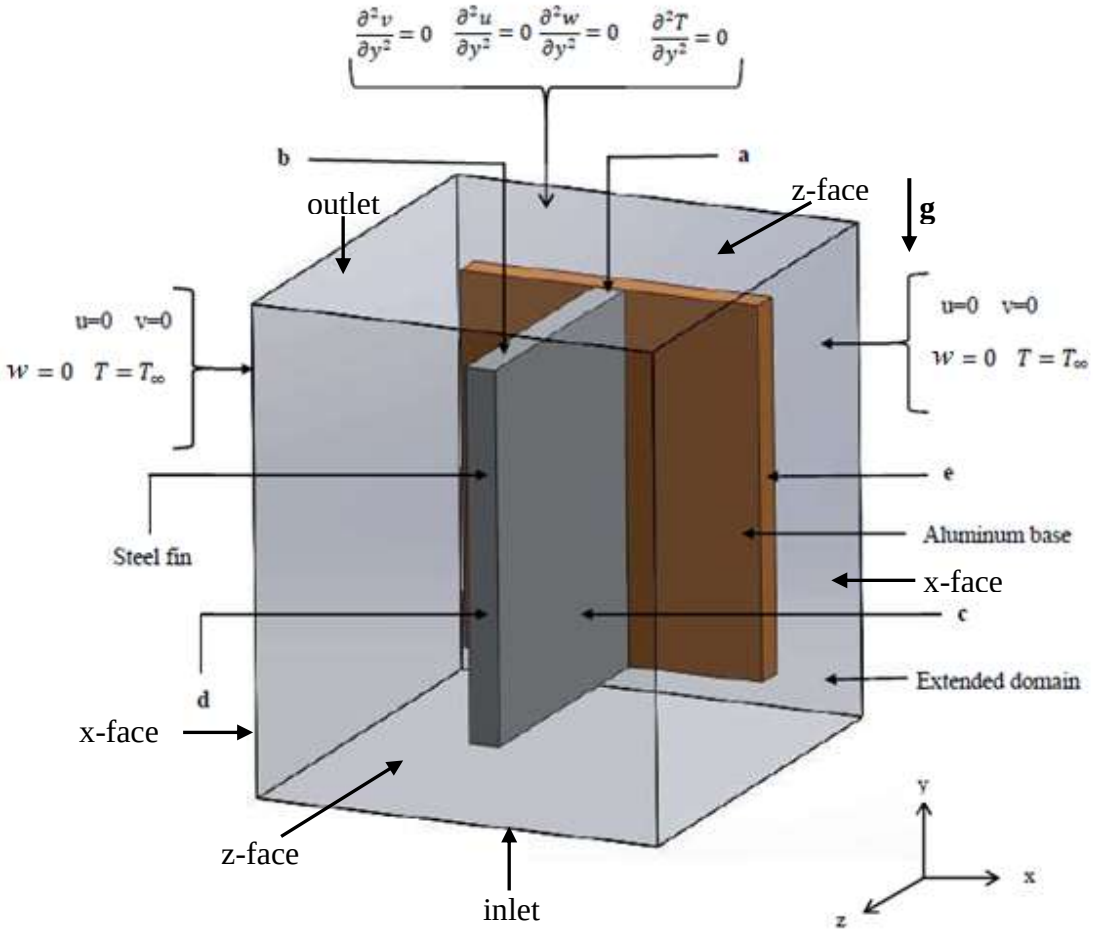

Figure 7.1 Numerical model.

The computational mesh model is shown in Figure 7.2. The governing equations of the present study is given as

Continuity:

$$\frac{\partial u}{\partial x}+\frac{\partial v}{\partial y}+\frac{\partial w}{\partial z}=0 \qquad (7.1)$$

X-momentum equation:

$$u\frac{\partial u}{\partial x}+v\frac{\partial u}{\partial y}+w\frac{\partial u}{\partial z}=-\frac{1}{\rho}\frac{\partial p}{\partial x}+\vartheta\left(\frac{\partial^2 u}{\partial x^2}+\frac{\partial^2 u}{\partial y^2}+\frac{\partial^2 u}{\partial z^2}\right) \qquad (7.2)$$

Y-momentum equation:

$$u\frac{\partial v}{\partial x}+v\frac{\partial v}{\partial y}+w\frac{\partial v}{\partial z}=-\frac{1}{\rho}\frac{\partial p}{\partial y}+\vartheta\left(\frac{\partial^2 v}{\partial x^2}+\frac{\partial^2 v}{\partial y^2}+\frac{\partial^2 v}{\partial z^2}\right)+g\beta(T-T_\infty) \quad (7.3)$$

Z-momentum equation:

$$u\frac{\partial w}{\partial x}+v\frac{\partial w}{\partial y}+w\frac{\partial w}{\partial z}=-\frac{1}{\rho}\frac{\partial p}{\partial z}+\vartheta\left(\frac{\partial^2 w}{\partial x^2}+\frac{\partial^2 w}{\partial y^2}+\frac{\partial^2 w}{\partial z^2}\right) \quad (7.4)$$

Energy equation (for fluid):

$$u\frac{\partial T}{\partial x}+v\frac{\partial T}{\partial y}+w\frac{\partial T}{\partial z}=\alpha\left(\frac{\partial^2 T}{\partial x^2}+\frac{\partial^2 T}{\partial y^2}+\frac{\partial^2 T}{\partial z^2}\right) \quad (7.5)$$

Energy equation (for solid):

$$k_s\left(\frac{\partial^2 T}{\partial x^2}+\frac{\partial^2 T}{\partial y^2}+\frac{\partial^2 T}{\partial z^2}\right)=0 \quad (7.6)$$

Figure 7.1 depicts the boundary conditions of the present problem. At the inlet, the following boundary conditions are imposed,

$$u=0\ v=0\ z=0\ T=T_\infty \quad (7.7)$$

At the outlet of the domain the following boundary condition is used,

$$\frac{\partial^2 v}{\partial y^2}=0 \qquad \frac{\partial^2 u}{\partial y^2}=0 \qquad \frac{\partial^2 z}{\partial y^2}=0 \quad \frac{\partial^2 T}{\partial y^2}=0 \quad (7.8)$$

The x-face of the domain is subjected to,

$$u=0 \quad v=0 \quad z=0 \quad \frac{\partial T}{\partial x}=0 \quad (7.9)$$

Also z-face of the domain is subjected to,

$$u=0 \quad v=0 \quad z=0 \quad \frac{\partial T}{\partial z}=0 \quad (7.10)$$

Region ‘a’ is solid-solid interface and the transfer of energy at this region is through conduction, where the wall of the fin and the aluminium base is treated as coupled wall.

$$k_{al}\frac{\partial T}{\partial n}=\ k_{ms}\frac{\partial T}{\partial n} \ \text{ and } \ T_{al}=T_{ms} \quad (7.11)$$

At regions ‘b’, ‘c’ and‘d’ the kind of boundary condition imposed is solid-liquid interface so the energy transfer between the fin faces to the air in the extended domain is by convection.

$$k_{ms}\frac{\partial T}{\partial n} = k_f\frac{\partial T}{\partial n} \text{ and } T_{ms} = T_{fluid} \tag{7.12}$$

Where k_{al} is thermal conductivity of aluminum, k_{ms} is thermal conductivity of mild steel and k_f is thermal conductivity of fluid.

At region ‘e’ i.e along the sides of the base insulation boundary condition is applied.

$$\frac{\partial T}{\partial x} = 0 \tag{7.13}$$

No slip condition is applied along all solid walls. All these regions are treated as interfaces.

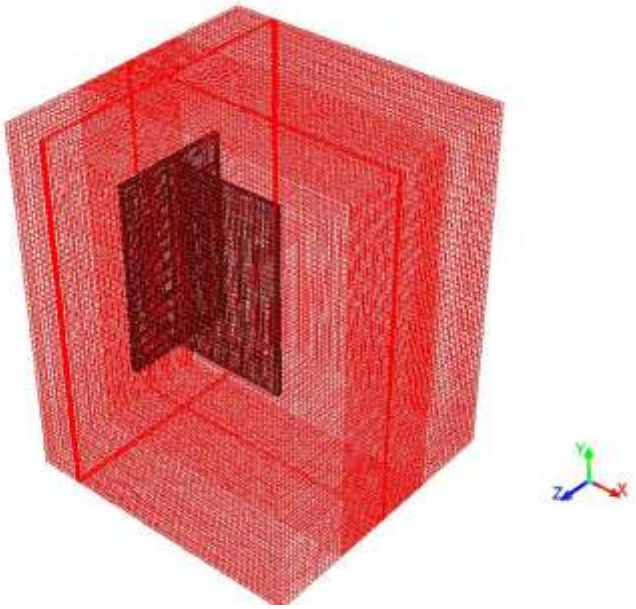

Figure 7.2 Computational mesh domain.

A grid independence study has been performed to find out the optimum number of nodes required for the numerical simulations. From Figure 7.3, 4,72,000 nodes are found to be optimum and the forward model computations are performed based on the optimum grid. Numerical simulations are carried out in a 32core 64GB RAM

workstation and the average time taken for obtaining a single forward solution was 45mins.

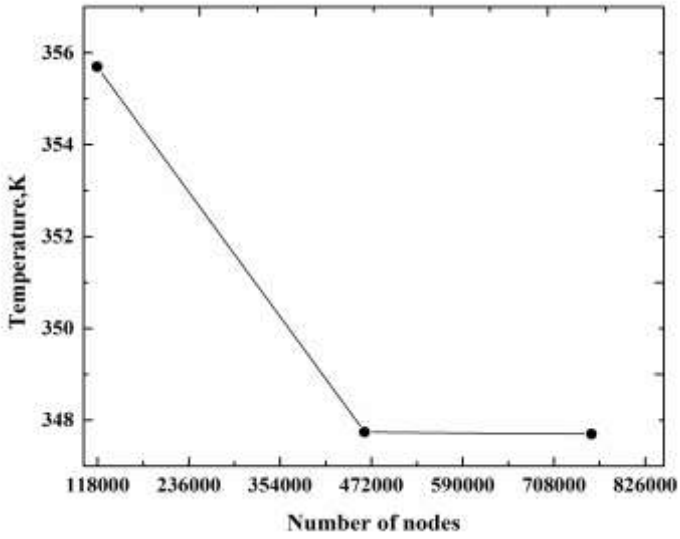

Figure 7.3 Grid Independence study.

7.3 EXPERIMENTAL SETUP

Chapter 3 provides the details about the experimental setup. The results of the steady state temperature distribution obtained from the vertical base fin for different power levels and simulation temperature results are compared and are shown in Figure 7.4.

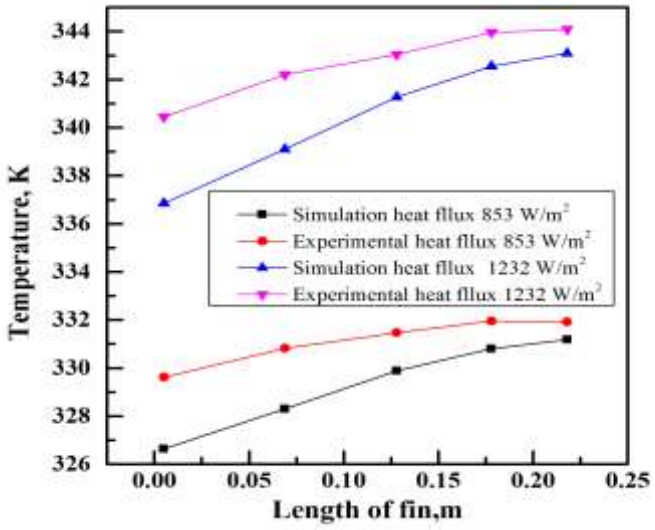

Figure 7.4 Comparison of temperature along the length of fin.

7.4 RESULTS AND DISCUSSION

Equation (7.1) - (7.13) is solved to obtain the temperature distribution along the length of the fin. Numerical simulations are carried out using different values of heat flux as input and the temperature contour and velocity contour are shown in Figures 7.5 and 7.6 respectively. The forward model consists of a 3D geometry which is modelled and meshed using ANSYS 14.5 with the selected grid size. The heat flux applied at the base is varied from 305-3300W/m^2. The selection of heat flux range confirms that the Rayleigh number does not exceed the critical value and the flow remains laminar.

Figure 7.5 Temperature contour along the height of fin obtained for heat flux of 1600 W/m^2

Steady state heat transfer simulations are carried out for different values of heat flux and the corresponding temperature data is obtained. Temperature along the height of fin is plotted against different values of heat flux. It can be observed that along the length of the fin there is a gradual increase in the temperature indicating that the heat transfer from the fin surface to ambient as y→L is decreasing because the cold air from the bottom receives more heat, raises upstream due to the density difference which is evident from the Figure 7.7. Information about the heat transfer coefficient along the length of the fin is shown in Figure 7.8 which also justifies the increase in temperature along the length of fin observed in Figure 7.7.

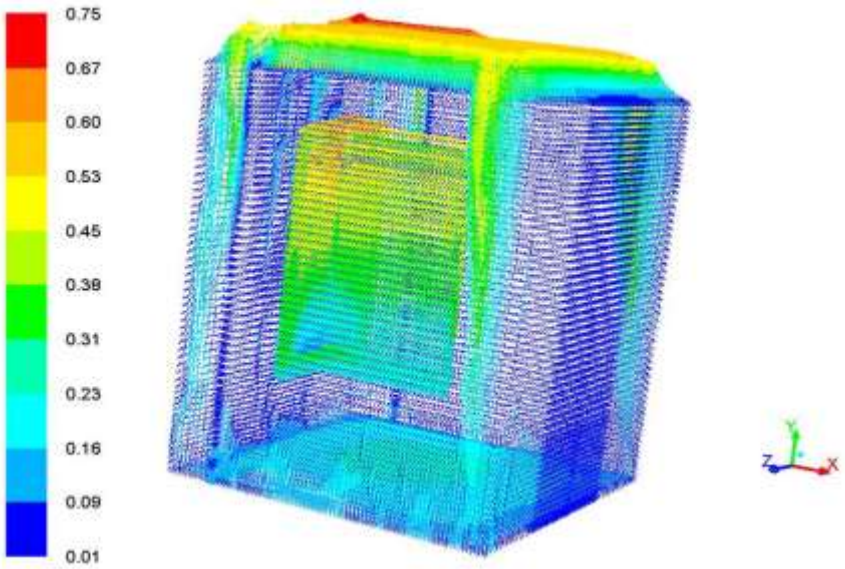

Figure 7.6 Velocity plot for heat flux of 1200W/m^2

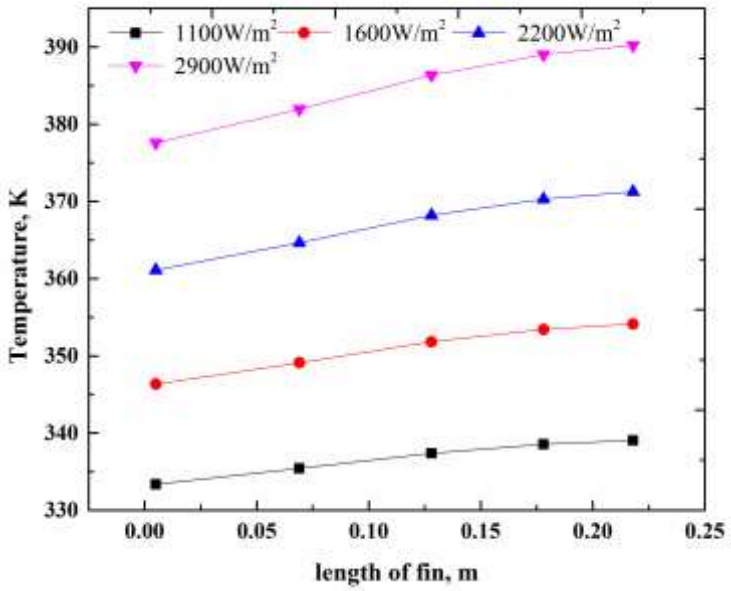

Figure 7.7 Temperature plot for different values of heat flux

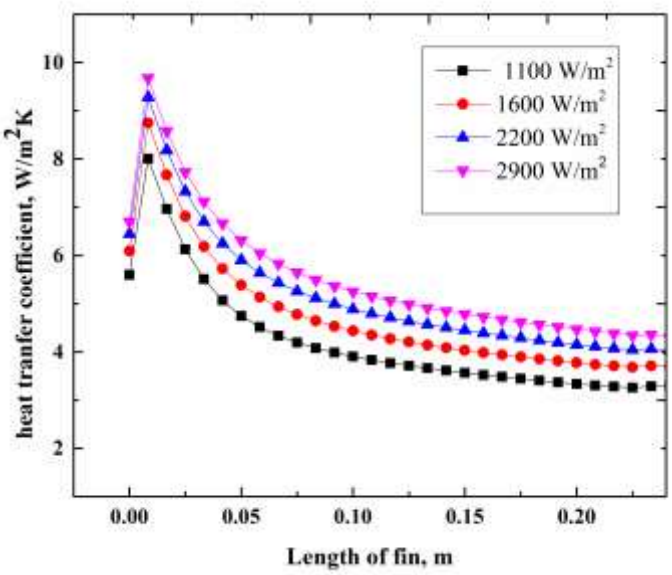

Figure 7.8 Heat transfer coefficient plot over the length of fin

7.4.1 ANN as forward model

The main aim of the present work is to minimize the computational cost of the forward model as well as the inverse model. Generally, any iterative technique used for the inverse estimation of unknown parameters requires forward model solution for every iteration thereby leading to more computational cost. In order to avoid this situation, a neural network can be trained between the known input and the temperature data. To develop a neural network for the forward model, the temperature distribution is obtained for the known values of the parameters involved in the mathematical model using CFD solution. Temperature data at 3 sensor locations have been considered. Therefore, training is done between the unknown heat flux or heat transfer coefficient and the temperatures. Neuron independence is carried out to fix the number of neurons while training the network for the forward and inverse models. Table 7.1 shows the comparison of simulation temperature and the ANN temperature. It is very much evident from the table that ANN can be used as an alternate for the conventional forward model.

Table 7.1 Comparison between simulation temperature and ANN temperature for simulated data

Location, m	Heat flux = 1100W/m^2		Heat flux = 1600W/m^2		Heat flux = 2200W/m^2	
	T_{CFD}, K	T_{ANN}, K	T_{CFD}, K	T_{ANN}, K	T_{CFD}, K	T_{ANN}, K
Base	363.43	363.43	389.49	389.52	419.77	419.78
0.005	333.36	333.35	346.33	346.32	361.10	361.09
0.178	338.54	338.53	353.42	353.42	370.30	370.30

Initially, ANN is trained using simulated measurements. The simulated data used for training is shown in Table A2 in Appendix. Later, experimental temperature is injected in to the simulated measurements one by one and training of the network is carried out. Hence, the forward model is now driven by the experimental input to accurately estimate the unknown parameters. To accomplish this, the experimental temperature injected into the forward model is classified as Model 1, Model 2, Model 3 and Model 4. Model 1 to Model 4 represents the experimental temperature injected as one temperature value, two temperature values, three temperature values and four temperature values respectively. The correlation coefficient for such an exercise is shown in Figure 7.9. Similarly, for the inverse analysis, a network is created based on the temperature data obtained from CFD simulations as input and the heat flux/heat transfer coefficient as output.

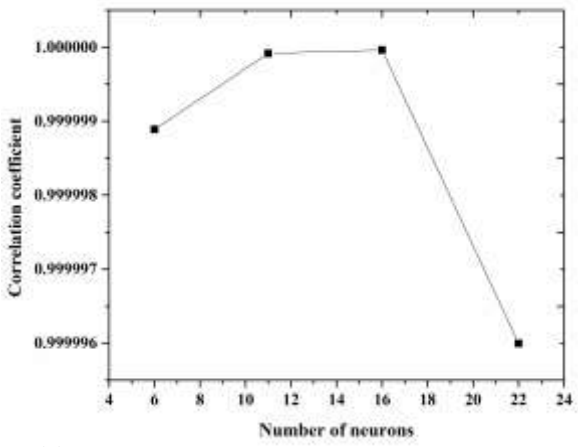

(a)

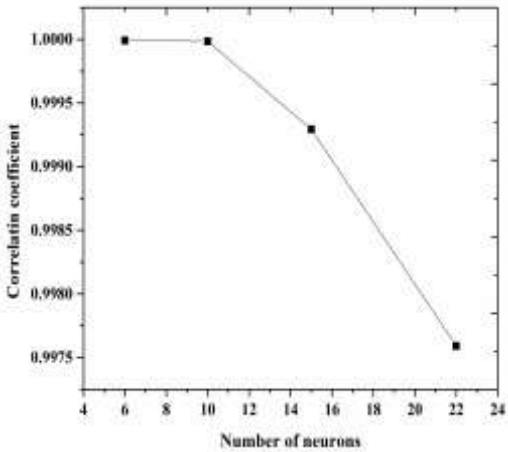

(b)

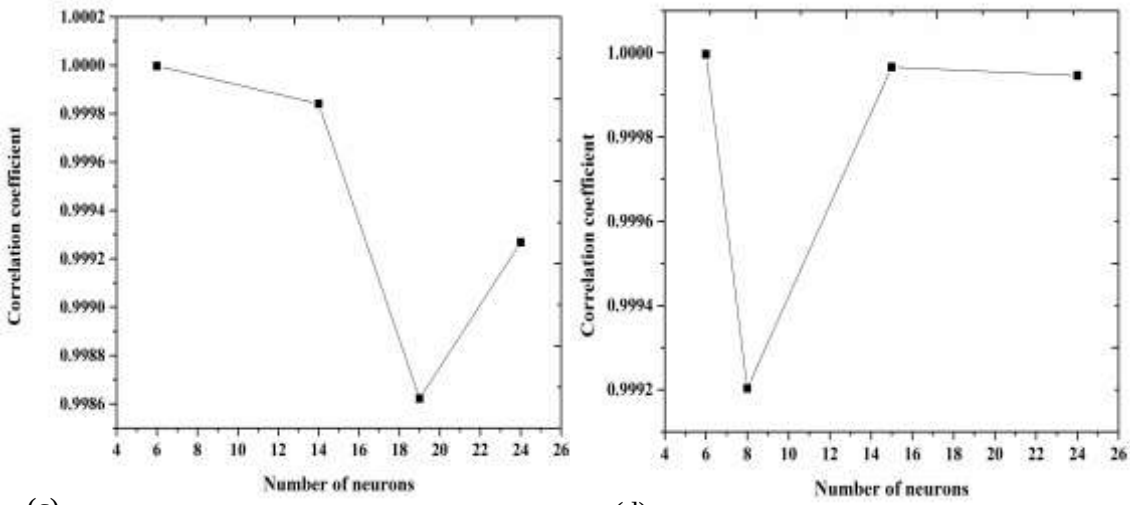

Figure 7.9 Correlation coefficient plot for forward model (a) one experiment value, (b) Two experiment values, (c) Three experiment values (d) Four experiment values.

Tables 7.2 to 7.5 show the comparison between ANN temperature and simulation temperature which is obtained by injecting experimental data one by one in to the simulation data. From these tables the maximum errors observed are 0.03%, 0.06%, 0.22% and 0.46% respectively. Figure 7.10 shows the mean absolute error obtained from Model 1 to 4.

Table 7.2 Comparison between simulation temperature and ANN temperature when single experiment value is considered (Model 1)

Location, m	q = 1100W/m^2		q = 1600W/m^2		q = 2200W/m^2	
	T_{CFD}, K	T_{ANN}, K	T_{CFD}, K	T_{ANN}, K	T_{CFD}, K	T_{ANN}, K
Base	363.43	363.391	389.49	389.490	419.77	419.717
0.005	333.36	333.465	346.33	346.328	361.10	361.046
0.178	338.54	338.6513	353.42	353.424	370.30	370.237

Table 7.3 Comparison between simulation temperature and ANN temperature when two experiment values is considered (Model 2)

Location, m	q = 1100W/m^2		q = 1600W/m^2		q = 2200W/m^2	
	T_{CFD}, K	T_{ANN}, K	T_{CFD}, K	T_{ANN}, K	T_{CFD}, K	T_{ANN}, K
Base	363.43	363.208	389.49	389.612	419.77	419.708
0.005	333.36	333.339	346.33	346.352	361.10	361.125
0.178	338.54	338.520	353.42	353.421	370.30	370.339

Table 7.4 Comparison between simulation temperature and ANN temperature when Three experiment values is considered (Model 3)

Location, m	Heat flux = 1100W/m^2		Heat flux = 1600W/m^2		Heat flux = 2200W/m^2	
	T_{CFD}, K	T_{ANN}, K	T_{CFD}, K	T_{ANN}, K	T_{CFD}, K	T_{ANN}, K
Base	363.43	363.136	389.49	389.503	419.77	420.046
0.005	333.36	334.115	346.33	346.252	361.10	360.726
0.178	338.54	338.783	353.42	353.328	370.30	370.398

Table 7.5 Comparison between simulation temperature and ANN temperature when four experiment values is considered (Model 4)

Location	q = 1100W/m^2		q = 1600W/m^2		q = 2200W/m^2	
	T_{CFD}, K	T_{ANN}, K	T_{CFD}, K	T_{ANN}, K	T_{CFD}, K	T_{ANN}, K
Base	363.43	362.332	389.49	389.421	419.77	419.811
0.005	333.36	334.922	346.33	346.583	361.10	360.838
0.178	338.54	339.088	353.42	353.533	370.30	370.187

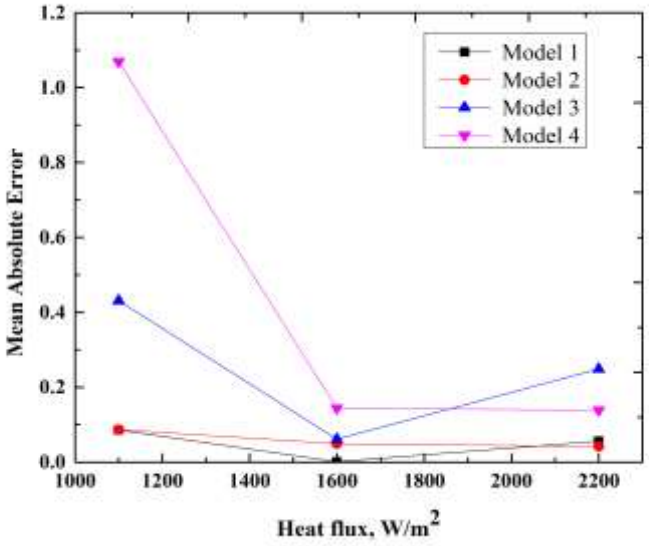

Figure 7.10 shows the Mean Absolute Error for the ANN data.

After establishing the network between heat flux and the temperature, an attempt has been made to estimate both heat flux and heat transfer coefficient simultaneously. As a result of this, the forward model now contains heat flux and heat transfer coefficient as input to the network and temperatures as output. Information about heat transfer coefficient along the length of the fin is shown in Figure 7.8. The number of neurons is fixed after carrying out neuron independence study. Table 7.6 shows the comparison of temperature between the simulated output and ANN.

Table 7.6 Heat flux and heat transfer coefficient as input to the network

Location, m	q =1500 W/m^2, h= 4.540W/m^{2}K		q = 2000 W/m^2, h = 4.924W/m^{2}K		q= 2700 W/m^2, h = 5.320W/m^{2}K	
	T_{CFD}, K	T_{ANN}, K	T_{CFD}, K	T_{ANN}, K	T_{CFD}, K	T_{ANN}, K
Base	384.36	384.101	409.79	409.869	444.43	444.626
0.005	343.80	343.686	356.23	356.239	372.93	372.995
0.178	350.53	350.423	364.76	364.785	383.76	383.742

7.4.2 ANN as Inverse model for single parameter estimation

For estimation purpose, the input and the output data used in Model 1 to 4 has now been interchanged to obtain Inverse Model 1 to 4. Nevertheless, the Inverse Model 1 to 4 contains heat flux as output and temperatures as input.

Before estimating the heat flux based on Models 1 to 4, an attempt has been made to estimate the heat flux for simulated data. The results of the estimation are shown in Table 7.7.

Table 7.7 Estimation of heat flux for the simulated data.

Actual heat flux,	Estimated heat flux,	Error percentage
1100	1099.78	0.020
1600	1599.7	0.018
2200	2198.65	0.061
2900	2915.44	0.532

ANN when used as inverse model produce a maximum error of 0.53% as seen from the table; therefore, this could be well attributed that the methodology proposed so far can be a potential tool for the estimation of heat flux for the experiment data as well. The results of inverse model is reported in Table 7.8 which shows the estimation of heat flux using the Inverse Models 1- 4.

Table 7.8 Estimation of heat flux using the Inverse Models 1- 4

Actual heat flux, W/m^2	Retrieved heat flux, W/m^2			
	Inverse Model 1	Inverse Model 2	Inverse Model 3	Inverse Model 4
1100	1102.7	1098.9	1099.6	1098.5
1600	1599.3	1599.4	1599.4	1599.0
2200	2197.1	2200.3	2199.2	2201.8

Temperature residual between the forward model heat flux and the estimated heat flux is shown in Table 7.9 the low residual value indicates the suitability of the model used in the inverse analysis.

Table 7.9 Temperature residual

Location, m	Temperature, K from forward model heat flux 2200W/m^2	Temperature, K from estimated heat flux 2198.65W/m^2	Residual
Base	403.344	402.812	1.32E-03
0.005	383.374	382.513	2.246E-03
0.178	377.558	376.277	3.393E-03

From the table it is observed that the maximum deviation in the estimated heat flux is 0.24%. Figure 7.11 shows the percentage deviation plot for the estimated heat flux when experimental data was injected to the simulation results.

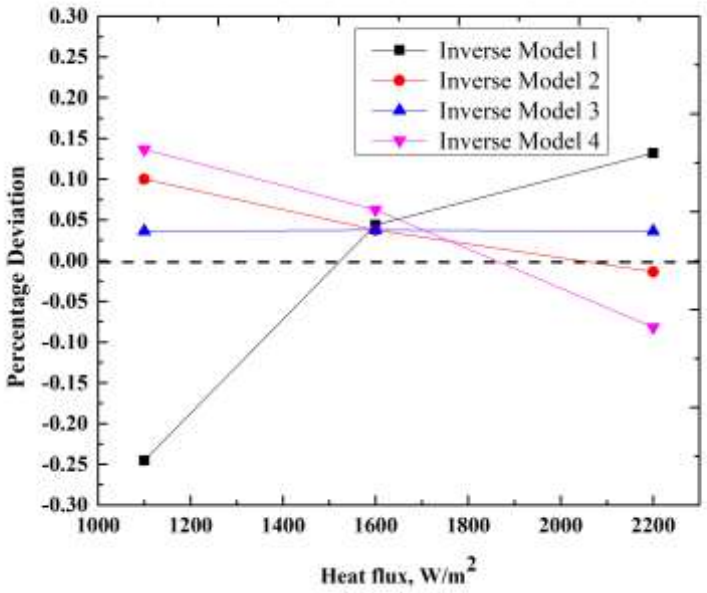

Figure 7.11 Percentage deviation plot for the retrieved heat flux

7.4.3 Simultaneous estimation of heat flux and heat transfer coefficient

The efficacy of the Neural network is further proved by simultaneous estimation of heat flux and heat transfer coefficient. NN is trained using temperature as the input, heat flux and heat transfer coefficient as the output. ANN when used as inverse tool in estimating heat flux yielded very good results as evident from Table 7.7. Table 7.10 and it further buttresses that the retrieved values of the unknown parameters for the experimental temperature with the maximum error of 6.2% and 2.1% for heat flux and heat transfer coefficient respectively.

Table 7.10 Estimation of heat flux and heat transfer coefficient for experimental data

Actual		Estimated		Error (%) Heat flux, W/m^2	Error (%) Heat transfer coefficient, W/m^2K
Heat flux, W/m^2	Heat transfer coefficient, W/m^2K	Heat flux, W/m^2	Heat transfer coefficient, W/m^2K		
853	3.78	823.64	3.71	3.44	1.64
1232	4.28	1155.6	4.37	6.20	2.10

7.5 CONCLUSIONS

3-D Computational model was created with appropriate boundary conditions, using a commercial software ANSYS-FLUENT. Initially, simulations were carried out to obtain the temperature data. Simulation results were used to train the NN and the accuracy of NN was shown in terms of Mean Absolute Error. In the first stage the heat flux was used as the input to NN and temperature was obtained as the output, later the same NN was then injected with experimental temperature in various stages to obtain Model 1 to Model 4. In the second stage, Inverse Models 1 – 4 were developed to estimate the unknown heat flux based on the temperature data. After establishing the robustness of the retrieval methodology, ANN was again applied for simultaneous estimation of heat flux and heat transfer coefficient based on the experimental temperature. Based on the proposed analysis, the following are the highlights of the work

(i) CFD simulations are replaced by the neural network model to reduce the computation time.

(ii) ANN driven by experimental temperature for effective estimation of unknown parameters

(iii) ANN was also used as inverse method thereby eliminating the process of iterative solutions to the proposed inverse problem.

(iv) The efficacy and robustness of the proposed methodology has been demonstrated through single parameter and multi-parameter estimations.

7.6 Closure

This chapter dealt with the use of ANN as both and forward models for single and multi-parameter estimations. The concept of experimental data driven ANN forward and inverse models has been established for the solution of inverse conjugate free convection heat transfer problem. The next chapter deals with the single and multi-parameter estimations for horizontal base orientation using ANN as the forward model and Bayesian Inference as a inverse model.

CHAPTER 8

SIMULTANEOUS ESTIMATION OF HEAT FLUX AND HEAT TRANSFER COEFFICIENT USING BAYESIAN INFERENCE FOR CONJUGATE HEAT TRANSFER FROM FIN

8.1 INTRODUCTION

This chapter deals with the simultaneous estimation of the heat flux and heat transfer coefficient using Bayesian framework. The computational model, which consists of a mild steel fin, is created using ANSYS. Steady state heat transfer experiments are conducted under natural convection. Initially, for the purpose of estimation, a two dimensional computational symmetric model is considered. The fin geometry is enclosed by an extended domain filled with air so as to account natural convection conjugate heat transfer. Grid independence study is carried out to fix the number of grids. Later, a 3-D model is developed to capture more physics of the problem and one can obtain the surface temperature of the fin to estimate the unknown parameters. The estimation process is classified into 2 stages. In the first case, for the 2D computational model, the heat flux is estimated using the simulated measurements. In the second case where 3D model is involved, simultaneous estimation of heat flux and heat transfer coefficient is attempted for experimental data. Additionally, ANN is used as the forward model within the Bayesian framework.

8.2 METHODOLOGY

8.2.1 2D Numerical Model

The problem includes a mild steel fin which is placed on an aluminium base plate and a heater is provided beneath the base plate to supply constant heat flux. The extended domain is modelled to study the convection effects and to capture the velocity profile. The medium considered for the extended domain is air which is considered to be of constant thermo-physical properties except for the density to model the natural convection. The problem is modelled as a two dimensional conjugate heat transfer problem. The fluid flow is symmetry and half of the physical domain is considered to save the computational cost. Grid independence study is carried out to fix the number of grids and simulation is carried out for various values of heat flux. The geometry

and boundary conditions considered for 2D simulation along with the dimensions (mm) is shown in Figure 8.1

$$\frac{\partial^2 v}{\partial y^2} = 0 \qquad \frac{\partial^2 u}{\partial y^2} = 0 \qquad \frac{\partial^2 T}{\partial y^2} = 0$$

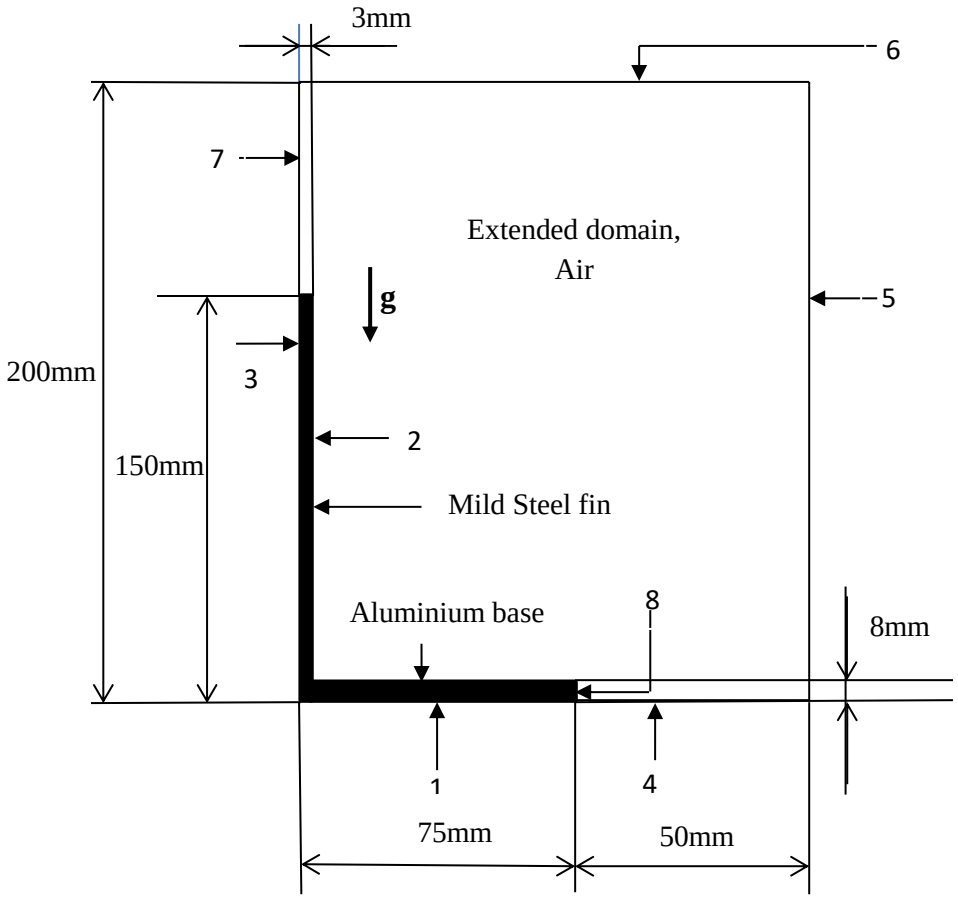

Figure 8.1 2D simulation model with boundary condition

Table 8.1 shows the boundary conditions used in the analysis. The location 2 of the simulation domain is the solid-fluid interface. Since the problem is conjugate heat transfer, the transfer of energy from aluminium base to steel fin is by conduction and from the fin wall to the fluid medium also from top of the aluminium base to the fluid medium is by convection. So, at the solid-fluid interfaces the transfer of energy will be by convection. At location 8 which is solid-fluid interface the information across the interface is prevented by providing insulation. At the solid liquid interface inflation layers are used for the flow of information from grid of one phase to the grid of other phase as well as between fin (solid) and base (solid).

Table 8.1 Types of boundary conditions for analysis

Boundary	Type of Boundary condition
1	$q = -k\frac{\partial T}{\partial y}$
2	Solid-fluid interface
3	$\frac{\partial T}{\partial x} = 0$
4	Pressure outlet
5	Pressure outlet
6	Pressure outlet
7	$\frac{\partial T}{\partial x} = 0$
8	Solid-fluid interface

The properties of the materials considered for the numerical analysis are given in Table 8.2. The governing equation along with the appropriate boundary conditions is solved using ANSYS fluent 14.5.

Table 8.2 Properties of the materials used in simulation

Properties	Mild Steel	Aluminium
Density (kg/m^3)	8030	2719
Specific heat (J/kgK)	502.48	871
Thermal conductivity (W/mK)	45	202.4

The numerical model is validated using analytical solution. The fundamental equations of the fluid flow are the continuity equation, momentum equations (Navier Stokes equation) and energy equation. All the cases considered in the present study involve laminar, two-dimensional, steady convection. The density changes are modelled with the Boussinesq approximation which treats the fluid density as a linear function of temperature for the buoyancy term in the momentum equation. Viscous

heat dissipation, compressibility effects are considered to be negligible. Based on the above assumptions, the governing equations can be written as follows.

Continuity:

$$\frac{\partial u}{\partial x} + \frac{\partial v}{\partial y} = 0 \tag{8.1}$$

X-momentum equation:

$$u\frac{\partial u}{\partial x} + v\frac{\partial u}{\partial y} = -\frac{1}{\rho}\frac{\partial p}{\partial x} + \nu\left(\frac{\partial^2 u}{\partial x^2} + \frac{\partial^2 u}{\partial y^2}\right) \tag{8.2}$$

Y-momentum equation:

$$u\frac{\partial v}{\partial x} + v\frac{\partial v}{\partial y} = -\frac{1}{\rho}\frac{\partial p}{\partial y} + \nu\left(\frac{\partial^2 v}{\partial x^2} + \frac{\partial^2 v}{\partial y^2}\right) + g\beta\,(T - T_\infty) \tag{8.3}$$

Energy equation (fluid):

$$u\frac{\partial T}{\partial x} + v\frac{\partial T}{\partial y} = \alpha\left(\frac{\partial^2 T}{\partial x^2} + \frac{\partial^2 T}{\partial y^2}\right) \tag{8.4}$$

Energy equation (solid):

$$k\left(\frac{\partial^2 T}{\partial x^2} + \frac{\partial^2 T}{\partial y^2}\right) = 0 \tag{8.5}$$

Equation (8.1) - (8.5) is solved for the appropriate boundary conditions (refer Figure 8.1) and the temperature distribution is obtained for the heat flux specified at the base.

8.2.2 Forward model verification

Any numerical simulation must be verified against analytical solution, considering one dimensional steady state fin the governing equation turns out to be ;

$$\frac{\partial^2 \theta}{\partial X^2} - (mL)^2\theta = 0 \tag{8.6}$$

Where $\theta = \frac{T - T_\infty}{T_o - T_\infty}$, $X = \frac{x}{L}$

θ is non dimensional temperature

X is non dimensional length

T_o = base temperature, K

T_∞= ambient temperature, K

fin constant , $m^2 = \frac{hp}{kA}$;

h= heat transfer coefficient, W/m^2K

p = perimeter of the fin, m

k = thermal conductivity of the fin material, W/m K

A= heat transfer area of fin, m^2

Writing the general solution in the form

$$\theta = C_1 e^{mx} + C_2 e^{-mx} \tag{8.7}$$

Using boundary conditions,

At x = 0, $\theta(0) = 1$

x= L, $h\theta(L) = -k \frac{d\theta}{dx}$

The expression for temperature distribution when subjected to the above boundary condition is obtained as (Incropera and DeWitt 2002),

$$\theta = \frac{\cosh m(L-x) + \left(\frac{h}{mk}\right) \sinh m(L-x)}{\cosh mL + \left(\frac{h}{mk}\right) \sinh mL} \tag{8.8}$$

For the known input and boundary conditions Equation (8.8) can be solved to obtain temperature distribution. Figure 8.2 shows the comparison of non-dimensional temperature along the length of the fin obtained from simulation and analytical method. Maximum difference of 1.47% is observed between the simulated and the analytical values.

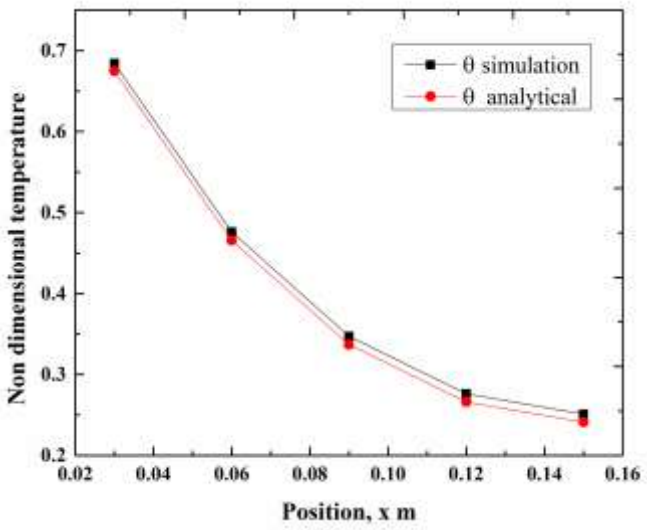

Figure 8.2 Comparison between simulation and analytical method

8.2.3 Grid independence test

Simulation is carried out using ANSYS 14.5 tool to obtain temperature distribution and velocity profile. Grid independence is carried out to fix the number of grids which helps reduce the computational cost and time. To carry out grid independence study, the temperature at five different locations (30mm, 60mm, 90mm, 120mm, 150mm) along the length of fin is considered. Maximum temperature difference is observed as 3.2°C between 18494 and 22722 nodes. Also, maximum of 1.2°C is observed between 25088 and 28457. When nodes of 18494 and 25088 are compared with the nodes of 28457, the average deviation in temperature for all five locations are found to be 0.28% and 0.19% respectively.

Table 8.3 Grid independence study

	Temperature at Position (x, y) mm				
Nodes	1.5,30	1.5,60	1.5,90	1.5,120	1.5,150
13294	392.67	377.62	365.89	359.00	355.66
18494	395.92	379.70	367.16	359.78	356.17
22722	394.53	376.74	363.83	356.47	352.97
25088	**396.32**	**379.83**	**367.57**	**360.04**	**356.67**
28457	396.86	381.05	368.64	360.96	356.65

Therefore, based on the above analysis 25088 nodes is considered for the present study. Table 8.3 shows the grid independence result for the geometry considered.

8.2.4 ANN as the forward model

ANN is a non-iterative method which can be used as forward model to obtain relation between input and output. Section (4.3) in chapter 4 provides the comprehensive information about neural network. ANN acts as a computational tool used to find out relation between large number of input and output data. These known inputs and outputs train the ANN function to give the corresponding unknown outputs to the various different inputs given. This is done by interconnected neurons and processing elements called nodes. Each node is associated with some weights which is used to determine the strength of the signal input to find the output as weighted sum of these different inputs. Figure 8.3 shows the depiction of a typical neural network model. Advantage of using ANN is their ability to large and complex systems with many interrelated parameters.

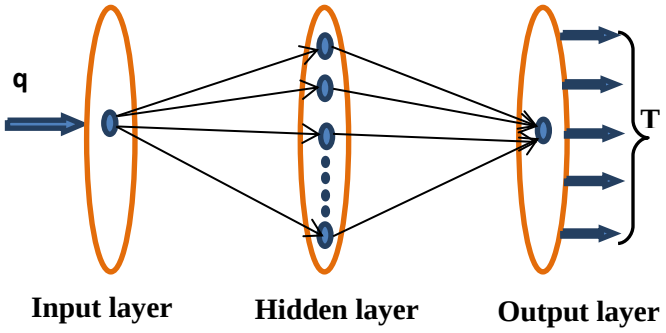

Figure 8.3 Layout of Neural Network

Training is accomplished using a set of network inputs for which the desired outputs are known. A single hidden layer is used in this work because of the linear relation between heat flux and temperature. The selection of the number of hidden neurons is based on the values of some of the common performance metrics used, which is given by the Equation (4.11) and (4.12). This is termed as neuron independence study.

The neuron independence study is carried out which is similar to grid independence study. Such a study is carried out by varying the number of neurons and the changes in training the network are observed. Table 8.4 shows the neuron

independence study and it can be seen that 8 neurons are sufficient for training the network. Training is done based on heat flux as input and the temperature distribution as output. To train the network, a large set of data is obtained from CFD simulations. A typical CFD solution takes 20 - 30 mins to converge whereas ANN takes only few seconds to provide the necessary output.

Table 8.4 Neuron independence study.

No.of neurons	MRE	R^2	R_{test}
4	0.00664	0.99993443	0.997818
6	0.00700	0.999922362	0.999949
8	**0.00608**	**0.999941288**	**0.999949**
10	0.00656	0.999938161	0.997362
13	0.00617	0.999940957	0.997676

Table 8.5 shows the comparison between the temperature obtained from CFD and ANN at a location (x, y), (1.5, 60) mm. A maximum error of 0.9% is noticed which justifies that ANN can be used as forward model without compromising the accuracy.

Table 8.5 Comparison between temperatures obtained from CFD and ANN

q, W/m^2	T_{CFD}	T_{ANN}	Error (%)
930	339.36	338.20	0.34
1050	340.04	343.11	0.90
1280	349.49	351.54	0.58
1450	355.93	356.12	0.05

8.2.5 Sensitivity study for single parameter heat flux

It is important to carry out the sensitivity analysis to determine the behaviour of the unknown parameter before attempting the estimation process. The sensitivity study is carried out to know the behaviour of the temperature with the changes in the estimated parameter. The sensitivity analysis is basically the Jacobian matrix that

investigates the behaviour between the inputs and the outputs. The objective of SA is to identify how the variability in an output quantity of interest (T_i) is connected to an input (P_j) in the model; the result is a sensitivity derivative$\left(\frac{\partial T_i}{\partial P_j}\right)$. Before addressing the estimation of the unknown parameters the behaviour of the determinant of the information matrix $\mathbf{J^T J}$ (Ozisik & Orlande 2000, Cole et al. 2009) is determined. The information matrix is also called as sensitivity matrix J and the entries of the matrix J_{ij} are called sensitivity coefficients. The sensitivity matrix (Ozisik & Orlande 2000) is defined as:

$$\boldsymbol{J(P)} = \left[\frac{\boldsymbol{\partial T^T(P)}}{\boldsymbol{\partial P}}\right]^{\boldsymbol{T}} = \begin{bmatrix} \frac{\boldsymbol{\partial T_1}}{\boldsymbol{\partial P_1}} & \frac{\boldsymbol{\partial T_1}}{\boldsymbol{\partial P_2}} & \frac{\boldsymbol{\partial T_1}}{\boldsymbol{\partial P_3}} & \cdots & \frac{\boldsymbol{\partial T_1}}{\boldsymbol{\partial P_N}} \\ \frac{\boldsymbol{\partial T_2}}{\boldsymbol{\partial P_1}} & \frac{\boldsymbol{\partial T_2}}{\boldsymbol{\partial P_2}} & \frac{\boldsymbol{\partial T_2}}{\boldsymbol{\partial P_3}} & \cdots & \frac{\boldsymbol{\partial T_2}}{\boldsymbol{\partial P_N}} \\ \vdots & \vdots & \vdots & & \vdots \\ \frac{\boldsymbol{\partial T_I}}{\boldsymbol{\partial P_1}} & \frac{\boldsymbol{\partial T_I}}{\boldsymbol{\partial P_2}} & \frac{\boldsymbol{\partial T_I}}{\boldsymbol{\partial P_3}} & \cdots & \frac{\boldsymbol{\partial T_1}}{\boldsymbol{\partial P_N}} \end{bmatrix}$$

The present work involves Navier Stokes equations and it is not easy to obtain the Jacobian Matrix. As a representative case, the steady state temperature using Green's function (Cole et al. 2009) is considered for a fin with high thermal conductivity and an attempt has been made to calculate the sensitivity coefficient. The steady state temperature is given as,

$$T(x,t) - T_\infty = \frac{qL}{k}\frac{\left(e^{-mx} - e^{-m(2L-x)}\right)}{mL(1+e^{-2mL})} \tag{8.9}$$

$$\frac{\partial \mathrm{T_i}}{\partial \mathrm{q}} = \left(\frac{\mathrm{e^{-mx_i} - e^{-m(2L-x_i)}}}{\mathrm{mL(1+e^{-2mL})}}\right)\frac{\mathrm{L}}{\mathrm{k}} \tag{8.10}$$

The sensitivity coefficient with respect to an unknown parameter $\boldsymbol{P}$ is determined by differentiating the solution with respect to $\boldsymbol{P}$. The plot of sensitivity coefficient is shown in Figure 8.4.When the determinant of $J^TJ \approx 0$, the inverse problem is then ill-conditioned. Therefore it is desirable to have linearly-independent sensitivity coefficients J_{ij} with large magnitudes, such that the inverse problem is not very sensitive to measurement errors and accurate estimates of the parameters can be obtained. From Figure 8.4 it is seen that the trend of the graph is decreasing and one can come to a conclusion that the estimation of heat flux is possible when the

temperature sensor is closer to the base of the fin due to high sensitivity coefficient J_{ij} and it tends to zero as we move from base of the fin towards tip.

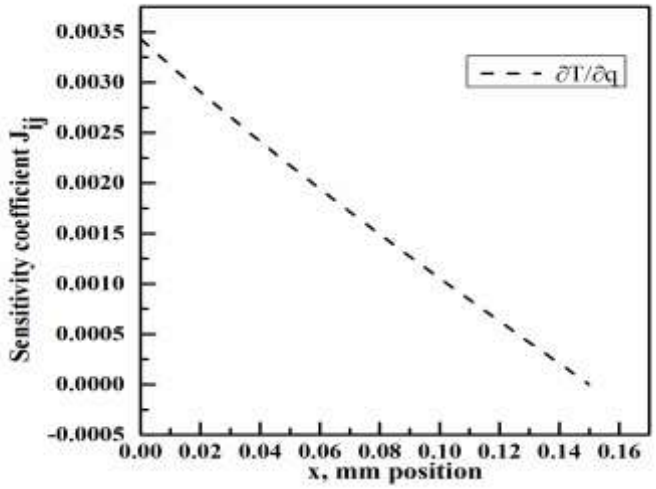

Figure 8.4 Plot of sensitivity coefficients along with positions.

8.2.6 3D computational model

Three dimensional computational model of the fin and the base assembly is created using ANSYS FLUENT. The computational model is shown in Figure 8.5 along with the boundary conditions. The numerical model consists of an extended domain in which air is present and Boussinesq approximation is incorporated so as to account for natural convection. Grid independence study which is shown in Table 8.6, is performed for a heat flux of 304 W/m^2. Based on the study, 1203824 nodes are considered for the numerical analysis.

The governing equations of the present study are given below which are same as the one used in chapter 7.

Continuity:

$$\frac{\partial u}{\partial x}+\frac{\partial v}{\partial y}+\frac{\partial w}{\partial z}=0 \tag{8.11}$$

X-momentum equation:

$$u\frac{\partial u}{\partial x}+v\frac{\partial u}{\partial y}+w\frac{\partial u}{\partial z}=-\frac{1}{\rho}\frac{\partial p}{\partial x}+\vartheta\left(\frac{\partial^2 u}{\partial x^2}+\frac{\partial^2 u}{\partial y^2}+\frac{\partial^2 u}{\partial z^2}\right) \tag{8.12}$$

Y-momentum equation:

$$u\frac{\partial v}{\partial x}+v\frac{\partial v}{\partial y}+w\frac{\partial v}{\partial z}=-\frac{1}{\rho}\frac{\partial p}{\partial y}+\vartheta\left(\frac{\partial^2 v}{\partial x^2}+\frac{\partial^2 v}{\partial y^2}+\frac{\partial^2 v}{\partial z^2}\right)+g\beta(T-T_\infty) \quad (8.13)$$

Z-momentum equation:

$$u\frac{\partial w}{\partial x}+v\frac{\partial w}{\partial y}+w\frac{\partial w}{\partial z}=-\frac{1}{\rho}\frac{\partial p}{\partial z}+\vartheta\left(\frac{\partial^2 w}{\partial x^2}+\frac{\partial^2 w}{\partial y^2}+\frac{\partial^2 w}{\partial z^2}\right) \quad (8.14)$$

Energy equation for fluid:

$$u\frac{\partial T}{\partial x}+v\frac{\partial T}{\partial y}+w\frac{\partial T}{\partial z}=\alpha\left(\frac{\partial^2 T}{\partial x^2}+\frac{\partial^2 T}{\partial y^2}+\frac{\partial^2 T}{\partial z^2}\right) \quad (8.15)$$

Energy equation for fin and base:

$$k_s\left(\frac{\partial^2 T}{\partial x^2}+\frac{\partial^2 T}{\partial y^2}+\frac{\partial^2 T}{\partial z^2}\right)=0 \quad (8.16)$$

Figure 8.5 depicts the materials used and the boundary conditions of the present problem. At the inlet, the following boundary conditions are imposed,

$$u=0\ v=0\ z=0\ T=T_\infty \quad (8.17)$$

At the outlet of the domain the following boundary condition is used,

$$\frac{\partial^2 v}{\partial y^2}=0 \qquad \frac{\partial^2 u}{\partial y^2}=0 \qquad \frac{\partial^2 z}{\partial y^2}=0 \qquad \frac{\partial^2 T}{\partial y^2}=0 \quad (8.18)$$

The x-face of the domain as represented in Figure5 is subjected to,

$$u=0 \quad v=0 \quad z=0 \quad \frac{\partial T}{\partial x}=0 \quad (8.19)$$

Also z-face of the domain is subjected to,

$$u=0 \quad v=0 \quad z=0 \quad \frac{\partial T}{\partial z}=0 \quad (8.20)$$

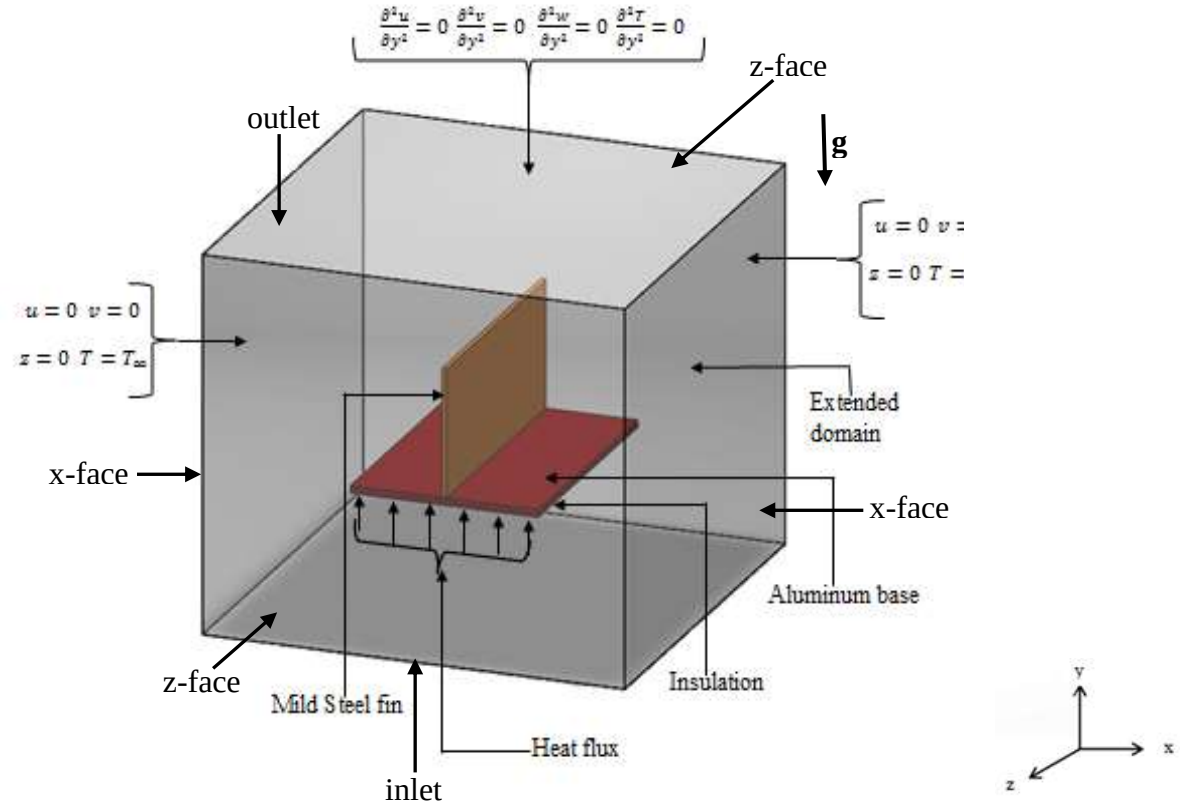

Figure 8.5 3D Computational Model

Along the sides of the fin, the kind of boundary condition imposed is solid-liquid interface hence the energy transfer between the fin faces to the air in the extended domain is by convection. The contact region between the fin and the base is defined as solid-solid interface and transfer of energy at this region is through conduction, where the wall of the fin and the aluminium base is treated as coupled wall. No slip condition is applied along all solid walls. All these regions are treated as interfaces

At region where aluminium base is in contact with fluid, the boundary condition is written as,

$$k_{al}\frac{\partial T}{\partial n} = k_f\frac{\partial T}{\partial n} \quad \text{and} \quad T_{aluminum} = T_{fluid} \tag{8.21}$$

Similarly, the region where mild steel is in contact with fluid, it can be written as,

$$k_{ms}\frac{\partial T}{\partial n} = k_f\frac{\partial T}{\partial n} \quad \text{and} \quad T_{mildsteel} = T_{fluid} \tag{8.22}$$

The contact region between base and fin is defined as

$$q_{cond,aluminum} = q_{cond,mild\ steel\ fin} \tag{8.23}$$

$$k_{al}\frac{\partial T}{\partial n} = k_{ms}\frac{\partial T}{\partial n} \quad \text{and} \quad T_{aluminum} = T_{mildsteel} \tag{8.24}$$

Table 8.6 Grid Independence test

Nodes	Maximum temperature, K
822494	325.76
1203824	**324.38**
2395862	325.14

8.2.7 Experimental setup

Steady state experiments are conducted on horizontal orientation of the base and the corresponding temperature distributions are recorded. One end of the calibrated thermocouples is placed along the length of the fin and the other end is connected to DAQ. The temperature distribution based on experiments and simulations is shown in Figure 8.6

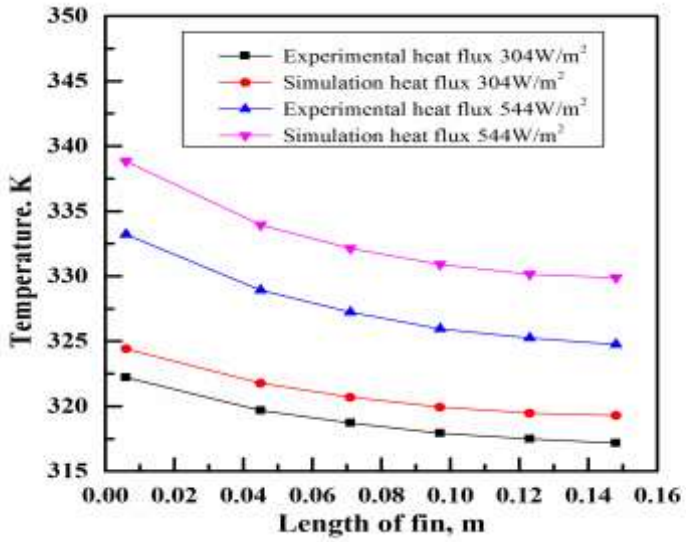

Figure 8.6 Comparison between simulation and experimental data

8.2.8 ANN as forward model for 3D model

Use of ANN as forward model and its advantage has already been discussed in the earlier chapters. It is pertinent to mention that the solution to the inverse problem

requires sampling of the unknown parameters using MCMC algorithm. Furthermore, the iterative process becomes cumbersome when CFD solutions are used as the forward model. Therefore, ANN replaces the conventional CFD solution in order to reduce the computational cost. Input in the form of heat flux and heat transfer coefficient is given to the neural network. The simulated data used for training the network is shown in Table A3 in Appendix. Similarly, neuron independence study is carried out to obtain reliable output from the neural network and is shown in Table 8.7. The comparison between the temperature obtained from simulation and neural network is shown in Table 8.8.

Table 8.7 Neuron independence study

Number of neurons	MRE	R^2
6	0.010602136	0.999848021
14	0.046005804	0.996379603
18	**0.005979928**	**0.999939249**

Table 8.8 Comparison of temperature between simulation and ANN

Location, m	q = 700W/m^2, h = 4.044W/m^{2}K		q = 1800W/m^2, h = 4.086W/m^{2}K		q = 2400W/m^2, h = 5.897W/m^{2}K	
	T_{CFD}	T_{ANN}	T_{CFD}	T_{ANN}	T_{CFD}	T_{ANN}
0.006	350.007	351.092	403.344	401.539	429.933	426.557
0.071	341.307	339.174	383.374	381.335	401.698	401.794
0.123	338.728	338.110	377.558	375.746	393.441	393.293

From the table, a maximum error of only 0.78% is observed between simulation and ANN. These results further corroborate the use of ANN as forward model.

8.2.9 Sensitivity study for two parameters

Sensitivity study for the two unknown parameters is discussed. The sensitivity coefficient is expressed as,

$$J_{ij} = \frac{\partial T_i}{\partial P_j} = \frac{T_i(P_1 \ldots\ldots, P_j + \Delta P_j \ldots\ldots, P_N) - T_i(P_1 \ldots\ldots, P_j \ldots\ldots, P_j)}{\Delta P_j} \quad (8.25)$$

Where J_{ij} is the sensitivity coefficient, T_i is the i^{th} estimated temperature, P_j is the j^{th} unknown parameter, ΔP_j is the change in the unknown parameter. When the magnitude of J_{ij} is small, it indicates that large changes in P_j results in small changes in T_i. In such case, the estimation of unknown parameters is exceedingly difficult.

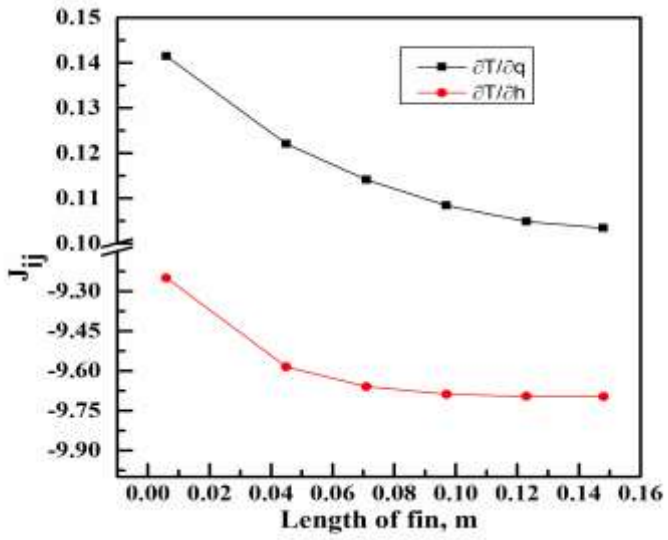

Figure 8.7 Sensitivity plot

The magnitude of the sensitivity coefficient of heat flux, shown in Figure 8.7, is found to be less and positive, while the other sensitivity coefficient is negative. The sensitivity coefficient of the heat flux and the heat transfer coefficient show linear dependence among them hence the simultaneous estimation of the heat flux and the heat transfer coefficient is more difficult without *a priori* information and also the magnitude of the sensitivity coefficient of the heat flux which is close to zero.

8.3 RESULTS AND DISCUSSION

8.3.1 Forward solution from CFD

The results of the 2D numerical model in terms of the temperature distribution and velocity plot for the heat flux value of 1280 W/m^2 are shown in Figure 8.8 and 8.9 respectively. The temperature decreases along the height of the fin as a result of natural convection where the cold air is able to absorb more heat at the bottom compared to the top portion of the fin.

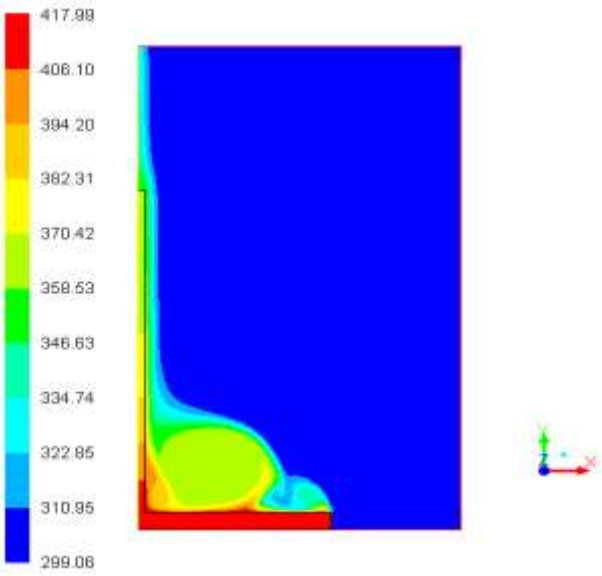

Figure 8.8 Temperature plot obtained from numerical simulation for heat flux value of 1200W/m^2

Numerical simulations are carried out with known boundary conditions and the convergence criterion is set to 1e-6. The heat flux applied at the base is varied from 1100 to 3100W/m^2. The heat flux range is selected such that the Rayleigh number is found to be 1.7e7 which is less than the critical value; thus, the flow is assumed to be laminar. Variation of temperature along the length of the fin for different heat flux is shown in Figure 8.10.

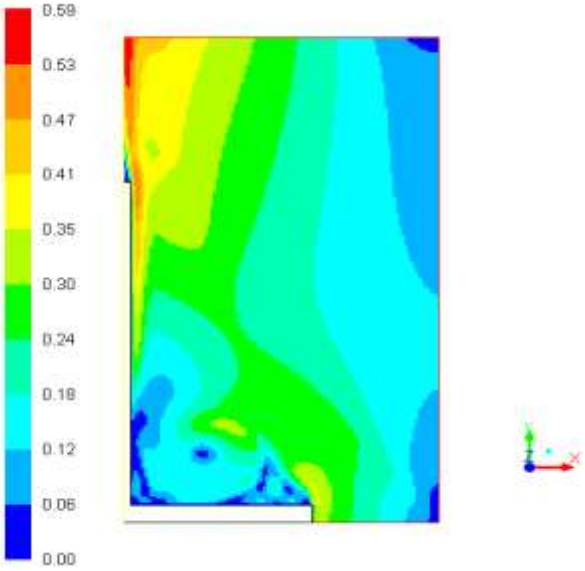

Figure 8.9 Velocity contour for heat flux of 1200W/m^2

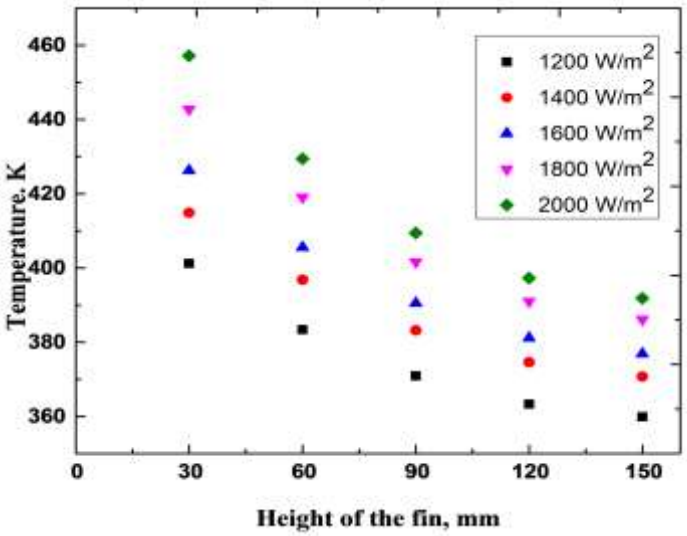

Figure 8.10 Temperature distributions along the height of the fin for different heat flux input

8.3.2 Estimation of single parameter heat flux using 2D numerical model.

Estimation of heat flux using Bayesian framework is initially attempted for simulated measurements. PPDF is calculated based on the Markov chain Monte Carlo method along with Metropolis-Hastings algorithm. In this work, heat flux is estimated with and without subjective prior. When uniform prior is considered, the PPDF is directly proportional to the likelihood function. The forward model measurement error is assumed to be 5% and the effect of number of samples on the estimation is discussed

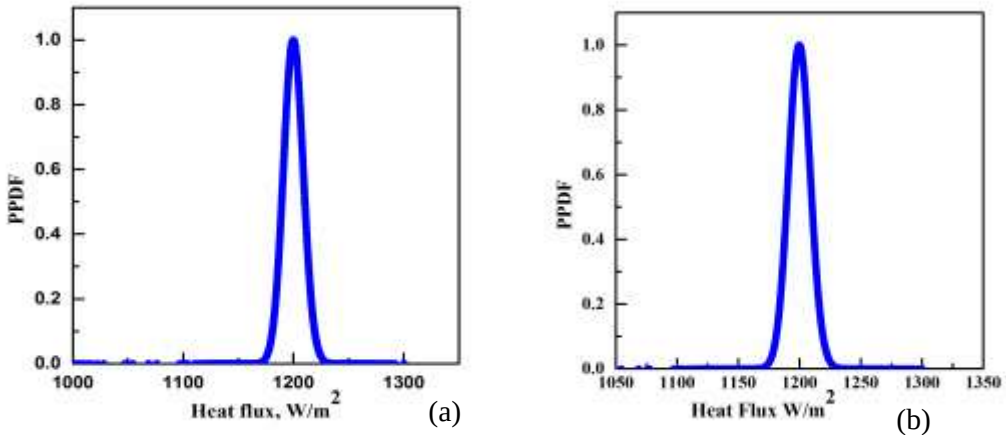

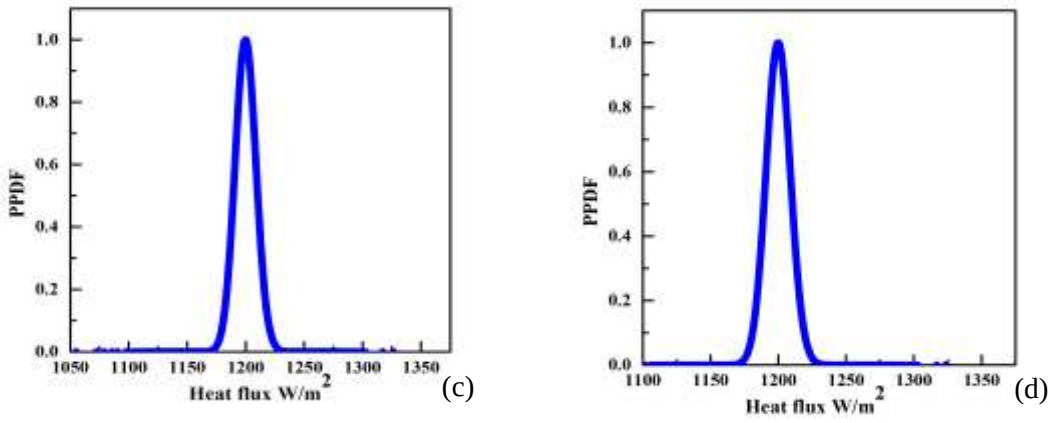

Figure 8.11 PPDF plot for (a)= 5000 samples (b) = 10000 samples (c) =15000 samples (d) = 20000 samples

in Table 8.9. It is observed that as the number of samples is increased the changes in the point estimates are negligible. Thus, the number of samples is limited to 5000 as a result of less computational time.

Table 8.9 Effect of sample size on Bayesian retrieval of heat flux

Heat flux, q W/m^2	Number of samples	Bayesian retrieved values for q(W/m^2)	
		Mean	SD
1200	5000	1200.27	10.005
	10000	1200.36	10.085
	15000	1200.26	10.194
	20000	1200.71	10.028

The PPDF of heat flux 1200W/m^2 plotted against different samples is shown in Figure 8.11. The mean and SD of the estimated heat flux is reported in Table 8.9 and there is no much difference in the values of the heat flux estimated for different samples.

Figure 8.12 represents the Markov states of the heat flux with initial guess of 800W/m^2 and is clearly seen that the samples oscillate with respect to the mean 1200W/m^2. When a Gaussian prior is incorporated, the PPDF now becomes Equation (5.4) given in chapter 5.

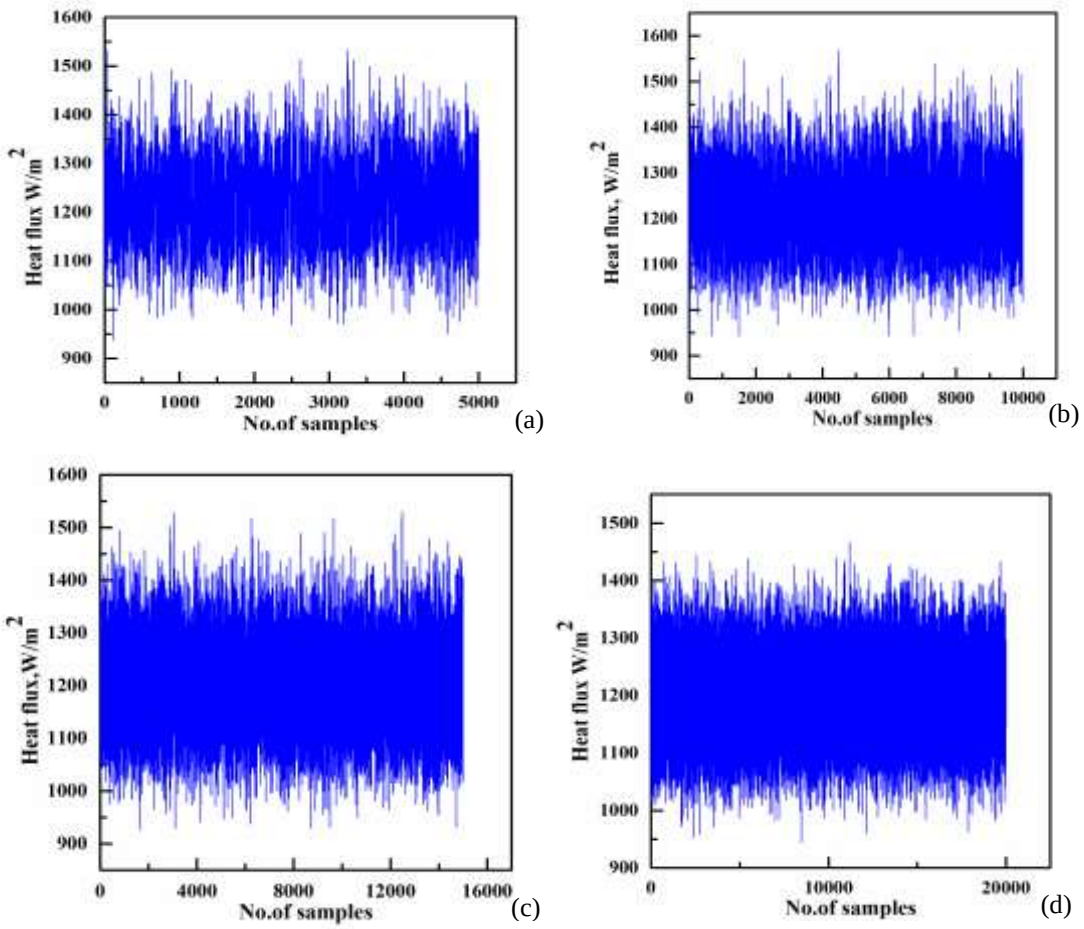

Figure 8.12 Frequency histogram data of heat flux 1200W/m^2 for (a) =5000samples (b) =10000samples (c) = 15000samples (d)=20000samples

Table 8.10 Retrieved values of heat flux using MH-MCMC with prior and without prior

Heat flux	Prior model	Number of samples =5000		Number of samples =10000	
		Mean	SD	Mean	SD
930	Uniform	929.76	8.675	929.93	8.552
	Normal	929.41	7.747	929.31	7.686
1050	Uniform	1050.25	8.587	1050.11	8.774
	Normal	1047.90	7.518	1048.10	9.428
1450	Uniform	1451.47	13.900	1451.26	15.351
	Normal	1447.00	14.905	1447.10	14.751

The expression for the Gaussian prior is given by Equation (5.3). From Table 8.10 it is seen that the assumed value of heat flux used to obtain simulated temperature and the heat flux estimated using MH-MCMC algorithm agrees very well for both the prior models considered. The estimated heat fluxes are reported as mean and standard deviation. There is no much difference between the heat flux values estimated by using uniform prior and normal prior. The use of Gaussian prior helps reduce the standard deviation of the estimates. Table 8.10 also shows the comparison between number of samples considered for the estimation process. There is no remarkable difference between the values estimated by using 5000 samples and 10000 samples. The concept of burn in has been adopted to avoid the influence of initial guess i.e., first 1000 samples are not considered to calculate mean and SD. The entire estimation procedure is repeated for different heat flux. As a result, the robustness of the Bayesian framework along with MH-MCMC algorithm is proved using simulated measurements and the estimation of boundary heat flux for the conjugate heat transfer problem is successfully demonstrated with and without prior knowledge. Figure 8.13 shows the posterior probability density function of the retrieved values of heat flux with uniform prior and normal prior respectively. Temperature residuals are calculated in order to assess the model used for the inverse analysis and for the retrieved value of 1447W/m^2 the value is found to be 5.47E-03.

Figure 8.14 shows the Markov chain of the heat flux 1200W/m^2. The robustness of the methodology is further tested for two different initial guesses i.e., 800W/$m^2$and 1800W/m^2 and the Markov states quickly converge to the actual heat flux of 1200 W/m^2 within 500 samples which are evident from Figure 8.14 (a) and (b) respectively.

8.3.3 Estimation of heat flux from perturbed data

In reality the temperature distribution cannot be pure and the presence of random noise is observed when experiments are performed. In view of this, the measurement data is contaminated with Gaussian errors that can cause large deviations of the final solution from the exact solution. To mimic experimental data, the simulated data is now added with noise at various levels i.e., the forward model is solved for the known heat flux and the temperature distribution obtained is perturbed by adding Gaussian

noise such as 0.1K and 0.5K. This represents noisy data similar to the experimental temperature. Therefore, the estimation of heat flux becomes challenging when the simulated measurements contain noise. The estimation results with 0.1K and 0.5K noise in the data are shown in Table 8.11.

With the noise level of (σ = 0.5K) which in terms of measurement level will be 3σ (1.5K), the error in the estimation is 1.2%. When prior information about the parameter is incorporated, even with the noisy data the estimated values are closer to the actual value compared to the uniform prior case. The PPDFs plot for the perturbed data for both uniform prior and normal prior at noise levels 0.1K and 0.5K are shown in Figures 8.15 and 8.16 respectively. When normal prior is used for estimation, the estimated values are closer to the actual value whereas the value obtained from uniform prior deviates from the actual value signifying that when non-informative prior is used, the standard deviation of the estimates reduces drastically. It has also been observed from Table 8.11 that the standard deviation of the estimates using normal prior is lesser than the uniform prior for all heat fluxes. This is due to the a priori information of the unknown parameter which simplifies the Markov chain process.

	Uniform prior	Normal prior
Heat flux, 930 W/m^2	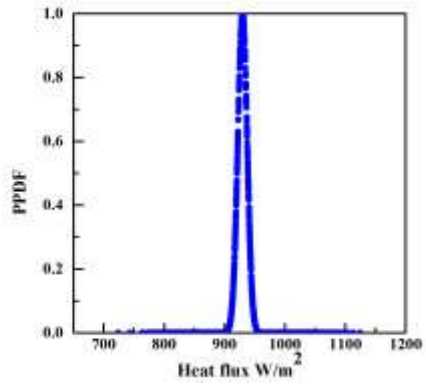	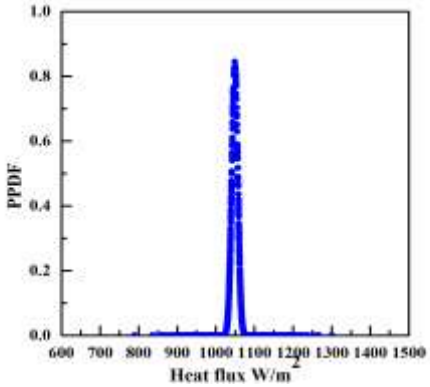
Heat flux, 1050 W/m^2	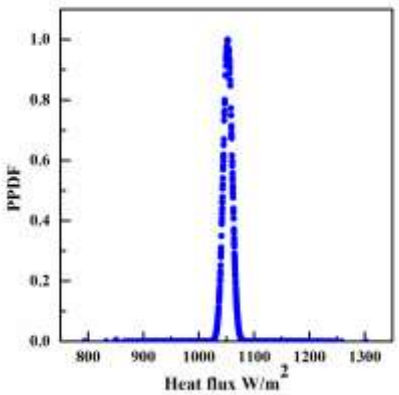	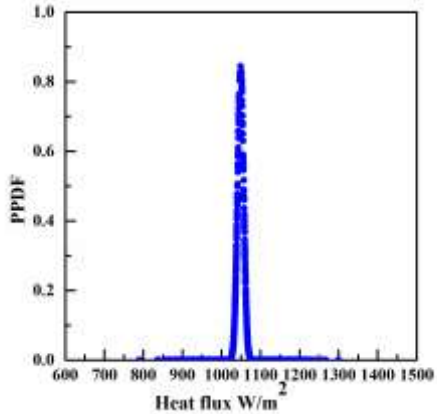
Heat flux, 1450 W/m^2	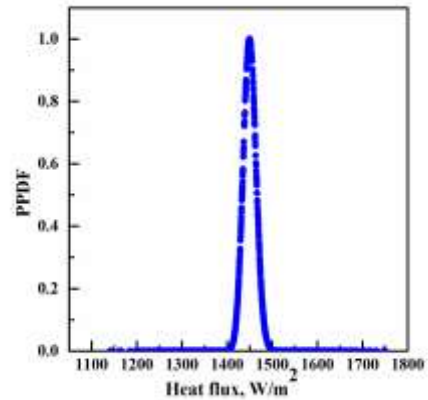	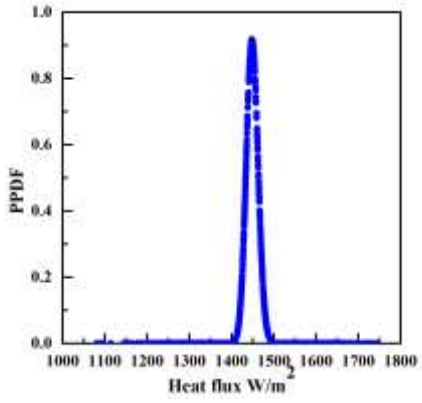

Figure 8.13 PPDF for different heat flux values with uniform and normal prior.

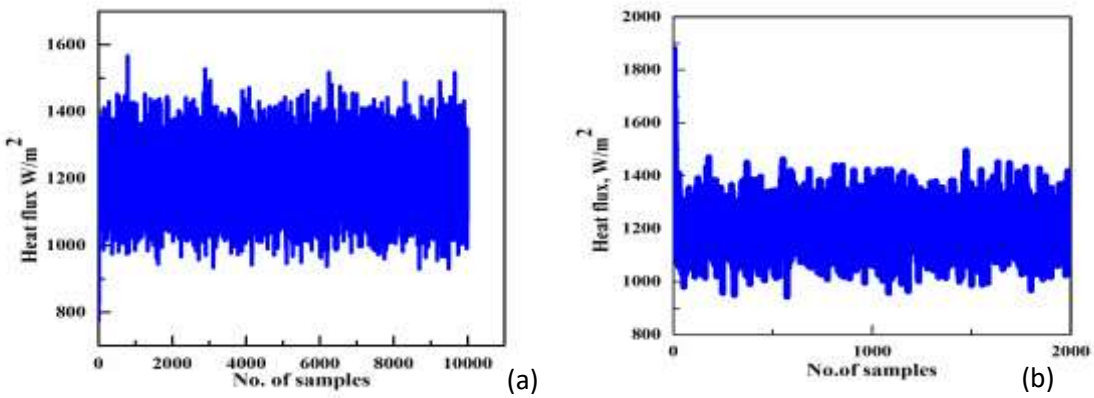

Figure 8.14 Sampling distribution for heat flux1200W/m^2 with initial guess (a) = 800W/m^2 (b) = 1800W/m^2.

Table 8.11 Estimation of heat flux for perturbed data at different noise levels.

Heat flux, W/m^2	Prior model	Noise level = 0.1K		Noise level = 0.5K	
		Mean	SD	Mean	SD
930	Uniform	932.17	8.533	942.28	8.731
	Normal	930.16	8.754	938.72	8.591
1050	Uniform	1052.6	8.902	1062.8	8.860
	Normal	1050.4	8.892	1059.2	8.317
1450	Uniform	1455.0	15.681	1473.4	16.036
	Normal	1451.5	17.103	1466.7	17.427

Table 8.12 Estimation of heat flux using Gaussian prior

Heat flux, W/m^2	Gaussian prior		q W/m^2, Retrieved	
	μ_p(q)	σ_p(q)	Mean	SD
930	850	45.5	926.65	9.240
	850	51	927.90	9.236
	850	76.5	928.61	8.999
1050	950	47.5	1045.9	7.803
	950	57	1046.0	9.309
	950	85.5	1048.4	8.933
1450	1350	65	1445.1	15.339
	1350	78	1446.3	16.656
	1350	117	1448.3	16.263

For the incorporation of Gaussian prior the standard deviation is considered as $\{\sigma_p$ = 0.05, 0.06, 0.09$\}$ of the Gaussian mean. Different combinations of Gaussian mean and standard deviation are considered. From Table 8.12, it also shows that when σ_p = 0.09 the mean estimate is closer to the actual value of the heat flux. For the heat flux of $930W/m^2$, several combinations of mean and standard deviation are used and it was observed that when the mean value was below $700W/m^2$ the estimated values are deviating from the actual values. Figure 8.17 shows the comparison of PPDF obtained for heat flux value of 1450 W/m^2 at 0.1 K noise levels, when uniform and normal prior are used during estimation. It is clearly observed that the standard deviation of the PPDF for normal prior is lesser than that of the standard deviation of the PPDF for uniform prior. This strongly proves the fact that incorporating prior information in the Bayesian framework will result in minimizing the uncertainty associated with the estimated parameters.

Noise level = 0.1K		
	Uniform a-priori	Normal a-priori
Heat flux, 930W/m^2	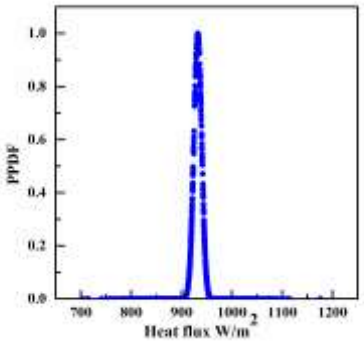	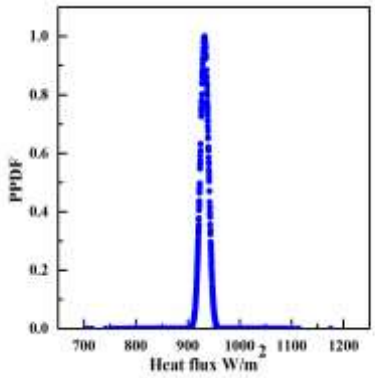
Heat flux, 1050W/m^2	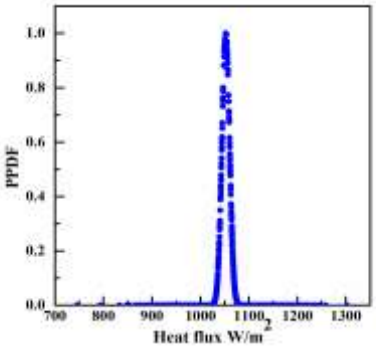	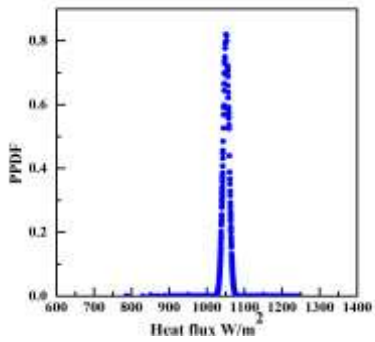
Heat flux,1450W/m^2	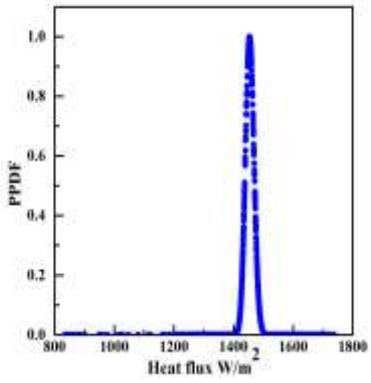	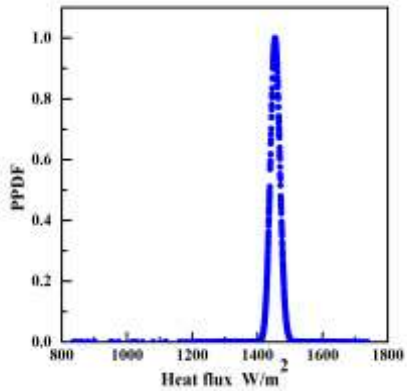

Figure 8.15 PPDF at noise level = 0.1K

Noise level = 0.5K		
	Uniform a-priori	Normal a-priori
Heat flux, 930W/m^2	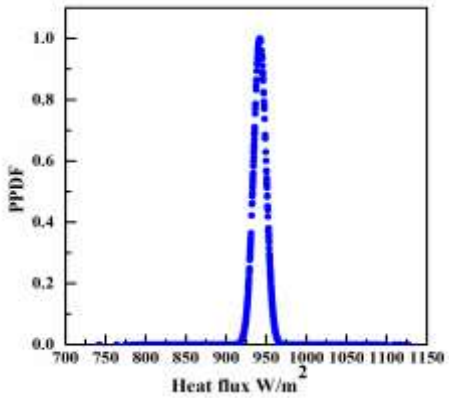	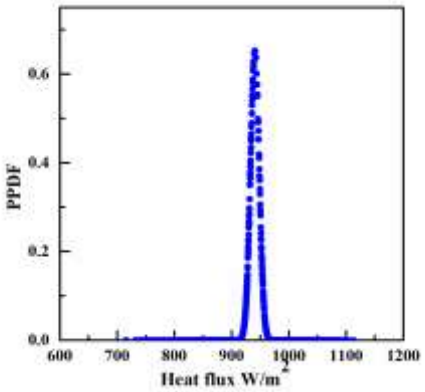
Heat flux, 1050W/m^2	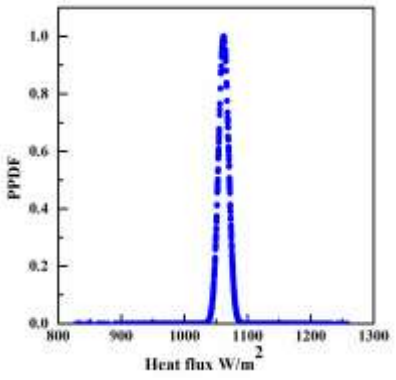	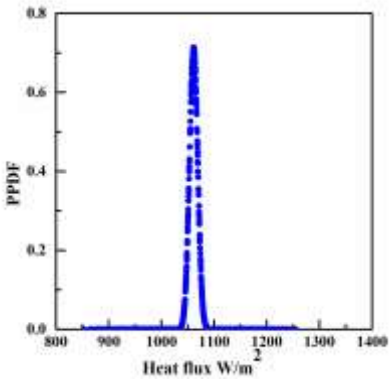
Heat flux,1450W/m^2	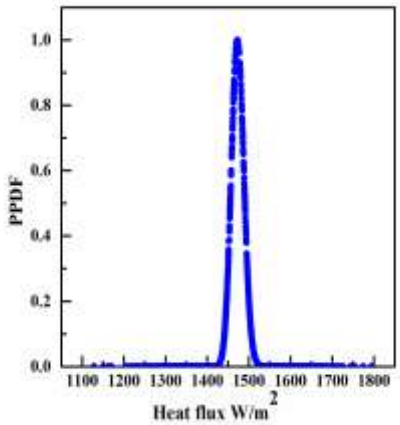	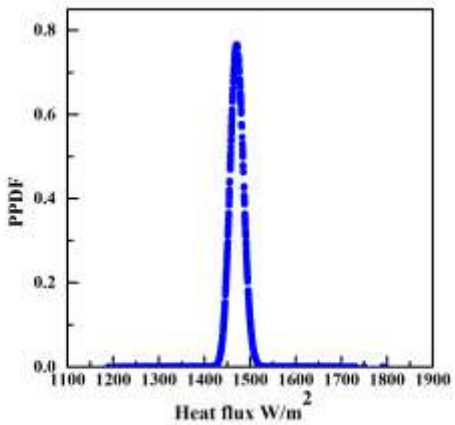

Figure 8.16 PPDF at noise level = 0.5K

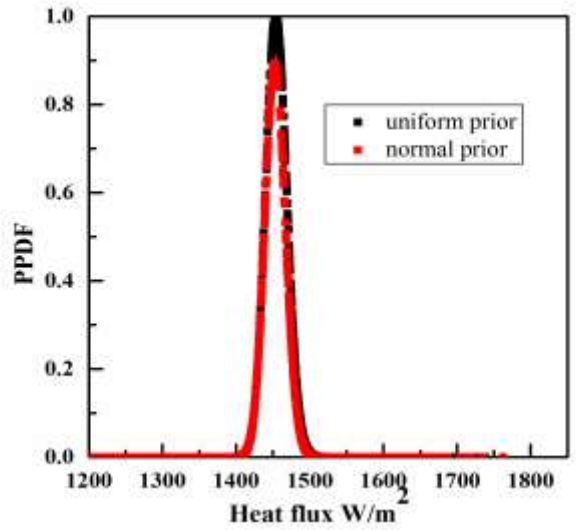

Figure 8.17 Comparison of PPDF for 1450 W/m^2 at 0.1K noise level.

8.3.4 Simultaneous estimation of heat flux and heat transfer coefficient for the experimental data

The primary aim of the work is the simultaneous estimation of heat flux and heat transfer coefficient from the available temperature data. Nevertheless, the Bayesian framework provides a window in to the simultaneous estimation of heat flux and heat transfer coefficient with the help of *a priori* knowledge. To accomplish this, the combination of MCMC-MH algorithm is used along with the prior information. Like previous analysis, the effect of sample size has been carried out for the simultaneous estimation of two unknown parameters. Three different samples 5000, 10000 and 20000 are considered and the estimation for heat flux value of 700W/m^{2}and heat transfer coefficient of 4.04W/m^{2}K in terms of mean and SD is shown in Table 8.13.

Table 8.13 Effect of sample size on estimation.

Number of samples	Heat flux, W/m^2		Heat transfer coefficient, W/m^{2}K		Time(s)
	Mean	SD	Mean	SD	
5000	686.48	23.488	3.70	0.388	548.9951
10000	688.12	23.854	3.73	0.374	1065.814
20000	687.81	22.569	3.75	0.387	2090.159

There is no much difference in the values of heat flux and heat transfer coefficient among the samples considered, as a result, sample size of 5000 has been selected for further study. Table 8.14 shows the results for the simultaneous estimation of the heat flux and heat transfer coefficient for the simulated data in terms of mean and SD. The value of σ_{prior} considered is 5% of the mean value.

Table 8.14 Simultaneous estimation for simulated data.

Actual		Retrieved Heat flux, W/m^2		Retrieved heat transfer coefficient, W/m^2K	
Heat flux, W/m^2	Heat transfer coefficient, W/m^2K	Mean	SD	Mean	SD
700	4.04	690.92	23.488	3.783	0.388
1000	3.86	990.36	37.110	3.890	0.300
1800	4.09	1778.42	77.271	3.864	0.307

The maximum error observed in the estimation of parameters from the Table 8.14 is 1.29%. The PPDF plot for heat flux value of $700W/m^2$ and heat transfer coefficient $4.04W/m^2K$ is shown in Figure 8.18 and PPDF plot for $1800W/m^2$ and heat transfer coefficient $4.09W/m^2K$ is shown in Figure 8.19. The temperature residual for the estimated heat flux is given in Table 8.15.

Table 8.15 Temperature residual

Location,m	Temperature from forward model heat flux $1800W/m^2$	Temperature from estimated heat flux 1778.42 W/m^2	Residual
0.006	419.770	419.730	9.4575E-05
0.071	354.164	353.993	4.8282E-04
0.123	364.521	364.462	1.6315E-04

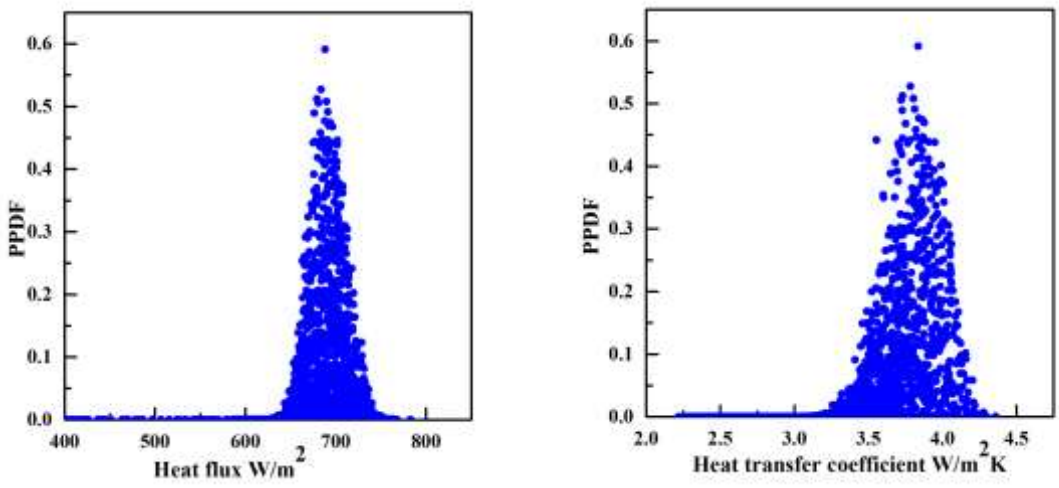

Figure 8.18 PPDF plot for heat flux 700W/m^2 and heat transfer coefficient 4.04W/m^{2}K with σ_{prior}= 5% of the mean.

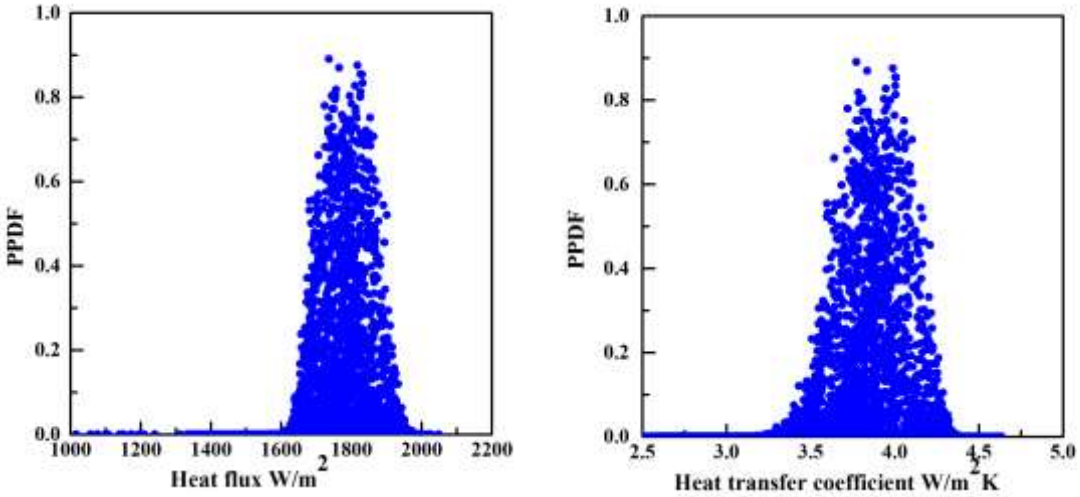

Figure 8.19 PPDF plot for heat flux 1800W/m^2 and heat transfer coefficient 4.09W/m^{2}K with σ_{prior}= 5% of the mean.

With the successful estimation of the parameters for the simulated data, the estimation is now extended to the measured data. Experiments are conducted for different power levels and the temperature is recorded. Now this information is used for the simultaneous estimation of the parameters. Table 8.16 shows the estimation of parameters with mean and SD. The Gaussian prior used for actual heat flux of

544W/m^2 and heat transfer coefficient of 3.89W/m^{2}K is, mean (q) =450, $\sigma(q)$=23 and mean (h)= 3.5, $\sigma(h)$=0.18 respectively. Similarly, for the heat flux of 853 W/m^2 and heat transfer coefficient of 2.57W/m^{2}K the Gaussian prior used is mean (q) = 780, $\sigma(q)$=39 and mean (h) =3, $\sigma(h) = 0.13$ respectively.

Table 8.16 Simultaneous estimation using experimental temperature

Actual		Retrieved Heat flux, W/m^2		Retrieved heat transfer coefficient, W/m^{2}K	
Heat flux, W/m^2	Heat transfer coefficient, W/m^{2}K	Mean	SD	Mean	SD
544	3.89	483.88	15.599	3.88	0.168
853	2.57	808.69	42.354	2.17	0.032

For the heat flux 544W/m^2 and heat transfer coefficient 3.89W/m^{2}K the error observed is 11% and 0.25% respectively. Similarly for the heat flux of 853W/m^2 and heat transfer coefficient 2.57W/m^{2}K the error observed is 5.19% and 15.56%. The PPDF plot for 544W/m^2 and 3.86W/m^{2}K is shown in Figure 8.20. And PPDF plot for 853W/m^2 and 2.57W/m^{2}K is shown in Figure 8.21.

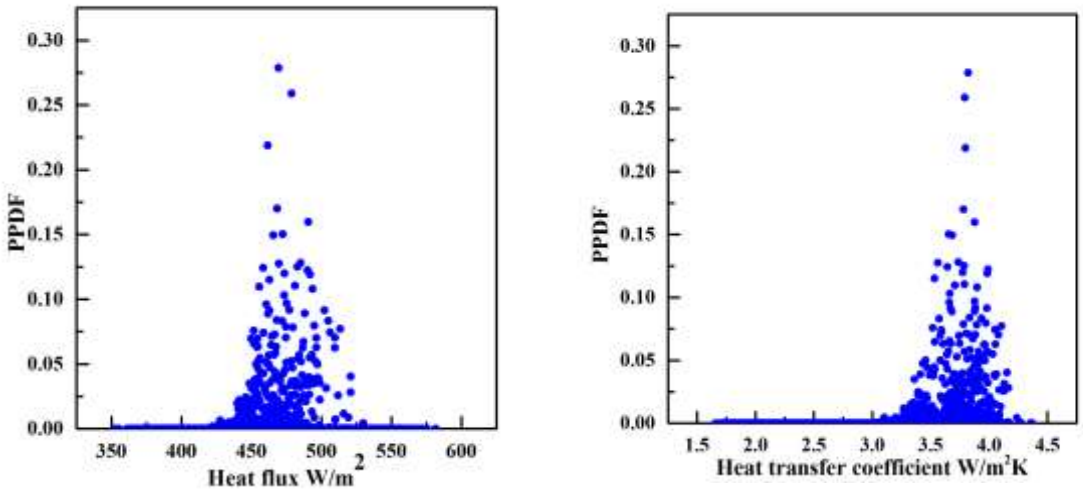

Figure 8.20 PPDF plot heat flux 544W/m^2 and heat transfer coefficient 3.89W/m^{2}K

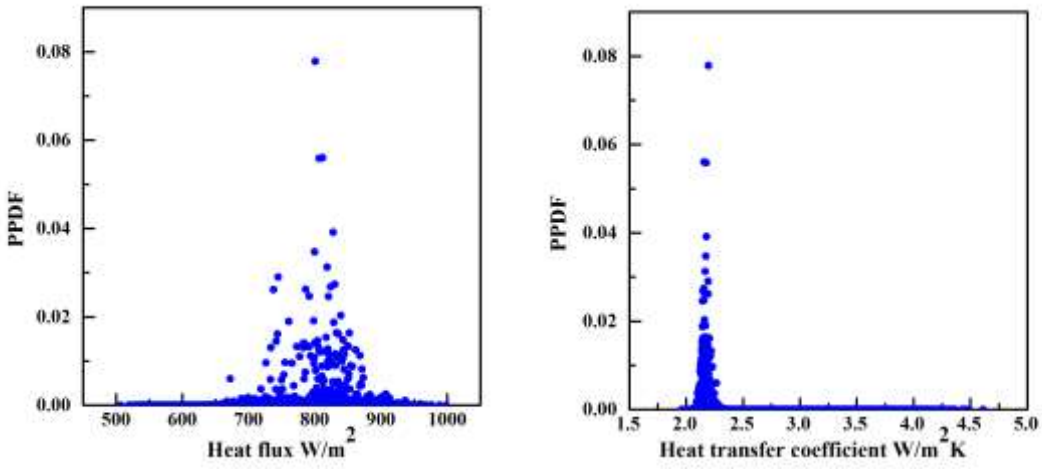

Figure 8.21 PPDF plot heat flux 853W/m^2 and heat transfer coefficient 2.57W/m^2K

8.4 CONCLUSIONS

In this chapter 2D and 3D computational model of steady state conjugate heat transfer from fin was considered. The fin setup was modelled using ANSYS fluent and simulations were carried out to obtain the temperature distribution. Grid independence study was carried out to fix the number of grids. The data obtained from simulation was used to train the network. ANN acts as the forward model to obtain temperature distribution for various heat fluxes. Validation of the ANN results is done with the output of CFD and a maximum error of 0.90% has been observed. Hence, CFD is replaced by ANN as the forward model. With ANN contributing as forward model, Bayesian inference method was successfully implemented as inverse method to estimate the unknown heat flux. The MCMC with MH algorithm has been explored to estimate the heat flux for the simulated data considering 2D simulation data. The unknown heat flux was also retrieved for the noisy simulated data with good accuracy. Gaussian prior has been incorporated for the unknown parameters. Steady state heat transfer experiments were conducted and simultaneous estimation of heat flux and heat transfer coefficient has been done, the data considered in this case is the 3D simulation data. Sensitivity study has also been discussed. The computation cost was drastically reduced with the use of ANN as the forward model.

8.5 Closure

This chapter dealt with the estimation of single parameter estimation and simultaneous estimation of two parameters for a conjugate heat transfer problem. Bayesian framework has been used as inverse model in conjunction with ANN for the estimation for both 2D and 3D geometric model. The next chapter deals with the application of the inverse problem for the simultaneous estimation of heat generation and heat transfer coefficient for a Teflon cylinder.

CHAPTER 9

AN MARKOV CHAIN MONTE CARLO-METROPOLIS HASTINGS APPROACH FOR THE SIMULTANEOUS ESTIMATION OF HEAT GENERATION AND HEAT TRANSFER COEFFICIENT FROM A TEFLON CYLINDER

9.1 INTRODUCTION

This chapter deals with the simultaneous estimation of volumetric heat generation and heat transfer coefficient of the Teflon cylinder from experimental data. Bayesian Inference along with MCMC-MH algorithm is used as the inverse method for the estimation process. ANN with back-propagation algorithm is used as the forward model to replace CFD simulation. Initially retrieval of volumetric heat generation is carried out as single parameter estimation later with the knowledge of volumetric heat generation, prior is incorporated within the Bayesian framework and simultaneous estimation of volumetric heat generation and heat transfer coefficient is accomplished.

9.2 FORWARD MODEL

Three-dimensional, steady state, conjugate heat transfer from a Teflon cylinder of dimensions 100 mm diameter and 100 mm length with uniform volumetric internal heat generation is considered. Volumetric heat generation takes place at the centrally located cylindrical aluminum heater. Temperature distribution is obtained throughout the Teflon cylinder. 3-D numerical model is created and cylindrical heater is placed at the center of the model. The material selected is Teflon and its properties are incorporated in the simulation. The internal heat generation q_v causes temperature distribution inside the cylinder and also on its surface. The velocity profiles and convection effects are studied by modeling an extended domain. Air is the medium considered for extended domain with constant thermo-physical properties except density where Boussinesq approximation is invoked to include natural convection. Meshing is done and grid independence study is carried out to fix the number grids for the numerical model. Computations are performed using the commercially available ANSYS FLUENT. A convergence criterion of 10^{-6} on the residual was used to declare convergence. Figure 9.1 shows the computational model used in this work.

The following equations are used to solve the conjugate heat transfer problem.

Continuity

$$\frac{1}{r}\frac{\partial(ru_r)}{\partial r}+\frac{1}{r}\frac{\partial(u_\theta)}{\partial \theta}+\frac{\partial u_z}{\partial z}=0 \tag{9.1}$$

r-momentum equation

$$\rho\left[u_r\frac{\partial u_r}{\partial r}+\frac{u_\theta}{r}\frac{\partial u_r}{\partial \theta}-\frac{u_\theta^2}{r}+u_z\frac{\partial u_r}{\partial z}\right] = -\frac{\partial p}{\partial r}+\rho g_r+\mu\left[\frac{1}{r}\frac{\partial}{\partial r}\left(r\frac{\partial u_r}{\partial r}\right)-\frac{u_r}{r^2}+\frac{1}{r^2}\frac{\partial^2 u_r}{\partial \theta^2}-\frac{2}{r^2}\frac{\partial u_\theta}{\partial \theta}+\frac{\partial^2 u_r}{\partial z^2}\right] \tag{9.2}$$

θ-momentum equation

$$\rho\left[u_r\frac{\partial u_\theta}{\partial r}+\frac{u_\theta}{r}\frac{\partial u_\theta}{\partial \theta}+\frac{u_r u_\theta}{r}+u_z\frac{\partial u_\theta}{\partial z}\right] = -\frac{1}{r}\frac{\partial p}{\partial \theta}+\rho g_\theta+\mu\left[\frac{1}{r}\frac{\partial}{\partial r}\left(r\frac{\partial u_\theta}{\partial r}\right)-\frac{u_\theta}{r^2}+\frac{1}{r^2}\frac{\partial^2 u_\theta}{\partial \theta^2}+\frac{2}{r^2}\frac{\partial u_r}{\partial \theta}+\frac{\partial^2 u_\theta}{\partial z^2}\right] \tag{9.3}$$

z-momentum equation

$$\rho\left[u_r\frac{\partial u_z}{\partial r}+\frac{u_\theta}{r}\frac{\partial u_z}{\partial \theta}+u_z\frac{\partial u_z}{\partial z}\right] = -\frac{\partial p}{\partial z}+\rho g_z+\mu\left[\frac{1}{r}\frac{\partial}{\partial r}\left(r\frac{\partial u_z}{\partial r}\right)+\frac{1}{r^2}\frac{\partial^2 u_z}{\partial \theta^2}+\frac{\partial^2 u_z}{\partial z^2}\right]+g\beta(T-T_\infty) \tag{9.4}$$

Energy equation

$$u_r\frac{\partial T}{\partial r}+\frac{u_\theta}{r}\frac{\partial T}{\partial \theta}+u_z\frac{\partial T}{\partial z}=\alpha\left[\frac{1}{r}\frac{\partial}{\partial r}\left(r\frac{\partial T}{\partial r}\right)+\frac{1}{r^2}\frac{\partial^2 T}{\partial \theta^2}+\frac{\partial^2 T}{\partial z^2}\right] \tag{9.5}$$

Solid region: Energy equation

$$\frac{1}{r}\frac{\partial}{\partial r}\left(kr\frac{\partial T}{\partial r}\right)+\frac{1}{r^2}\frac{\partial}{\partial \theta}\left(k\frac{\partial T}{\partial \theta}\right)+\frac{\partial}{\partial z}\left(k\frac{\partial T}{\partial z}\right)+q_v=0 \tag{9.6}$$

Equation (9.1) – (9.6) are solved subject to the following boundary conditions to obtain the temperature distribution on the Teflon cylinder.

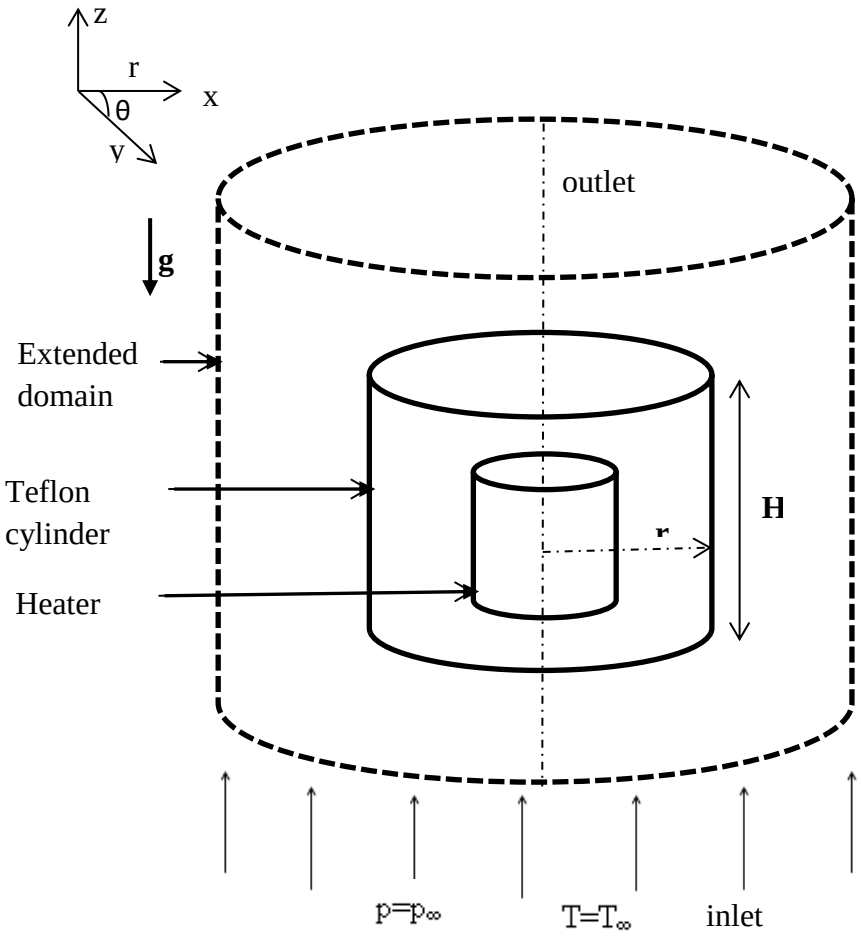

Figure 9.1 Numerical Model

Boundary Conditions:

On the outer surface of the Teflon cylinder, the boundary condition imposed is given as

$$k_{teflon}\frac{\partial T}{\partial n} = k_{fluid}\frac{\partial T}{\partial n} \text{ and } T_{teflon} = T_{fluid} \tag{9.7}$$

For the extended domain:

$$u_r \rightarrow 0,\ u_\theta \rightarrow 0,\ u_z \rightarrow 0,\ T \rightarrow T_\infty \text{ when } r \rightarrow \infty \tag{9.8}$$

Extended domain inlet:

$p=p_\infty$ and $T=T_\infty$ (9.9)

No slip and impermeability conditions are specified at the solid-fluid interfaces i.e, $u_r = u_\theta = u_z = 0$. At the inlet of the extended domain a uniform pressure $p=p_\infty$ and temperature $T=T_\infty$ is specified. Similarly, at the outlet of the extended domain the flow variables are imposed to zero such that there is no diffusion. It should also be noted that the heat generation term q_v (W/m^3) in Equation (9.6) is constant for the heater and is zero elsewhere in the solid region.

A grid independence study has been carried out to determine the optimum grid size for meshing the whole domain to obtain a balance between computational cost and accuracy. The domain is meshed with a coarse mesh and the case is run with the convergence criteria of 10^{-6}. The grid is then refined and cases are studied until the solution becomes invariant. The optimum grid size is selected after carrying out many trials. Table 9.1 represents the details of study considered for heat generation of $q_v = 5x10^5$ W/m^3. From the study, the grid size of 110000 is selected as optimum grid.

T**able 9.1** Results of the grid independence study.

No. of nodes	Temperature(K)				
	T_a	T_b	T_c	T_d	T_e
50000	340.95	340.63	341.02	339.17	463.91
75000	341.69	341.86	342.21	341.31	464.78
90000	341.56	343.03	343.11	339.86	465.24
110000	**339.83**	**339.71**	**335.16**	**332.15**	**463.06**
120000	339.37	338.62	334.18	331.3	463.09

9.3 EXPERIMENTAL SETUP

Chapter 3 provides the information on the Teflon experimental setup used in this work along with pictorial representation. Table 9.2 shows the thermocouple locations on the Teflon cylinder in terms of x, y and z dimensions. Steady state experiments are carried out for different power supply and temperatures are measured using thermocouple. The process of experiment includes heating, steady state and cooling. Temperature during all these stages is recorded. Steady state is said to have been reached when the temperature difference does not vary by more than 0.2°C for time

span of 10 minutes. The measured temperature for different volumetric heat generation is shown in Table 9.3.

Table 9.2 Points on the Teflon cylinder considered for temperature measurement

Points	Dimensions (mm)
A	(24,0,75)
B	(34,0,77)
C	(41,0,75)
D	(40,0,90)
E	(35,0,85)
F	(30,0,80)
G	(25,0,30)
H	(35,0,15)
I	(28,0,5)
J	(50,0,50)

9.4 ANN AS FORWARD MODEL

The estimation process is an iterative process and the forward model is executed for every sample generated using the inverse algorithm. In order to reduce the computational cost involved in the inverse methodology, the forward model is solved for a set of input data (heat generation W/m^3) and corresponding temperature distribution is obtained thereby developing a relationship between the input and the output. To create the relationship between the input and output data ANN is employed. Therefore, in the inverse process when a sample is accepted instead of running the forward model the ANN model is executed to obtain the temperature distribution thereby reducing the computational cost. The detailed study of ANN is provided in chapter 4. Training is accomplished using a set of network inputs for which the desired outputs are known. Table 9.4 shows the neuron independence study. The selection of the number of hidden neurons is based on the values of some of the common performance metrics used, as mentioned by Equation (4.11) and (4.12) in chapter 4.

Table 9.3 Temperature distribution for different heat flux

Power (W)	2.72	3.63	4.80	5.73	6.51
q_v (W/m^3)	128347.8	171386.2	226466.3	270270.8	307113.7
Heater temperature (K)/Location	336	350	358	366	372
T_a	317	324	327	332	334
T_b	313	317	320	323	325
T_c	311	315	317	320	321
T_d	309	312	314	316	317
T_e	310	315	317	319	321
T_f	313	318	321	325	326
T_g	318	325	329	334	336
T_h	310	313	315	317	318
T_i	310	311	313	316	317
T_j	311	314	318	321	324

Table 9.4 Results of the neuron independence study

No. of neurons in the hidden layer	MRE	R^2
5	0.010137	0.99974
10	**0.0000175**	**0.99999**
15	0.0019204	0.99988

9.5 INVERSE METHOD

The Bayesian inference algorithm is explained in detail in chapter 5. Bayesian Inference along with MCMC-MH algorithm is used as the inverse method for the estimation of volumetric heat generation and heat transfer coefficient. Mathematically for the retrieval problem, the Bayes theorem can be stated as

$$P\,(q_v|T) = \frac{P(T|q_v)\,P(q_v)}{P(T)} \tag{9.10}$$

where q_v represents the state vector (volumetric heat generation) and *T* represents the measurement vector. $P(q_v)$ is the prior probability density function (PDF) of the state q_v.$P(T|q_v)$ is the conditional probability density function of the measurements given the state vector, and $P\,(q_v|T)$ is the posterior probability density function of the state vector. $P(T|q_v)$ is the likelihood probability density function and assuming a normal distribution it can be written as

$$P(T|q_v) = \frac{1}{(2\pi\sigma^2)^{0.5}}\, e^{-\sum_{i=1}^{n}\frac{(\mathbf{T}_{exp}-\mathbf{T}_{network})^2}{2\sigma^2}} \tag{9.11}$$

The uncertainty σ is due to the measurement errors and the error in the forward model. For a uniform prior, $P(q_v)$is automatically set to 1 and the PPDF now becomes,

$$P\,(q_v|T) = \frac{1}{(2\pi\sigma^2)^{\frac{N}{2}}}\; e\left(\frac{-\sum_{i=1}^{N}(\mathbf{T}_{exp}-\mathbf{T}_{network})^2}{2\sigma^2}\right) \tag{9.12}$$

where the normalizing constant in the denominator of Equation (9.10) is left out for convenience. In Equation (9.12), N represents the total number of temperatures measured in the experiment.

For simplicity, let χ^2be defined as

$$\chi^2 = \frac{\sum_{i=1}^{N}(T_{exp,i}-T_{network,i})^2}{\sigma^2} \tag{9.13}$$

When prior information is incorporated, a frequently employed prior is the Gaussian prior given below:

$$P(q_v) = \frac{1}{\sqrt{2\pi\sigma_p^2}} e\left\{\frac{-(\emptyset-\mu_p)^2}{2\sigma_p^2}\right\} \tag{9.14}$$

$$P(q_v|T) = \frac{1}{(2\pi\sigma^2)^{\frac{N}{2}}} e\{\frac{-\chi^2}{2}\} \times \frac{1}{\sqrt{2\pi\sigma_p^2}} e\{\frac{-(\emptyset-\mu_p)^2}{2\sigma_p^2}\} \quad (9.15)$$

Equation (9.15) represents the posterior probability density function of obtaining the state vector q_v for a given set of temperature measurements after our prior knowledge of parameters and the forward model have been incorporated in the analysis. The PPDF is discrete and has to be numerically evaluated for every assumed value of q_v. To derive point estimates of q_v from Equation (9.15), further processing of the PPDF is required. Two frequently used estimators are the (i) maximum a posteriori (MAP) and (ii) mean or expectation. In order to determine the mean and SD, the process becomes iterative process and large number of data must be sampled. Samples are drawn with the help of Metropolis-Hastings (MH) algorithm.

9.5.1 Metropolis-Hastings Algorithm

Markov chain Monte Carlo method is implemented using Metropolis-Hastings algorithm. The Markov chain suggests the generation of samples from the posterior. The unknown parameters are initially guessed and the forward model is solved to obtain temperature distribution. The temperature distribution is now compared with the experimental temperature distribution and the probability is calculated using Equation (9.15). The current state of heat generation and heat transfer coefficient is moved to the next state with the help of Metropolis Hastings algorithm based on the acceptance criteria. Similarly, many such samples are generated and finally the PPDF is obtained. The detailed explanation of the algorithm and the flow chart is shown in Chapter 5.

9.6 RESULTS AND DISCUSSION

9.6.1 Forward Solution from Numerical Model

Numerical simulations are carried out with appropriate boundary conditions and with fixed convergence criteria. The computational model is shown in Figure 9.1. The volumetric heat generation value, q_v applied to the heater is varied from $1x10^5$ to $5x10^5$ W/m^3. The selection of q_v range confirms that the Rayleigh number does not exceed the critical value and the flow remains laminar. Figures 9.2 and 9.3 show the temperature distribution and velocity contours for $q_v = 4.5x10^5$W/m^3, respectively. As

a result of natural convection conjugate heat transfer, the boundary layer grows from leading edge to the trailing edge. Heat has to be dissipated from the heater to the Teflon cylinder and then to the boundary layer. As a result of heat flux across the boundary layer and because of the fact that the boundary layer becomes thicker at the top, the temperature at the top of the Teflon is slightly higher than the bottom of the Teflon and it is clearly seen in Figure 9.4.

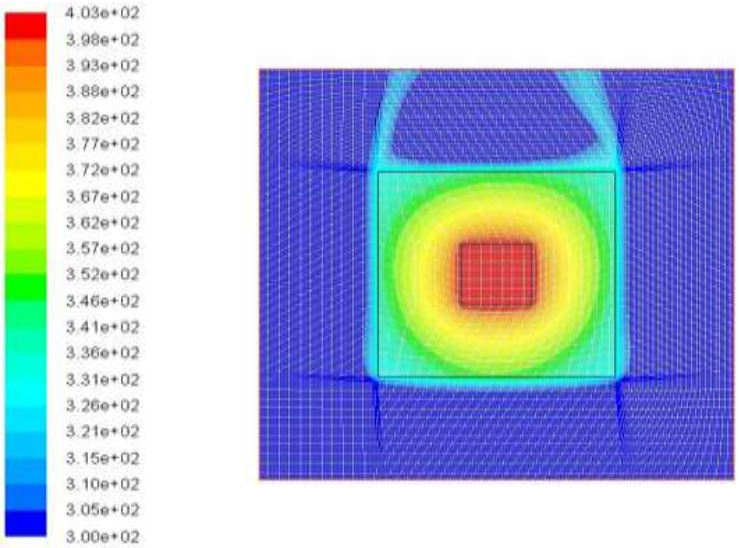

Figure 9.2 Temperature (K) distribution in the Teflon cylinder for $q_v = 4.5x10^5$ W/m^3 (Longitudinal mid-section)

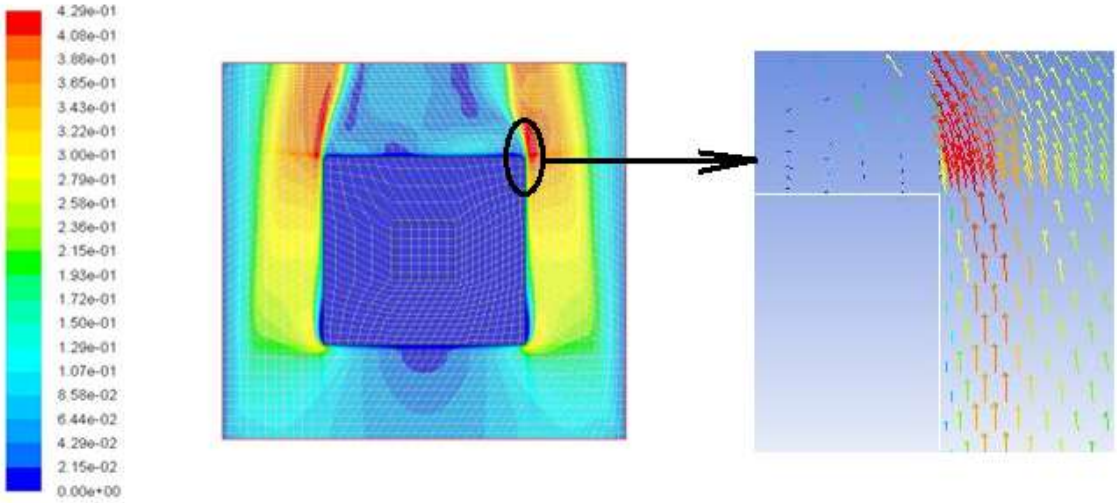

Figure 9.3 Velocity (m/s) contours for $q_v = 4.5x10^5$ W/m^3 (Longitudinal mid-section)

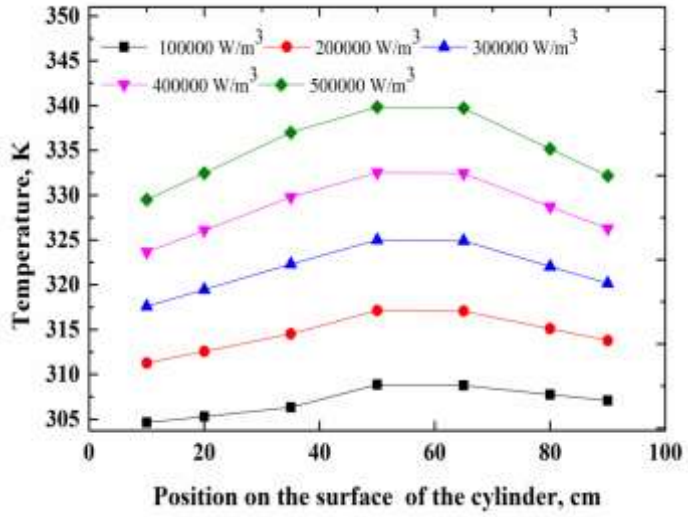

Figure 9.4 Variation of temperature on the surface of the Teflon cylinder for different q_v

9.6.2 Forward Solution from ANN

The temperature data obtained from full numerical simulations and ANN are compared for different values of q_v at (50, 0, 50) (mm) on the Teflon cylinder to test the adequacy of the network and the results of such an exercise is shown in Table 9.5. The accuracy of the ANN is clearly evident from this comparison. Typically, one FLUENT simulation takes 20 to 30 mins to reach convergence. In the MH algorithm, the samples are accepted or rejected by solving the forward model and comparing their probabilities thereby resulting in huge computational times. ANN provides the output for a given set of inputs based on the correlation developed during the training phase almost instantaneously. So the computation of the conventional forward model is now eliminated by using the ANN as the forward model.

Table 9.5 Comparison between full numerical solution and ANN

q_v, W/m^3	$T_{CFD,}$ K	T_{ANN}, K	Error (%)
100000	308.85	307.89	0.31
200000	317.14	316.28	0.27
300000	324.99	323.72	0.39
400000	332.54	331.44	0.33

9.6.3 Single Parameter estimation q_v

The experimental temperature data at various locations of the Teflon cylinder are available. The objective is to estimate q_v given the temperature data for different power inputs. To establish the MCMC method driven by Bayesian approach, first numerically obtained temperature data for assumed values of q_v are used. In order to reduce computational time and cost, a trained neural network is used as forward model which replaces the numerically obtained temperature data. For these temperature data obtained from neural network, the MCMC method driven by Bayesian approach, the value of q_v is retrieved.

Table 9.6 Effect of sample size on Bayesian retrieval of q_v

No. of samples	Bayesian retrieved value of qv, W/m^3	
	Mean	SD
5000	216571.5	407.57
7500	216571.5	407.58
10000	216571.5	407.57

Samples 5000, 7500, 10000 were selected to study the retrieval methodology. The burn in concept is incorporated to cut off the effect of initial guess on the parameter estimation. The burn-in considered in the present study is 2000 samples (i.e. the first 2000 samples) are not used for calculating mean and SD. Table 9.6 reports the retrieved values of q_v for various values of samples considered.

Table 9.7 Estimation of q_v from experimental temperatures

Actual q_v (W/m^3)	Bayesian retrieved values of q_v (W/m^3)		Error (%)
	Mean	SD	
128347.83	125549.8	780.19	2.18
171386.16	166296	476.96	2.97
226466.26	216571.5	407.57	4.37
270270.76	259249.1	1145.77	4.08
307113.71	296780.2	387.689	3.36

To obtain consistent solution to the samples driven by MCMC, the entire retrieval is carried out for 5000 samples. Table 9.7 shows the mean and SD of the retrieved values of q_v using the MCMC-MH method for the experimental temperature. The standard deviations that show the uncertainty in the retrieved parameter is also reported in Table 9.7. Figures 9.5 and 9.6 show the PPDF for the retrieval of q_v and Figures 9.7 and 9.8 show the variation of the mean of the PPDF with respect to iterations for heat generation q_v= 216571.5W/m^3 with different initial guesses.

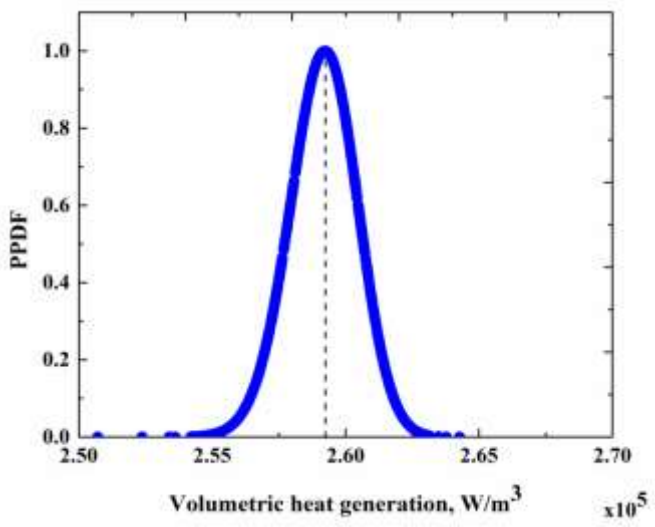

Figure 9.5 PPDF for q_v = 259248.7W/m^3

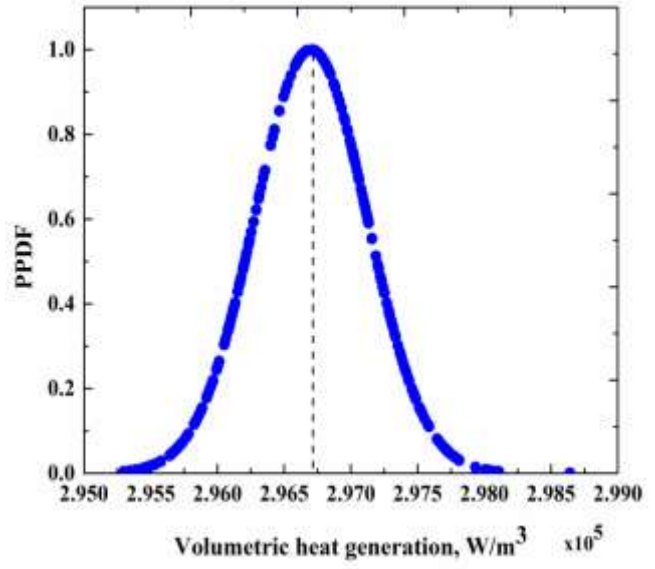

Figure 9.6 PPDF for q_v = 296780.2 W/m^3

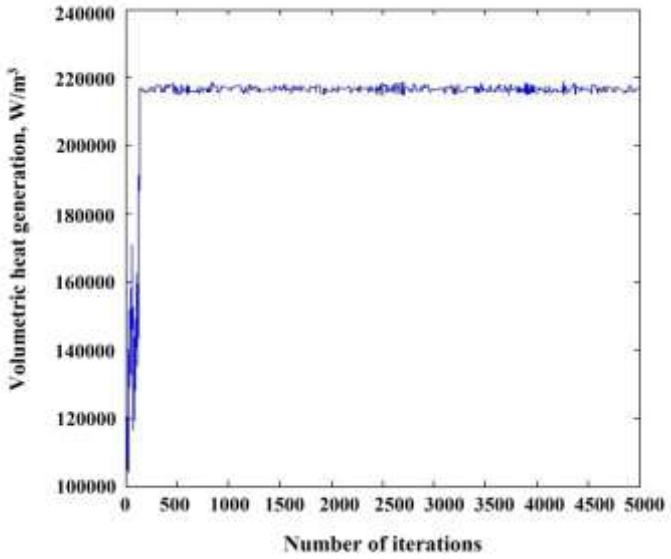

Figure 9.7 Sampling history with initial guess $q_v = 1x10^5$ W/m^3

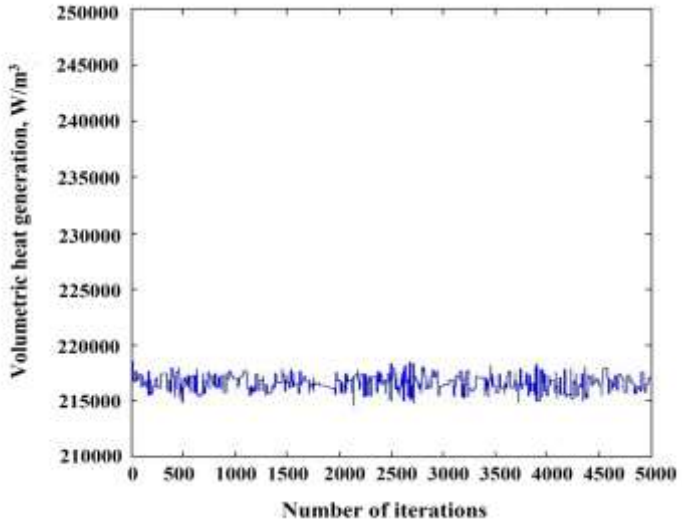

Figure 9.8 Sampling history with initial guess $q_v = 2.5x10^5$ W/m^3

Figure 9.9 shows a parity plot between simulated temperature and experimental temperature for q_v=307113.7 W/m^3. It is clear from the Figure 9.9 that the simulated temperature and experimental temperature agree very well with the maximum deviation of 0.48%.

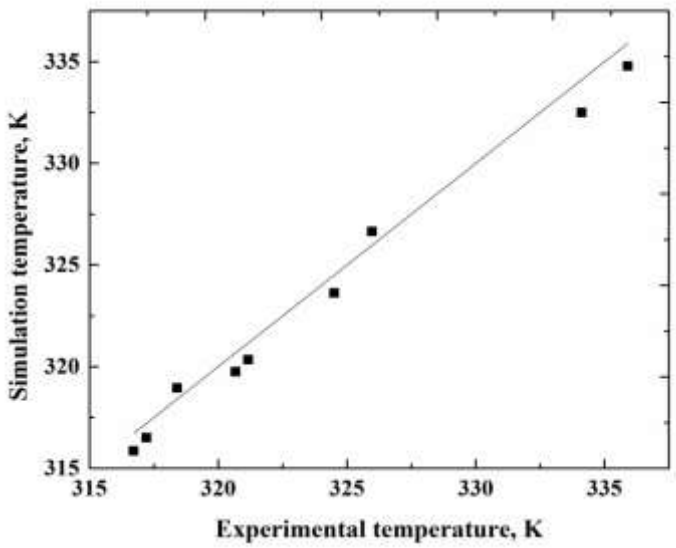

Figure 9.9 Parity plot for 307113.7 W/m^3

9.6.4 Single parameter retrieval of h from known q_v

The sole idea of this work is simultaneous retrieval of heat generation q_v and heat transfer coefficient h for the temperature data. In order to obtain the prior information of these parameters estimation is carried out separately as single parameter estimation on heat transfer coefficient 'h' and heat generation q_v. In this section retrieval of heat transfer coefficient 'h' is attempted for the known heat generation 'q_v'.

Table 9.8 Estimation of h for known q_v

	Bayesian retrieved values of h (W/m^{2}K)	
q_v (W/m^3)	Mean	SD
171386.16	3.34	0.047
226466.26	3.8	0.028

Table 9.8 shows the mean and SD of the retrieved values of h using the MCMC-MH method. The standard deviations showing the uncertainty in the retrieved parameter is also reported. Figure 9.10 and 9.11 shows the PPDF for the retrieval of h and Figure 9.12 and 9.13 shows the variation of the mean of the heat transfer coefficient with respect to iterations.

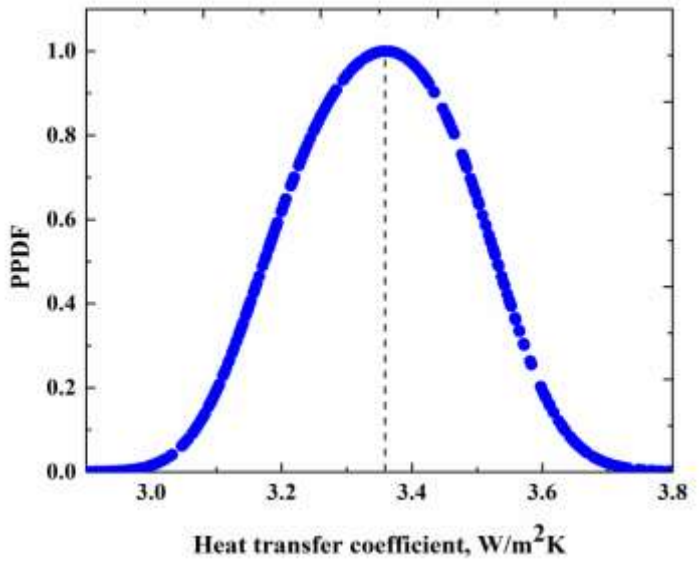

Figure 9.10 PPDF for h = 3.36 W/m^{2}K

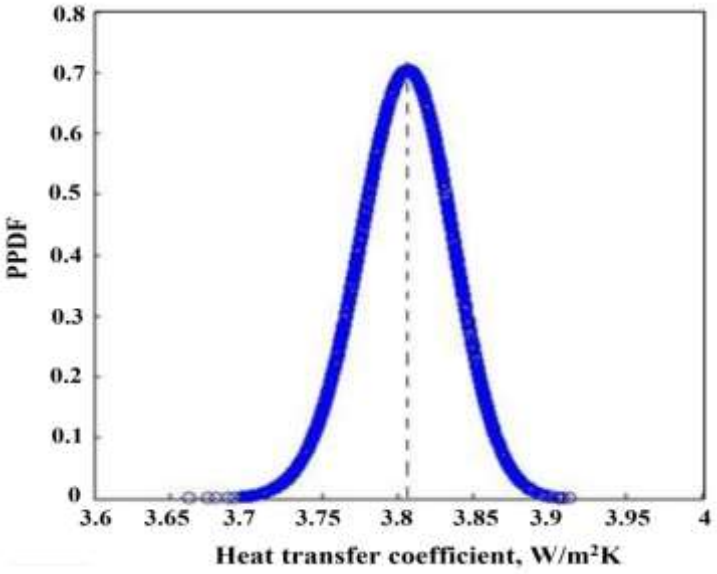

Figure 9.11 PPDF for h = 3.81 W/m^{2}K

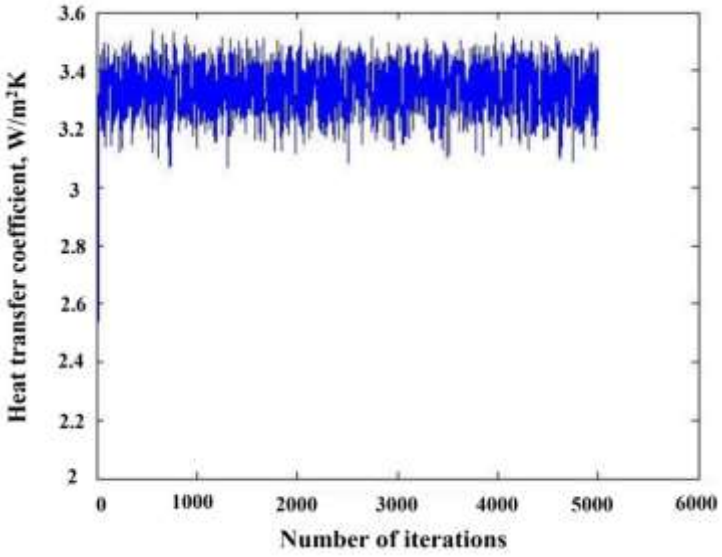

Figure 9.12 Sampling history for h = 3.36 W/m^{2}K

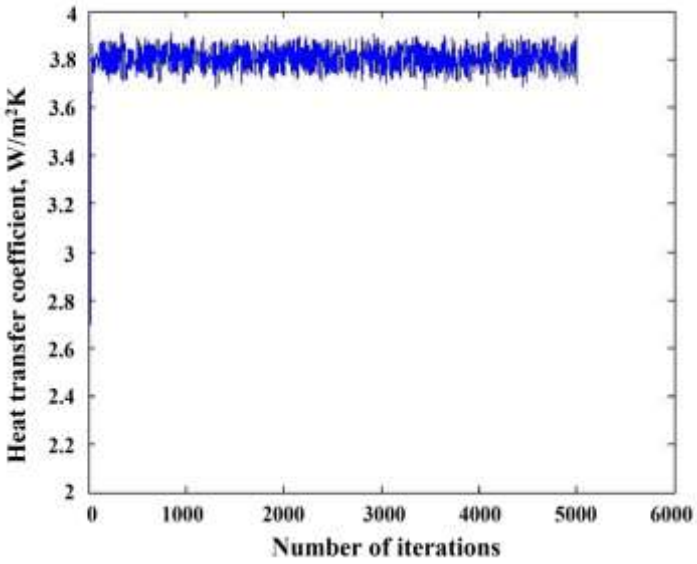

Figure 9.13 Sampling history for h = 3.81 W/m^{2}K

9.6.5 Two Parameter estimation

Estimation of volumetric heat generation and heat transfer coefficient as single parameter estimation has been carried out successfully and reported as well. In this section, the results of simultaneous retrieval of q_v and h are reported. Now the problem is modified into two parameter estimation. Same temperature data is used for the estimation which was earlier used for single parameter estimation. The parameters

can be correlated parameters and in such a situation without prior information one cannot estimate the unknown parameters. Under such circumstances adequate prior information can be injected with the help of single parameter retrievals. In the present study, appropriate Gaussian prior is specified for both heat transfer coefficient and heat generation. For the first case a Gaussian prior with a mean value of 200000W/m^3 for q_v, a standard deviation for the prior is also required and is assumed to be 1000 W/m^3. Table 9.9 reports the results of the simultaneous retrieval of q_v and h by injecting appropriate Gaussian priors.

Table 9.9 Estimation of q_v and h for experimental temperatures

Gaussian prior	q_v (W/m^3)			h (W/m^2K)		
	Actual	Mean	SD	Actual	Mean	SD
Mean (k)=200000, σ(k)=1000. Mean (h)= 3, σ(h)=0.5	226466.3	199948	1011.24	3.12	3.03	0.28
Mean (k)=350000, σ(k)=800. Mean (h)= 3,σ(h)=0.5	370152.4	350014	852.45	4.18	4.03	0.34

It is seen from Table 9.9 that the unknown parameters have been retrieved simultaneously with reasonable standard deviation. Figure 9.14 shows the sampling history and PPDF plot for q_v = 350014 W/m^3 and h = 4.032 W/m^2K with the initial guess of q_v = 380000 W/m^3 and h = 2.5 W/m^2K respectively**.** The exercise is repeated for different combination of volumetric heat generation and heat transfer coefficient and the results are extracted. Figure 9.15 shows the sampling history and PPDF for the retrieval of q_v = 199948 W/m^3 and h = 3.031 W/m^2K with initial guess of q_v = 225000W/m^3 and h = 4.5 W/m^2K respectively.

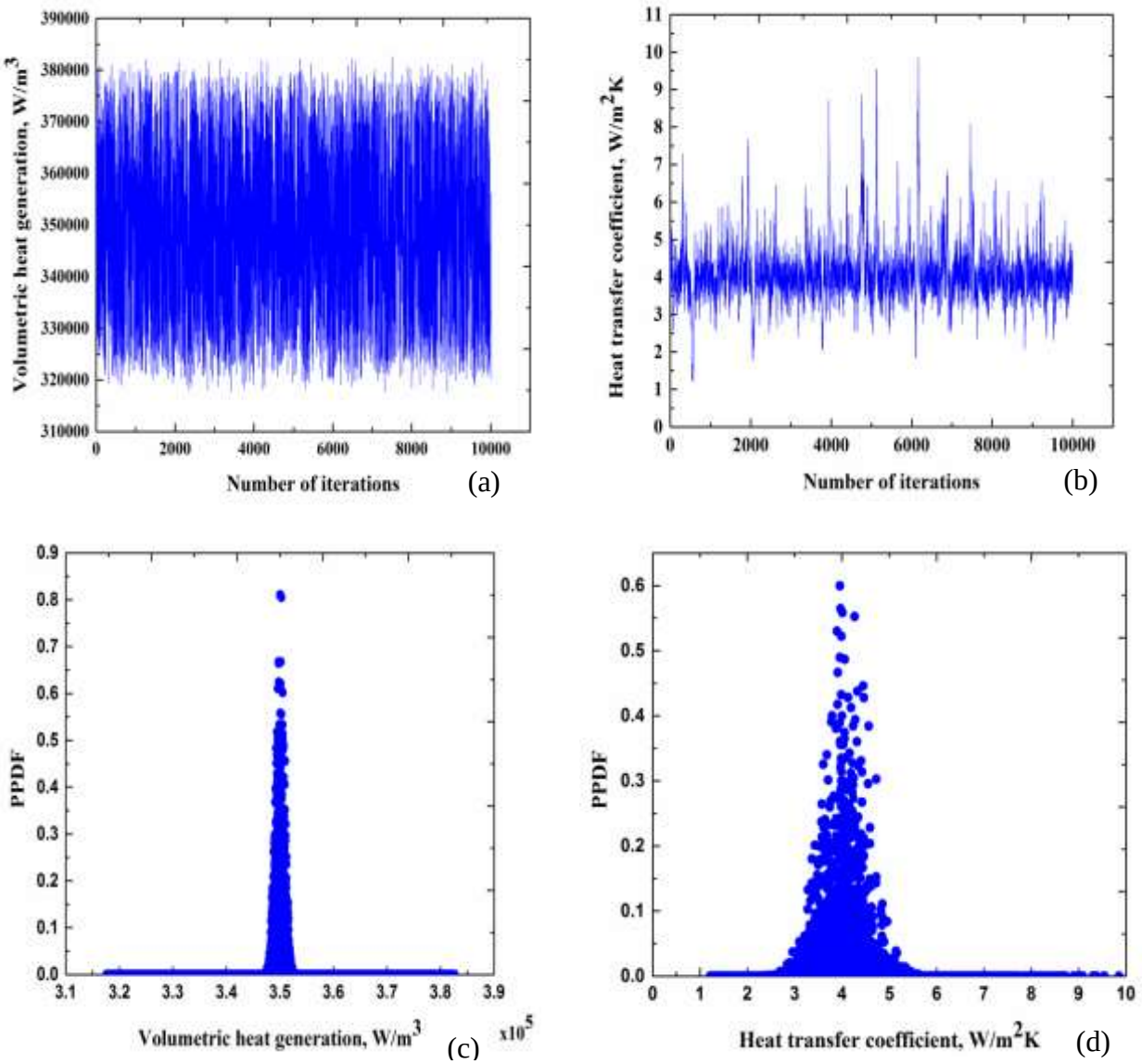

Figure 9.14 (a) sampling history for q_v= 350014 W/m^3 (b) sampling history for h = 4.032 W/m^{2}K (c) PPDF for q_v= 350014 W/m^3 (d) PPDF for h = 4.032 W/m^{2}K

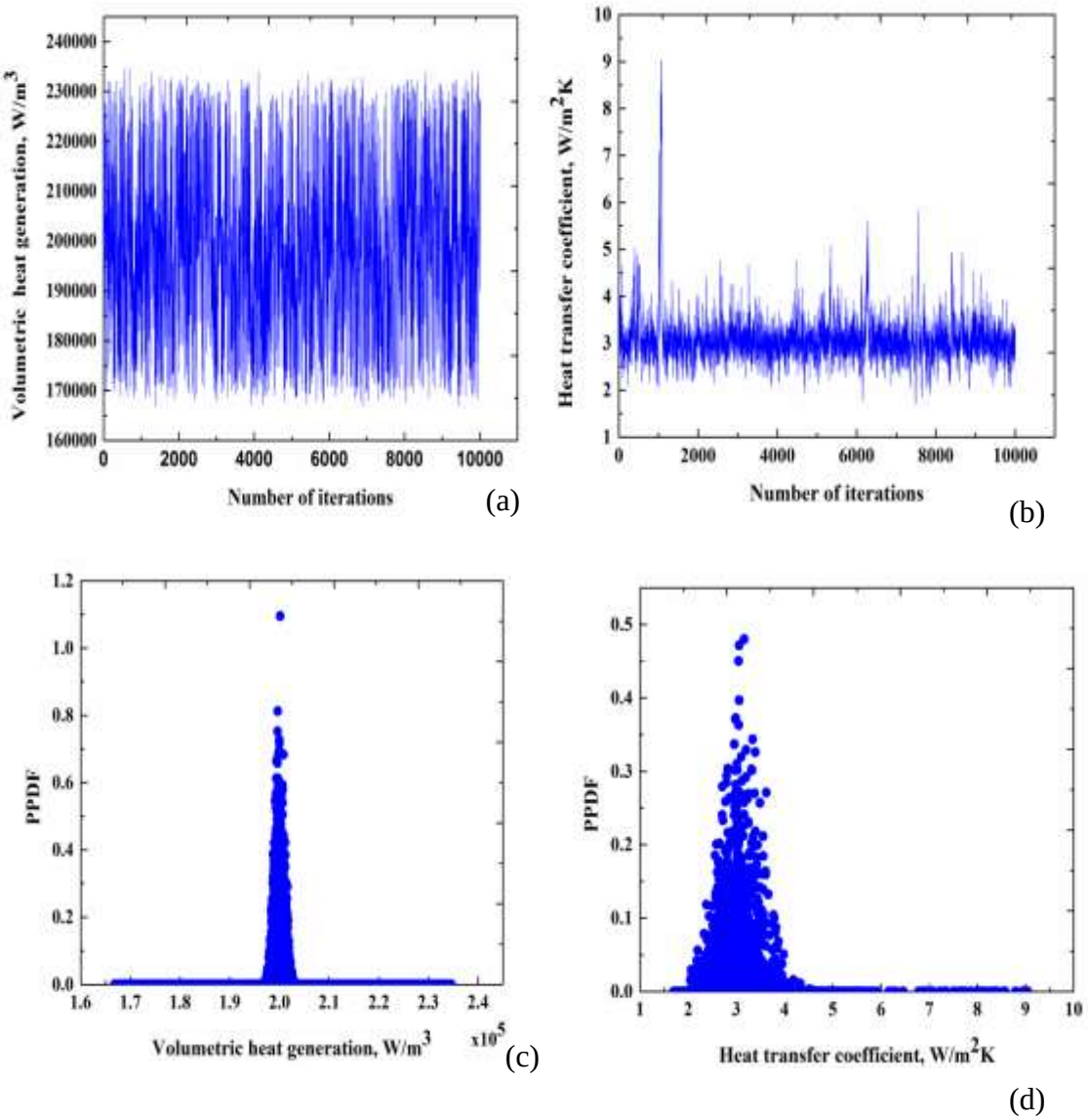

Figure 9.15 (a) sampling history for q_v= 199948W/m^3 (b) sampling history for h = 3.031 W/m^{2}K (c) PPDF for q_v= 199948W/m^3 (d) PPDF for h = 3.031 W/m^{2}K

9.7 CONCLUSIONS

Volumetric internal heat generation rate, q_v has been estimated for a Teflon cylinder using an inverse heat transfer model with the experimentally obtained surface temperature as the input. The forward model for three dimensional conjugate heat transfer has been solved using the commercially available Fluent 14.5. q_v is assumed to be known and the temperature values are obtained. ANN is then used to replace the forward model to save computational cost. Simulation data is used to train network. Single parameter estimation of q_v and h is carried out initially using MCMC-MH

technique and later simultaneous estimation of both q_v and h from the experimentally obtained temperature is carried out. A maximum error of 0.39% is observed between temperature obtained from Computational Fluid Dynamics and ANN. The unknown q_v and h was retrieved for the obtained experimental temperature data and the maximum retrieved parameter error was found to be 4.37%. Thus the MCMC-MH method is a powerful optimization technique for the simultaneous estimation of volumetric heat generation and heat transfer coefficient from surface temperature data.

9.8 Closure

This chapter reported the multi-parameter estimation in terms of volumetric heat generation and heat transfer coefficient considering experimental temperature on the surface of the Teflon cylinder. MCMC-MH algorithm was used as the inverse algorithm with *apriori* information obtained from single parameter estimation.

CHAPTER 10

CONCLUSIONS

The thesis is directed towards estimation of unknown parameters from a natural convection conjugate heat transfer problem. The estimation is carried out considering steady state condition. Numerical simulations of conjugate heat transfer model are carried to obtain temperature data for the given input. ANN replaces the conventional CFD solutions as fast forward model. The inverse part includes the use of methods such as GA, ANN and Bayesian Inference for the estimation of unknown parameters. In fact, ANN is used as both forward and inverse models in the estimation process. The corner stone of the work is the use of the hybrid method in the process of estimation, where stochastic method GA is combined with the deterministic method LM for estimation. The estimation is initiated using simulated data considering the 2D model in order to justify its robustness and later measured data has been used. Both 2D and 3D computational models have been used in this work. Also, steady state experiments on Teflon cylinder is conducted for simultaneously estimating heat generation and heat transfer coefficient.

The thesis started with the introduction to the estimation methods. A brief introduction to the forward model and the inverse model was provided and the methods appearing under forward and inverse models were also discussed in **Chapter 1**. The concept of estimation procedure was explained with the sketch. Finally the organization of the thesis was presented. **Chapter 2** provided literature review about the techniques used in the inverse estimation and its advantages. The experimental setup, horizontal and vertical orientation of the fin, Teflon cylinder, data acquisition system, calibration of the thermocouples, along with other instrumentations were discussed in **Chapter 3** with pictorial view. **Chapter 4** discussed about the forward problem used in the estimation process. Numerical simulations and Artificial Neural Network (ANN) were explained in detail.

Chapter 5 provided the idea about the inverse method used in the present work. Genetic Algorithm (GA) was discussed with its phenomena such as crossover and mutation. Use of ANN as inverse method was highlighted. Bayesian Inference along

with the sampling algorithm MCMC-MH was explained in the form of flow chart. In **Chapter 6** 2D horizontal base model was considered for the estimation of heat flux for the measured data using GA as the inverse method. ANN was used as the forward model. A hybrid method was proposed in this chapter wherein LM was combined with GA for the retrieval process. **Chapter 7** dealt with the use of ANN as both forward and inverse models for the estimation of heat flux and heat transfer coefficient for 3D vertical base setup. This chapter also showed the effect of injecting experimental data into the simulated data in the retrieval process.

Chapter 8 showed the simultaneous estimation of heat flux and heat transfer coefficient for the 3D horizontal base conjugate heat transfer problem using experimental data. ANN was used as the forward model. Bayesian Inference along with MCMC-MH sampling algorithm was used as the inverse method. The process began with the single parameter estimation for the simulated data considering the 2D model and later extended to 3D model and experimental data was considered for the simultaneous estimation of heat flux and heat transfer coefficient. *Apriori* information was incorporated in the estimation process. A study on sensitivity coefficient was also provided.

Finally **Chapter 9** dealt with the application of Bayesian inference to a different problem wherein a low thermal conductivity Teflon cylinder was used. Cylindrical heater was used as the heat source and MCMC-MH algorithm has been adopted for the estimation of heat generation and heat transfer coefficient for the Teflon cylinder. Once again ANN was used as the forward model. This problem can be related to the investigation of the presence of tumor in the human body.

10.1 SCOPE FOR FUTURE WORK.

1. The estimation of the parameters can be extended to 3D transient heating or cooling problems along with conjugate approach.
2. Delayed Acceptance Metropolis-Hastings algorithm can be used to improve the computational time of Markov Chain Monte Carlo methods.
3. Model reduction using Approximation Error Model (AEM) can be used for the inverse conjugate heat transfer problems wherein the statistical aspect of the

approach is retained during estimation of unknown parameters within the Bayesian framework.

APPENDIX

1. Calculation of the Rayleigh Number for Vertical orientation.

Surface temperature for the maximum heat flux considered (3300 W/m^2) is 394.96K

$T_s = 394.96K \quad T_\infty = 303K \quad k_{air} = 0.0242W/mk \quad \vartheta = 1.789 * 10^{-5}\, m^2/s$

$g = 9.81\, m/s^2 \quad Pr = 0.732\ for\ air \quad L = 0.250m \quad T_f = \frac{T_s + T_\infty}{2} = 348.98K$

$\beta = \frac{1}{T_f} = 0.0028K^{-1}$

$$Ra = \frac{g * \beta * (T_s - T_\infty) * L^3}{\vartheta^2} * Pr$$

$$\boldsymbol{Ra = 9.0268 * 10^7}$$

2. Calculation of the Rayleigh Number for Horizontal orientation.

Surface temperature for the maximum heat flux considered (3500 W/m^2) is 439.11K

$L = 0.150m \quad T_s = 439.11K \quad T_f = \frac{T_s + T_\infty}{2} = 371.05K \quad \beta = \frac{1}{T_f} = 0.00269K^{-1}$

$$Ra = \frac{g * \beta * (T_s - T_\infty) * L^3}{\vartheta^2} * Pr$$

$$\boldsymbol{Ra = 2.7725 * 10^7}$$

Table A1: Properties of materials used in simulations

Properties	Aluminum	Mild steel	Teflon
Density(kg/m^3)	2719	8030	2200
Specific heat (J/kgK)	871	502.48	1100
Thermal conductivity (W/mK)	202.4	45	0.25

Table A2: Simulated data used for neural network training for Vertical base 3D model

Heat flux, W/m^2	Heat transfer coefficient, W/m^2K	Base	0.005m	0.178m
305	2.38	318.45	310.48	312.12
400	2.74	323.84	313.46	315.57
544	3.15	333.02	317.81	320.60
700	3.51	341.75	322.33	325.84
853	3.78	350.18	326.63	330.79
1000	4.00	358.10	330.68	335.46
1232	4.28	370.41	336.85	342.55
1400	4.46	379.16	341.22	347.58
1500	4.54	384.36	343.80	350.53
1700	4.72	394.64	348.83	356.29
1800	4.79	399.69	351.32	359.13
1900	4.86	404.78	353.79	361.96
2000	4.92	409.79	356.23	364.76
2400	5.16	429.71	365.90	375.78
2500	5.24	434.64	368.24	378.43
2600	5.27	439.53	370.56	381.08
2700	5.32	444.43	372.93	383.76
2784	5.37	448.52	374.89	385.95
3200	5.53	459.04	384.45	396.82
3300	5.58	473.49	386.74	399.38

Table A3 Simulated data used for neural network training for Horizontal base 3D model

Heat flux, W/m^2	Heat transfer coefficient, W/m^2K	0.006	0.071	0.123
304	4.438	324.40	320.69	319.46
400	3.369	330.08	325.08	323.59
544	3.885	338.83	332.13	330.14
853	2.565	357.09	346.81	343.77
1000	3.862	365.57	353.20	349.62
1100	3.730	369.17	356.27	352.47
1232	2.415	377.06	362.03	357.70
1500	3.177	390.45	371.98	366.62
1600	4.264	395.77	376.05	370.43
1680	3.775	400.81	381.18	375.26

1900	5.117	407.06	384.07	377.56
2000	3.315	412.70	389.26	382.34
2200	3.974	420.74	395.75	388.31
2500	5.713	435.99	407.29	398.82
2600	2.502	443.10	411.61	402.47
2700	4.750	448.10	416.04	407.08
2784	3.104	451.77	418.34	408.61
2900	5.555	451.39	417.77	407.85
3200	5.361	463.98	427.76	417.31
3300	5.127	469.09	431.79	421.22
3500	5.000	475.73	436.04	424.63

Bayesian Inference

Single Parameter with normal prior

```
clc;
clear all;
m(1) =2.4;
mew_prior = 3;
sigma_prior = 0.01*mew_prior;
sigma1 = 0.01;
j=2;
n=10000;
%t_meas= input('enter Texp =  ')
t_meas=[357.1012
  346.7650
  343.7256]

while j<n
 u = rand;
 %---------------------
% q_mstar = P(m*)
%---------------------
q_mstar(j-1) = rand;
 %------------------
% sigma for P(m*)
%------------------
sigma = 0.02*m(j-1);
```

```
temp(j-1) = rand;
 if temp(j-1)>0.5
    m_star(j-1) = m(j-1) - sqrt(-2*sigma^2*log(q_mstar(j-1)));
else
    m_star(j-1) = m(j-1) + sqrt(-2*sigma^2*log(q_mstar(j-1)));
end
 % sqrt(2*pi*sigma1^2) IGNORED FOR NORMALIZATION PURPOSE
 %-------------------------------------------------
% CALCULATING t_sim and t_meas
t_sim =oneD_fin_150mm_steady_input_m(m(j-1));
% CALCULATING PPDF
% TAKING PRIOR VALUE AS 1
 X = (((t_sim-t_meas)'*(t_sim-t_meas))/(2*sigma1*sigma1*10000));
P_m0(j-1) = exp(-1*X)*exp(-(m_star(j-1)-
mew_prior)^2/2/sigma_prior^2);
  %-------------------------------------------------
% CALCULATING P(m0) or P(m(j-1))

%P_m0(j-1) = exp(-1*X/(2*sigma^2));
 %-------------------------------------------------
% CALCULATING P(m_star)
 sum1(j-1) = 0;
t_sim1 =oneD_fin_150mm_steady_input_m(m_star(j-1));
X = (((t_sim1-t_meas)'*(t_sim1-t_meas))/(2*sigma1*sigma1*10000));
 P_mstar(j-1) = exp(-1*X)*exp(-(m_star(j-1)-
mew_prior)^2/2/sigma_prior^2);
 %-------------------------------------------------
 % CALCULATING A
 A1 = P_mstar(j-1)/P_m0(j-1);
A(j-1) = min(1,A1);

% METROPOLITAN HASTINGS CHECK
count = 0;
 if u<A(j-1)
    m(j) = m_star(j-1);
    count= count + 1;
 else
    m(j) = m(j-1);
```

```
 end
 j = j+1;
 %-----------------------------------------------
end
plot(m_star,P_mstar)
hist(P_mstar,20)
 %-----------------------------------------------
%VALUE FOR M FOR WHICH MAX PPDF IS OBTAINED
j=2;
max_p = P_m0(1);
while j<n
       if max_p < P_m0(j-1)
        max_p = P_m0(j-1);
      count = j;
    else
        j = j+1;
    end
end
 %m(count)
Mean= sum(P_mstar.*m_star)/sum(P_mstar)
Var=sum(((m_star-Mean).^2).*P_mstar)/sum(P_mstar.*m_star);
Std_dev= sqrt(Var)
[M,I]= max(P_mstar);
MAP=m_star(I)
```

Single parameter with uniform prior

```
clc;
clear all;
m(1) = 1000;
%------------------
% sigma1 for PPDF
%------------------
lambda = 10;
sigma1 = 0.01;
j=2;
n=20000;
t_meas= input('enter Texp =  ')
while j<n
u = rand;
```

```
%--------------------
% q_mstar = P(m*)
%--------------------
q_mstar(j-1) = rand;
 %------------------
% sigma for P(m*)
%------------------
 sigma = 0.02*m(j-1);
 temp(j-1) = rand;
 if temp(j-1)>0.5
    m_star(j-1) = m(j-1) - sqrt(-2*sigma^2*log(q_mstar(j-1)));
else
    m_star(j-1) = m(j-1) + sqrt(-2*sigma^2*log(q_mstar(j-1)));
end
 % sqrt(2*pi*sigma1^2) IGNORED FOR NORMALIZATION PURPOSE
 %-------------------------------------------------
% CALCULATING t_sim and t_meas
 t_sim =oneD_fin_150mm_steady_input_m(m(j-1));
%-------------------------------------------------
 % CALCULATING PPDF
% TAKING PRIOR VALUE AS 1
X = (((t_sim-t_meas)*transp(t_sim-t_meas))/(2*sigma1*sigma1*1000));
P_m0(j-1) = exp(-1*X);
%-------------------------------------------------
% CALCULATING P(m0) or P(m(j-1))
%-------------------------------------------------
% CALCULATING P(m_star)
 sum1(j-1) = 0;
  t_sim1 =oneD_fin_150mm_steady_input_m(m_star(j-1));
X = (((t_sim1-t_meas)*transp(t_sim1-t_meas))/(2*sigma1*sigma1*1000));
 P_mstar(j-1) = exp(-1*X);
 %-------------------------------------------------
 % CALCULATING A
 A1 = P_mstar(j-1)/P_m0(j-1);
A(j-1) = min(1,A1);

% METROPOLITAN HASTINGS CHECK
count = 0;
 if u<A(j-1)
```

```
    m(j) = m_star(j-1);
    count= count + 1;
 else
    m(j) = m(j-1);
 end
 j = j+1;
 %-----------------------------------------------
end
plot(m_star,P_mstar)
hist(P_mstar,20)
 %-----------------------------------------------
%VALUE FOR M FOR WHICH MAX PPDF IS OBTAINED
j=2;
max_p = P_m0(1);
while j<n


    if max_p < P_m0(j-1)
        max_p = P_m0(j-1);
      count = j;
    else
        j = j+1;
    end
end
 %m(count)
Mean= sum(P_mstar.*m_star)/sum(P_mstar)
Var=sum(((m_star-Mean).^2).*P_mstar)/sum(P_mstar);
Std_dev= sqrt(Var)
[M,I]= max(P_mstar);
MAP=m_star(I)
```

Two parameter with prior model

```
clc
clear all
tic
load '18neurons.mat'   loads the trained neural network
n=5000; %iterations
m(n,2)=zeros; % initialise storage for parameters q n h
m(1,1)= 500; %initial guess for q
```

```
m(1,2)=4; %initial guess for h
sigma1=0.05; %std dev for the PPDF,varying this will vary the maximum
PPDF value.also small std dev.
j=2
while j<n
    u=rand;
    q_mstar((j-1),1) = rand; %required to obtain new value of q
    sigmaa = 0.05*m((j-1),1);%lowering this would result in estimates
far from the required value.
    temp((j-1),1) = rand;
    if temp(j-1)>0.5
        %finding new value of q
    m_star((j-1),1) = m((j-1),1) - sqrt(-2*sigmaa^2*log(q_mstar((j-
1),1)));%to find new value of q
    else
    m_star((j-1),1) = m((j-1),1) + sqrt(-2*sigmaa^2*log(q_mstar((j-
1),1)));
    end
    %finding new value of h
    q_mstar((j-1),2)=rand;
    sigmab=0.05*m((j-1),2);
     temp((j-1),2) = rand;
    if temp(j-1)>0.5
    m_star((j-1),2) = m((j-1),2) - sqrt(-2*sigmab^2*log(q_mstar((j-
1),2)));
    else
    m_star((j-1),2) = m((j-1),2) + sqrt(-2*sigmab^2*log(q_mstar((j-
1),2)));
    end
    %calculation simulated temp for initial guess value of q n h
    t_sim= neuralnetwork_for_fin_m( m(j-1,1),m(j-1,2) );
%     q_h = [m(j-1,1);m(j-1,2)];
    t_meas=[333.205914
327.242272
325.231468];
% t_sim=sim(network1,q_h);
% calculating the likelihood
X = (((t_sim-t_meas)'*(t_sim-t_meas))/(2*sigma1*sigma1*1000));
P_m0(j-1) = exp(-1*X); %PPDF for initial guess of q n h
```

```
%calculation of simulated temp for nxt value of q n h
t_sim1=neuralnetwork_for_fin_m( m_star(j-1,1),m_star(j-1,2) );
% q_h = [m_star(j-1,1);m_star(j-1,2)];
    t_meas=[333.205914
327.242272
325.231468];
% t_sim1=sim(network1,q_h);
%calculating likelihood
X = (((t_sim1-t_meas)'*(t_sim1-t_meas))/(2*sigma1*sigma1*1000));
P_mstar(j-1) = exp(-1*X); %PPDF for new value of q n h

% calculating acceptance ratio
A1=P_mstar(j-1)/P_m0(j-1);
A(j-1)= min(1,A1);

% METROPOLITAN HASTINGS CHECK
count = 0;
 if u<A(j-1)
    m(j,1) = m_star((j-1),1);
    count= count + 1;
 else
    m(j,1) = m((j-1),1);
 end
 if u<A(j-1)
    m(j,2) = m_star((j-1),2);
    count= count + 1;
 else
    m(j,2) = m((j-1),2);
 end
 j = j+1
end
Mean1= sum(P_mstar'.*m_star(:,1))/sum(P_mstar)
Mean2= sum(P_mstar'.*m_star(:,2))/sum(P_mstar)
Var1=sum(((m_star(:,1)-Mean1).^2).*P_mstar')/sum(P_mstar')
Var2=sum(((m_star(:,2)-Mean2).^2).*P_mstar')/sum(P_mstar')
Std_dev1= sqrt(Var1)
Std_dev2= sqrt(Var2)
```

```
[M,I]= max(P_mstar);
MAP=m_star(I,:)
toc
subplot(1,2,1);
plot(m_star(:,1),P_mstar);
xlabel('heatflux');ylabel('PPDF');
title('PPDF plot for q');

subplot(1,2,2);
plot(m_star(:,2),P_mstar);
xlabel('heat transfer coefficient');ylabel('PPDF');
title('PPDF plot for h');
```

REFERENCES

Adili, A., Hasni, N., Kerkeni, C., Nasrallah, S. B., (2010), "An inverse problem based on genetic algorithm to estimate thermophysical properties of fouling." Int. J. Therm. Sci., 49, 889-900.

Arash, J., Pouria, A. and Mohammad, N. M. J. (2014). "Optimization of a novel carbon dioxide cogeneration system using artificial neural network and multi-objective genetic algorithm." Appl. Therm. Eng., 64, 293-306.

Arnout, W. (2009). "Using the Inverse Heat Conduction Problem and thermography for the Determination of Local Heat Transfer Coefficients and Fin Effectiveness for Longitudinal Fins." Ph.D thesis, Sint-Pietersnieuwstraat 41, 9000 Gent, Belgium.

Balaji, C. and Padhi, T. (2010). "A new ANN driven MCMC method for multi-parameter estimation in two-dimensional conduction with heat generation." Int. J. Heat Mass Transfer 53, 5440–5455.

Balaji, C. and Thaseem, T. (2009). "An example of Bayesian Inference in thermal sciences." Reson., 14, 1171-1182. https://doi.org/10.1007/s12045-009-0112-7

Balázs, C., Gyula, G. (2012). "Simultaneous identification of temperature-dependent thermal properties via enhanced genetic algorithm." Int. J. Thermophys, 33, 1023–1041.

Balázs, C., Woodbury, K. A. and· Gyula, G., (2013). "Inverse Identification of Temperature-Dependent Volumetric Heat Capacity by Neural Networks." Int. J. Thermophys., 34, 284–305. DOI 10.1007/s10765-013-1410-6

Beck, J. V., Blackwell, B. and Clair, C. S. (1985). " Inverse Heat Conduction: Ill-posed problems." New York, Wiley.

Charles, J., Mrinal, K. S. and Paul L. S. (2004). "An Efficient Stochastic Bayesian Approach to Optimal Parameter and Uncertainty Estimation for Climate Model Predictions." J. Climate, 17, 2828-2841.

Cheung, S. H. and Beck, J. L. (2009). "Bayesian Model Updating Using Hybrid Monte Carlo Simulation with Application to Structural Dynamic Models with Many Uncertain Parameters." J. Eng. Mech. 135, 243-255.

Chyi-Tsong, C. and Hung-I, C. (2013), "Multi-objective optimization design of plate-fin heat sinks using a direction-based genetic algorithm." J. Taiwan Inst. Chem. E., 44 257–265.

Cole, K.D, Tarawneh, C. and Wilson, B. (2009). “Analysis of flux-base fins for estimation of heat transfer coefficient.” Int. J. Heat Mass Transfer, 52, 92–99.

Damian, S. (2008). “Using genetic algorithms for the determination of an heat transfer coefficient in three-phase inverse Stefan problem.” Int. Commun. Heat Mass., 35, 149–156.

Deng, S. and Hwang, Y. (2006). “Applying neural networks to the solution of forward and inverse heat conduction problems.” Int. J. Heat Mass Transfer, 49, 4732–4750.

Diego, C.K., Navier-Cotta, C.P., Joao, V.C.A., Cotta, R.M. and Orlande, H.R.B. (2012). “Theoritical- experimental analysis of heat transfer in nonhomogeneous solids via improved lumped formulation, integral transforms and infrared thermograpghy.” Int. J. Therm. Sci., 62, 71-84.

DOI: 10.1080/08916152.2013.871867

Dong, L., Xiaojing, L. and Yanhua, Y. (2017). “Investigation of uncertainty quantification method for BE models using MCMC approach and application to assessment with FEBA data.” Ann. Nucl. Energy, 107, 62–70.

Dorfman, A.S. (2006). “Conjugate problems in convective heat transfer.” CRC Press, Taylor & Francis group, Boca Raton, Florida.

Elham, H., Mohammad, A. S. and Salman, M. (2016). “Accurate prediction of nanofluid viscosity using a multilayer perceptron artificial neural network (MLP-ANN).” Chemometr. Intell. Lab., 155, 73–85.

Elham, S., Saeed, S., Mohammad, E. A. and Mitra, N. (2016). “Parameter estimation of breast tumour using dynamic neural network from thermal pattern.” J. Adv. Res., 7, 1045–1055

Ewa, M., Jolanta, D., and Grażyna, K. (2013). “Application of sensitivity analysis in microscale heat transfer.” Comput. Assist. Meth. Eng. Sci., 20, 113–121.

Fudym, O., Orlande, H.R.B., Bamford, M. and Batsale, J.C. (2008). “Bayesian approach for thermal diffusivity mapping from infrared images with spatially random heat pulse heating.” J. Phys. Conf. Ser., 135, 012042.

Fung-Bao, L. (2008). “A modified genetic algorithm for solving the inverse heat transfer problem of estimating plan heat source.” Int. J. Heat Mass Transfer, 51, 3745–3752.

Ghadimi, B., Kowsary, F. and Khorami, M. (2015). “Heat flux on-line estimation in a locomotive brake disc using artificial neural networks.” Int. J. Therm. Sci., 90, 203-213.

Giralomi, M. (2008). “Bayesian inference for differential equations.” Theor. Comput. Sci., 408, 4-16.

Gnanasekaran, N. (2011). “A Bayesian approach for multi-parameter estimation using heat transfer experiments.” Ph. D thesis, IITM, India.

Gnanasekaran, N. and Balaji, C. (2011). “A Correlation For Nusselt Number Under Turbulent Mixed Convection Using Transient Heat Transfer Experiments.” Front. Heat Mass Transfer (FHMT), 2, 023008. DOI: 10.5098/hmt.v2.2.3008

Gnanasekaran, N. and Balaji, C. (2011). “A Bayesian approach for the simultaneous estimation of surface heat transfer coefficient and thermal conductivity from steady state experiments on fins.” Int. J. Heat Mass Transfer 54, 3060–3068.

Gnanasekaran, N. and Balaji, C. (2013). “Markov Chain Monte Carlo (MCMC) approach for the determination of thermal diffusivity using transient fin heat transfer experiments.” Int. J. Therm. Sci. 63, 46-54.

Goldberg, D.E. (2006). “Genetic algorithms.” Pearson Education, India.

Guanghui, S., Morita, K., Fukuda, K., Pidduck, M., Dounan, J. and Jaakko, M. (2003). “Analysis of the critical heat flux in round vertical tubes under low pressure and flow oscillation conditions, Applications of artificial neural network.” Nucl. Eng. Des. 220, 17-35.

Hadamard,J. (1923). “Lectures on Cauchy’s Problem in Linear Differential Equations.” New Haven, CT , Yale University Press.

Hamidreza, N. and Woodbury, K. A. (2014). “Application of Artificial Neural Network As Digital Filter For Online Heat Flux Estimation.” Pro. ASME Int. Mechanical Engineering Congress and Exposition, Montreal, Quebec, Canada.

Hamilton, F. C., Marcelo, J. C., Rogério, N. C. and Albino, J.K.L. (2014). “Heat transfer coefficient estimation of an internal combustion engine using particle filters.” Inverse Probl. Sci. En. 22(3), 483–506.
http://dx.doi.org/10.1080/17415977.2013.797411

Hamzaoui, Y.E., Rodríguez, J.A., Hernandez, J.A., Victor. S. (2015). “Optimization of operating conditions for steam turbine using an artificial neural network inverse.” Appl. Therm. Eng., 75, 648-657.

Hao, P. and Xiang, L. (2008). “Optimal design approach for the plate-fin heat exchangers using neural networks cooperated with genetic algorithms.” Appl. Therm. Eng. 28. 642–650.

Hotta, T. K., Balaji, C. and Venkateshan, S. P. (2015). “Experiment Driven Ann-GA Based Technique for Optimal Distribution of Discrete Heat Sources Under Mixed Convection.” Exp. Heat Transfer, 28(3), 298-315.
http://dx.doi.org/10.1080/17415970600844242

Imani, Ranjbar, A. A. and Esmkhani, M. (2006). “Simultaneous estimation of temperature-dependent thermal conductivity and heat capacity based on modified genetic algorithm.” Inverse Probl. Sci. En., 14(7), 767–783.

Incropera, F. P. and David P. De W. (2002). “Fundamentals of Heat and Mass Transfer.” fifth ed., New York, John Wiley & Sons, Chapter 3.

Jambunathan, K., Hartle, S. L., Ashforth-Frost, S. and Fontama, V. N. (1996). “Evaluating convective heat transfer coefficients using neural networks.” Int. J. Heat Mass Transfer, 39 (11), 2329-2332.

Jesus, E. M. R., Carlos, P. T., Felix F. G. N. and Juan De D. O. D. (2014). “Thermodynamic properties of refrigerants using artificial neural networks.” Int. J. Refrig., 46, 9-16.

Jingbo, W. and Zabaras, N. (2005). “Hierarchical Bayesian models for inverse problems in heat conduction.” Inverse Probl., 21, 183–206. Doi:10.1088/0266-5611/21/1/012

José, O. V., Gwendolyn, M. and ·Claudio, A. F. (2011). “Heat Capacity of Ionic Liquids Using Artificial Neural Networks and the Concept of Mass Connectivity.” Int. J. Thermophys., 32, 942–956. DOI 10.1007/s10765-011-0954-6

Juan, A. L. (2011). “Autoignition Temperature Prediction Using an Artificial Neural Network with Particle Swarm Optimization.” Int. J. Thermophys., 32, 957–973, DOI 10.1007/s10765-011-0956-4

Julien, B., Orlande, H. R. B., Nathan, M. and Sihem, G., (2016). “Bayesian inference for estimating thermal properties of a historic building wall.” Build. Environ., 106, 327-339.

Kaipio, J. and Somersalo, E., (2004). “Statistical and Computational Inverse Problems.” Applied Mathematical Sciences 160, New York, USA, Springer-Verlag.

Kaipio, J. P. and Colin F. (2011). “The Bayesian Framework for Inverse Problems in Heat Transfer.” Heat Transfer Eng., 32(9), 718-753.
DOI:10.1080/01457632.2011.525137

Kemal, E., Aytunc, E. and Ibrahim, D. (2007). “Heat transfer analysis of phase change process in a finned-tube thermal energy storage system using artificial neural network.” Int. J. Heat Mass Transfer, 50, 3163–3175.

Konda,R., B., Gnanasekaran, N. and Balaji, C. (2012). “Estimation of thermo-physical and transport properties with Bayesian inference using transient liquid crystal thermography experiments.” J. Physics: Conference Series 395, 012082.

Kumar, S., Kumar, H. and Gnanasekaran, N. (2016). “A neural network based method for estimation of heat generation from a teflon cylinder.” Front. Heat Mass Transfer (FHMT) 7-15.

Liang, Y., Fenglian, Y. and Chuli, Fu. (2009). “A Bayesian inference approach to identify a Robin coefficient in one-dimensional parabolic problems” J. Comput. Appl. Math., 231, 840-850.

Ling, Z., Nan, Z., Fuyun, Z. and Youming, C. (2004). “A genetic-algorithm-based experimental technique for determining heat transfer coefficient of exterior wall surface.” Appl. Therm. Eng., 24, 339–349.

Louis, G., Maxime, T.G., François, M. P. (2009), “Review of utilization of genetic algorithms in heat transfer problems.” Int. J. Heat Mass Transfer, 52, 2169–2188.

Masoud, A., Karim Nazari, N., Nima, S., Mohammad, R. S., Kherbeet, A.S., Somchai, W. and Mahidzal. D. (2016). “Prediction of dynamic viscosity of a hybrid nano-lubricant by an optimal artificial neural network.” Int. Commun. Heat Mass., 76, 209–214.

Miroslav, R., Woodbury, K. A., Kral, J. and Brezina, T. (1995). “Genetic Algorithm In Solution Of Inverse Heat Conduction Problems.” Numer. Heat Tr. B- Fund., 28, 293-306.

Mitra, S. and Balaji, C. (2010). “A neural network based estimation of tumour parameters from a breast thermogram.” Int. J. Heat Mass Transfer, 53, 4714–4727.

Mohammad, H. E. (2017). “Designing a neural network for predicting the heat transfer and pressure drop characteristics of Ag/water nanofluids in a heat exchanger.” Appl. Therm. Eng., 126, 559–565.

Mohammad, H. E., Seyfolah, S., Nima, S., Masoud, A. and Sara, R. (2015). “Designing an artificial neural network to predict thermal conductivity and dynamic viscosity of ferromagnetic nanofluid.” Int. Commun. Heat Mass., 68 50–57.

Mohsen, A., Hajar, A., Armin, Z. and Mohammad, V. T. (2017). “Application of artificial neural network method to exergy and energy analyses of fluidized bed dryer for potato cubes.” Energy, 120, 947-958.

Morales, L.I., Conde-Gutierrez, R.A., Hernandez, J.A., Huicochea, A., Juarez-Romero, D. and Siqueiros, J. (2015). “Optimization of an absorption heat transformer with two-duplex components using inverse neural network and solved by genetic algorithm” Appl. Therm. Eng., 85, 322-333.

Mota, C. A. A., Orlande, H. R. B., Carvalho, M. O. M. D., Kolehaminen, V. and Kaipio, J. P. (2010). “Bayesian estimation of temperature-dependent thermophysical properties and transient boundary heat flux.” Heat Transfer Eng. 31, 570-580.

Naoya, K., Shunsuke, M., Koichi, T., Kazuyoshi, S., Tomohiko, T. and Yukitaka, S. (2016). “Predicting maximum depth of corrosion using extreme value analysis and Bayesian inference.” Int. J. Pres. Ves. Pip., 146, 129-134.

Naveira-Cotta, C. P., Cotta, R. M. and Orlande, H. R. B. (2010).“Inverse Analysis of forced convection in micro channels with slip flow via integral transforms and Bayesian inference.” Int. J. Therm. Sci., 49, 879-888.

Naveira-Cotta, C. P., Cotta, R. M. and Orlande, H. R. B. (2011). “Inverse Analysis with integral transformed temperature fields: Identification of thermophysical properties in heterogrneous media.” Int. J. Heat Mass Transfer, 54, 1506-1519.

Orlande, H. R. B., Dulikravich, G. S., Markus, N., Daniel, W. and Marcelo J. C. (2014). “Accelerated Bayesian Inference For The Estimation Of Spatially Varying Heat Flux In A Heat Conduction Problem.” Numer Heat Tr. A-Appl., 65, 1–25. DOI: 10.1080/10407782.2013.812008

Orlande, H.R.B., Marcelo J. C. and Dulikravich, G. S. (2008). “Approximation of likelihood function in the Bayesian technique for solution of inverse technique.” Inverse Probl. Sci. En., 16(6), 677-692. DOI: 10.1080/17415970802231677

Ozisik, M. N. and Orlande, H. R. B. (2000). “Inverse Heat Transfer: Fundamentals and Applications.” New York, Taylor and Francis.

Parthasarathy, S. and Balaji, C. (2008). “Estimation of parameters in multi-mode heat transfer problems using Bayesian inference-effect of noise and a prior.” Int. J. Heat Mass Transfer 51, 2313-2334.

Patrick, H., Christian P., Jeff, H. and Kevin, A. (2007), “Nonlinear Bayesian Algorithms for Gas Plume Detection and Estimation from Hyper-spectral Thermal Image data.” Sensors, 7, 905-920.

Pereyra, S., Lombera, G.A., Frontini, G. and Urquiza, S.A. (2014). “Sensitivity Analysis and Parameter Estimation of Heat Transfer and Material Flow Models in Friction Stir Welding.” Mat. Res., 17(2), 397-404..

Phippe, L., Frederic, M., Harry, B., Francois, G. and Laetitia, A. (2006). “Bayesian Parameter Estimation of Convective Heat Transfer Coefficients of a Roof Mounted Radiant Barrier System.” J. Sol. Energy Eng., 128, 213-225.

Ponnada, S., Rajesh, B. and Balaji, C. (2016). “Geometric Optimization of a PCM-Based Heat Sink—A Coupled ANN and GA Approach.” Heat Transfer Eng., 37(10), 875-888. DOI: 10.1080/01457632.2015.1089749

Premachandran, B. and Balaji, C. (2006). “Conjugate mixed convection with surface radiation from a horizontal channel with protruding heat sources.” Int. J. Heat Mass Transfer 49, 3568–3582.

Renjith, R. R., Venugopal, G. and Rajkumar, M. R. (2015). “Bayesian Inference for Parameter Estimation in Transient Heat Transfer Experiments.” J. Heat Transfer, 137 121011-1-7, [DOI: 10.1115/1.4030955.

Reza, B. and Masoud, R. (2012). “Prediction of heat transfer and flow characteristics in helically coiled tubes using artificial neural networks.” Int. Commun. Heat Mass., 39, 1279–1285.

Reza, P., Hasan, D. and Seyed, H. T. (2014), “Solving an inverse heat conduction problem using genetic algorithm: sequential and multi-core parallelization approach.” Appl. Math. Model., 38, 1948-1958.

Sablani, S. S. (2001). “A neural network approach for non-iterative calculation of heat transfer coefficient in fluid–particle systems.” Chem. Eng. Process., 40, 363–369.

Sablani, S.S., Kacimov, A., Perret, J., Mujumdar, A.S. and Campo, A., (2005). “Non-iterative estimation of heat transfer coefficients using artificial neural network models.” Int. J. Heat Mass Transfer, 48, 665–679.

Sepehr, S. and Hassan, H. (2010). “Thermal-economic multi-objective optimization of plate fin heat exchanger using genetic algorithm.” Appl. Energ., 87, 1893–1902.

Shubhankar. C., Prasanta, K. D. (2015). “Application of Bayesian Inference Technique for the reconstruction of an isothermal hot spot inside a circular disc from peripheral temperature measurement – A critical assessment.” Int. J. Heat Mass Transfer, 88, 456–469.

Sivanandam, S.N. and Deepa, S.N. (2008). “Introduction to Genetic Algorithms.” New York, Springer.

Somasundharam, S. and Reddy, K. S. (2016). “Inverse estimation of thermal properties using Bayesian inference and three different sampling techniques.” Inverse Probl. Sci. Eng. DOI: 10.1080/17415977.2016.1138946

Soteris, A. K. and Milorad, B. (2000). “Artificial neural networks for the prediction of the energy consumption of a passive solar building.” Energy, 25, 479–491.

Swati, V. and Balaji, C. (2007). “Multi-parameter estimation in combined conduction–radiation from a plane parallel participating medium using genetic algorithms.” Int. J. Heat Mass Transfer, 50, 1706–1714.

Tan, C.K., Ward, J., Wilcox, S.J. and Payne, R. (2009). “Artificial neural network modelling of the thermal performance of a compact heat exchanger.” Appl.Therm. Eng., 29, 3609–3617.

Unal, A., Aydin, K.M. and Feridun, O.A. (2009). “Estimation of heat transfer in oscillating annular flow using artificial neural networks.” Adv. Eng. Softw., 40, 864–870.

Unal, A., Aydin, K.M. and Selma, A. (2016). “Prediction of heat transfer on a flat plate subjected to a transversely pulsating jet using artificial neural networks.” Appl. Therm. Eng., 100, 412–420.

Venugopal, G., Suryakant, Balaji, C. and Venkateshan, S.P. (2009). "A hybrid optimization technique for developing heat transfer correlations based on transient experiments." Int. J. Heat Mass Transfer, 52, 1954–1964.

Wang, J. and Zabaras, N. (2004). "A Bayesian inference approach to the inverse heat conduction problem." Int. J. Heat Mass Transfer, 47, 3927-3941.

Woodbury, K. A. and Suprasanna, D. (2006). "Comparison between the performance of binary coding and real number encoding in genetic algorithms applied to the IHCP." Pro. IMECE, ASME Int. Mechanical Engineering Congress and Exposition, Chicago, Illinois, USA.

Woodbury, K. A., Courtney, G., John, B. and Charles, K. (2004). "An inverse method using a genetic algorithm to determine spatial temperature distribution from infrared tranmissivity measurements in a gas." Pro. HT-FED04, ASME Heat Transfer /Fluids Engineering Summer Conference, Charlotte, North Carolina USA.

Xiang, M, and Zabaras, N. (2009). "An efficient Bayesian inference approach to inverse problems based on an adaptive sparse grid collocation method." Inverse Probl., 25, 035013. Doi:10.1088/0266-5611/25/3/035013

Xu, W. and Tomasz, K. (2017). "Inverse uncertainty quantification of reactor simulations under the Bayesian framework using surrogate models constructed by polynomial chaos expansion." Nucl. Eng. Des., 313, 29–52.

Yasar. I. (2003). "A new approach for the prediction of the heat transfer rate of the wire-on-tube type heat exchanger—use of an artificial neural network model." Appl. Therm. Eng., 23, 243–249.

Yegnanarayana, B. (2005). "Artificial Neural Networks." Prentice-Hall of India Private Limited, New Delhi.

Youssef, M. and Dongbin, X. (2009). "A Stochastic Collocation Approach to Bayesian Inference in Inverse Problems." Commun. Comput. Phys., 6(4), 826-847.

Zabaras, N. (1988). "Inverse Problems in Heat Transfer1, Handbook of Numerical Heat Transfer." John Wiley & Sons, Inc., US, Chapter-17, 525-558

Zeke, S.H. C., Ngan, H.W., Rad, A.B., David, A.K. and Kasabov, N. (2006). "Short-term ANN load forecasting from limited data using generalization learning strategies." Neurocomputing, 70, 409–419.

Zixi, H., Zhewei, Y. and Jinglai, L. (2017). "On an adaptive preconditioned Crank–Nicolson MCMC algorithm for infinite dimensional Bayesian inference." J. Comput. Phys., 332, 492–503.

LIST OF PUBLICATIONS

INTERNATIONAL JOURNAL

1. **Harsha, K.**, Sharath, K., Gnanasekaran, N. and Balaji, C. (2018). "A Markov Chain Monte Carlo-Metropolis Hastings Approach for the Simultaneous Estimation of Heat Generation and Heat Transfer Coefficient from a Teflon Cylinder." Heat Transfer Eng., 39(4), 339-352. DOI: 10.1080/01457632.2017.1305823
2. **Harsha, K.** and Gnanasekaran, N. (2018). "A Bayesian inference approach - estimation of heat flux from fin for perturbed temperature data." Sadhana, (2018) 43:62. https://doi.org/10.1007/s12046-018-0861-7.
3. **Harsha K.,** Vishweshwara, P.S., Gnanasekaran, N. and Balaji, C. (2018). "A Combined ANN-GA and Experimental Based Technique for the Estimation of the Unknown Heat Flux for a Conjugate Heat Transfer Problem." Heat and Mass Transfer, Springer. https://doi.org/10.1007/s00231-018-2341-3
4. **Harsha, K**. and Gnanasekaran, N. (2017). "A synergistic combination of Asymptotic Computational Fluid Dynamics and ANN for the estimation of unknown heat flux from fin heat transfer." Alexandria Engineering Journal, Elsevier. http://dx.doi.org/10.1016/j.aej.2017.01.034
5. Sharath, K, **Harsha K.** and Gnanasekaran, N. (2016). "A neural network based method for estimation of heat generation from a teflon cylinder." Front. Heat Mass Transfer (FHMT), 7, 15. DOI: 10.5098/hmt.7.15.
6. Amey, S. K., **Harsha K.** and Gnanasekaran, N. (2015). "A New Forward Model Approach for a Mild Steel Fin under Natural Convection Heat Transfer." Int. conference on Computational Heat and Mass Transfer-2015, Procedia Engineering 127, 317-324.

INTERNATIONAL CONFERENCE

1. **Harsha, K**., Sharath, K., Sagar, K. S. and Gnanasekaran, N. (2014). "Hybrid Monte Carlo approach for estimation of heat flux from fin for perturbed temperature data." 23rd Int. Conference on Interdisciplinary Mathematical,

Statistical and Computational Techniques,(IMSCT 2014- FIMXXIII), Dec.18-20, NITK, Surathkal.

2. **Harsha, K**., Sharath, K., Sagar, K. S. and Gnanasekaran, N. (2015). "Synergistic approach for the simultaneous estimation of heat transfer coefficient and heat flux using fin from steady state heat transfer experiments." 6th Int. Symp. on Advances in Computational Heat Transfer (CHT-15), May 25-29, Rutgers University, Piscataway, USA.
3. **Harsha, K**., Amey, S. K. and Gnanasekaran, N. (2015). "Estimation of heat transfer coefficient of a mild steel fin using inverse heat transfer approach." Int. Conference on Computer Aided Engineering (CAE-2015), Department of Mechanical Engineering, GITAM University, School of Technology, Hyderabad, India.
4. **Harsha, K**. and Gnanasekaran, N. (2015). "Simultaneous estimation of heat transfer coefficient and thermal diffusivity for rectangular fin under heating and cooling process." Proceedings of the 23rd National Heat and Mass Transfer Conference and 1st International ISHMT-ASTFE Heat and Mass Transfer Conference IHMTC2015, December 17-20, Thiruvananthapuram, India.
5. **Harsha, K**., Vishweshwara, P.S., and Gnanasekaran, N. (2017). "The use of GA and PSO for the inverse estimation of heat flux in a conjugate heat transfer problem." Proc. of the 24thNational and 2nd Int. ISHMT-ASTFE Heat and Mass Transfer Conference (IHMTC-2017), December 27-30, BITS Pilani, Hyderabad, India.
6. Gnanasekaran, N., **Harsha, K**., and Balaji, C. (2018). "MCMC and approximation error model for the simultaneous estimation of heat flux and heat transfer coefficient using heat transfer experiments." Proc. of the 16th Int. Heat Transfer Conference, IHTC-16, 2018, August 10-15, Beijing, China.
7. Gnanasekaran, N. and **Harsha, K**. (2018). "Accelerating MCMC using model reduction for the estimation of boundary properties within Bayesian framework." Int. Conference Numerical Heat Transfer and Fluid Flow, January 19-21, NIT Warangal, India.

BIO-DATA

Personal details:

Name	HARSHA KUMAR MK
Phone	09980019001
Email	harsha84.nitk@gmail.com
Address	SRI DURGA, D.No:2-86/6(1), Behind Paramjyothi Bajana Mandhir Alape, Bajal, Mangalore-575007

Work Experience:

Total experience of 7 years 4 months in teaching and 4 years 2 months in research.

1) Worked as lecturer in S N S Polytechnic College, Bajpe, Mangalore for the duration of 3 months in the year 2006.
2) Worked as Lecturer in Canara Engineering College, Benjanapadavu, Mangalore from 09/11/2006 to 31/07/2011 and Assistant professor from 01/08/2011 to 26/12/2013.
3) Research Scholar in the department of Mechanical Engineering, National Institute of Technology Karnataka, Surathkal, from December 2013 till date.

Subjects Handled:

Modeling and Finite Element Analysis (MFEA), Operations Research (OR), Basic Thermodynamics (BTD), Applied Thermodynamics (ATD), Computer Aided Engineering Drawing (CAED), Manufacturing Process I,II and III, CAD/CAM, Automotive Engineering, Elements Of Mechanical Engineering, CAMA(Computer Aided Modeling and Analysis).

Technical Skills:

Analysis Languages Matlab, Ansys, Pro e, Solid Edge

Educational Qualifications:

Degree	Board/University	Percentage	Year of Passing
M.Tech (Energy System Engineering)	NMAMIT, Nitte, (Karnataka)	9.24 CGPA	2010
B.Tech (Mechanical Engineering	Malnad College Of Engineering, Hassan, (Karnataka), VTU	65.14%	2006
P.U.C	Milagres P.U. College, Mangalore (Karnataka)	80.66%	2002
S.S.L.C	Milagres High School, Mangalore (Karnataka)	72.48%	2000

Achievements:

1. Received best paper award for the paper titled, "Accelerating MCMC using model reduction for the estimation of boundary properties within Bayesian framework" at International Conference Numerical Heat Transfer and Fluid Flow, NIT Warangal, India, Jan 19-21, 2018.

Industrial Training Undergone:

1) Kudremukh Iron Ore company, Baikampady during the year 2004 for the duration 20 days.
2) Mangalore Refinery And Petrochemicals Ltd. Surathkal during the year 2005 for the duration of 25 days.
3) Suzlon Composites, Padubidri during the year 2009 for the duration of 2 months.

Number of publications: 6

Number of conferences: 7

Number of seminars and workshops Attended: 14

Other Activities:

1) Appointed as the secretary of Association of Canara Mechanical Engineers (ACME), CEC since 2010.
2) Was coordinator in the project of MODROBS, which included acquiring grant from AICTE, New Delhi, for the advancement of CIM and CAMA lab. And a grant of Rs 9,00,000/- was sanctioned by AICTE for the procurement of Vertical Milling Machine (CNC) which has been installed in the college in the year 2012.